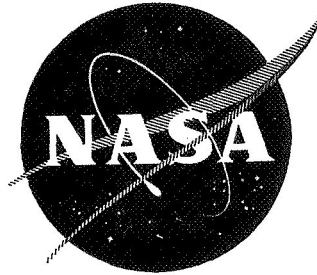CASE FILE
COPY

CADMIUM ELECTRODE MECHANISM
ELECTRODE MORPHOLOGY AND CAPACITY

by

F. G. Will and H. J. Hess

GENERAL ELECTRIC CORPORATE RESEARCH AND DEVELOPMENT

prepared for

NATIONAL AERONAUTICS AND SPACE ADMINISTRATION

NASA Lewis Research Center
Contract NAS 3-12968
J. Stewart Fordyce, Project Manager

NOTICE

This report was prepared as an account of Government-sponsored work. Neither the United States, nor the National Aeronautics and Space Administration (NASA), nor any person acting on behalf of NASA:

A.) Makes any warranty or representation, expressed or implied, with respect to the accuracy, completeness, or usefulness of the information contained in this report, or that the use of any information, apparatus, method, or process disclosed in this report may not infringe privately-owned rights; or

B.) Assumes any liabilities with respect to the use of, or for damages resulting from the use of, any information, apparatus, method or process disclosed in this report.

As used above, "person acting on behalf of NASA" includes any employee or contractor of NASA, or employee of such contractor, to the extent that such employee or contractor of NASA or employee of such contractor prepares, disseminates, or provides access to any information pursuant to his employment or contract with NASA, or his employment with such contractor.

FINAL REPORT

CADMIUM ELECTRODE MECHANISM
ELECTRODE MORPHOLOGY AND CAPACITY

by

F. G. Will and H. J. Hess

GENERAL ELECTRIC CORPORATE RESEARCH AND DEVELOPMENT
P. O. Box 8
Schenectady, New York   12301

prepared for

NATIONAL AERONAUTICS AND SPACE ADMINISTRATION

March 15, 1971

Contract NAS 3-12968

NASA Lewis Research Center
Cleveland, Ohio
J. Stewart Fordyce, Project Manager
Direct Energy Conversion Division

FOREWORD

The research described herein was done in the Physical Chemistry Laboratory of the General Electric Research and Development Center under NASA Contract NAS 3-12968 with Dr. J. Stuart Fordyce, Direct Energy Conversion Division, NASA-Lewis Research Center, as Project Manager.

TABLE OF CONTENTS

ABSTRACT

Changes in the capacity and morphology of cadmium film elec-
trodes during cycling in 0.1 to 6N potassium hydroxide solutions
were studied, using in-situ microscopy and scanning electron
microscopy. In stirred bulk solutions under conditions of uniform
current distribution a dissolution mechanism dominates in con-
centrated hydroxide and accounts for the large initial capacities
and for the pronounced changes in morphology and loss of capacity
on cycling. In dilute hydroxide, a solid state mechanism pre-
vails and explains the small capacities and the lack of changes
in morphology and capacity. In the case of thin electrolyte films,
simulating the non-uniform current distribution in a single pore
of a battery plate, dissolution and precipitation of cadmium
species causes substantial loss of capacity during cycling, while
the remaining capacity is due to small particles reacting via a
solid state mechanism.

SUMMARY

The capacity of cadmium battery plates often decreases gradually on continuous cycling. Certain changes in the morphology and passivation phenomena have been found to accompany this loss of capacity. The problem has not been fully identified and the mechanism leading to the loss of capacity is not understood. The present study is aimed at establishing the correlation between morphology and capacity of cadmium electrodes on repeated charge and discharge.

The study was performed on electrodes consisting of thin layers of cadmium and cadmium oxide on an inert conducting substrate. Two different geometries were chosen for the study: 1) The test electrode was contained in bulk solutions of potassium hydroxide in such a way that uniform current distribution and minimization of concentration changes in the electrolyte resulted. 2) A miniature cadmium electrode, covered with a thin film of electrolyte, was positioned side-by-side to the counter electrode. The resulting nonuniform current distribution and lack of electrolyte convection simulates conditions in a single pore of a battery plate. In-situ microscopy and scanning electron microscopy were applied to examine the changes in morphology during cycling.

In bulk solutions of 6N KOH, prolonged discharge and especially continuous cycling leads to a drastic loss in capacity and complete change in morphology due to dissolution of cadmium species. Between 70 and 80% of the cadmium dissolves during a typical discharge. Extensive charging leads to electrodeposition of dissolved cadmium species and to the recovery of nearly theoretical capacities. Precipitation of particles is not observed. With decreasing KOH concentration the changes in morphology and capacity on cycling become substantially smaller. Also the capacities which are obtained are much decreased. In 0.1N KOH no significant dissolution occurs, and the charge and discharge

1

occurs via a solid state transport mechanism. The capacities obtained in this case correspond to only a few atom layers.

In the case of thin films of KOH electrolyte, the initial changes in the morphology and capacity of cadmium oxide films deposited electrophoretically were studied extensively, using optical and scanning electron microscopy. Discharge leads to the formation of well-crystallized $Cd(OH)_2$ particles which do not contribute to the capacity on subsequent cycling. The crystals are formed by precipitation and account for the large observed loss in capacity on cycling. The remaining capacity is due to the charge and discharge of particles of the original size via a solid state transport mechanism. On continued cycling, the capacity further decreases, accompanied by the formation of a brown layer and a change in the shape of the discharge curve. This suggests the formation of passivating cadmium oxide layers. The effects of electrolyte film thickness, different methods of preparing the electrodes and temperature were investigated. The electrolyte film thickness was found to have very little effect on the cycling behavior. The mechanically more rigid structure of electrodes prepared by painting cadmium oxide-binder mixtures on the substrate leads to a smaller loss of capacity on cycling. Increasing the temperature was found to enhance the loss of capacity on cycling, accompanied by drastic changes in the morphology which could be detected in the microscope during the very first discharge.

INTRODUCTION

Cadmium battery plates often exhibit a gradual decrease of their capacity when they are repeatedly charged and discharged.[1] A certain part of the "lost" capacity may be regained by changing the conditions of charging and discharging. Another part of the capacity, however, is lost irreversibly. The phenomenon is more pronounced in sealed cells working with a minimum of electrolyte than in flooded, vented cells.

Studies of Cd battery plates with microscopy, x-ray diffraction and electron microscopy techniques have shown that the decrease of the plate capacity is related, at least in part, to changes in the plate morphology.[1-3] Migration of Cd species from the interior of the plate to its surface accompanied by an increase in the size of the particles has been demonstrated. This migration becomes more pronounced as the number of cycles and the rate of charging and discharging increases. Recently it was shown that the loss of capacity on cycling can be substantially reduced by adding certain metal oxides to the battery plate.[4]

Numerous studies have dealt with the mechanism of the Cd electrode in bulk solutions of alkali. These studies have established the solubility of Cd as a function of electrolyte concentration and temperature.[5-7] No full agreement exists with regard to the nature of the dissolved Cd species. Authors in the past have alternately proposed a dissolution-precipitation[8-14] and a solid state transport mechanism for the Cd electrode.[15-17] Recent results obtained with a ring-disc electrode seem to show that in concentrated alkaline solutions the discharge occurs solely by a dissolution-precipitation mechanism and that both mechanisms enter when charging the electrode.[18] The proposed mechanism involves the formation of $Cd(OH)_3^-$ ions as an intermediate species in solution:[18-19]

3

$$Cd + 3\ OH^- \rightleftharpoons Cd(OH)_3^- + 2e^- \qquad\qquad [1]$$

$$Cd(OH)_3^- \rightleftharpoons Cd(OH)_2 + OH^- \qquad\qquad [2]$$

The mechanism of the Cd electrode is complicated by the formation of passivating layers. Certain experimental evidence suggests the formation of CdO films as the cause for passivation.[20-21] However, CdO has so far escaped positive identification. The mechanism is further complicated by the formation of several phases of $Cd(OH)_2$.[22-25]

The behavior of battery plates on cycling and the mechanism of Cd electrodes in bulk electrolytes have both been studied. However, a gap exists in our understanding of the effects of repeated charging and discharging on the morphology of smooth Cd electrodes in bulk electrolyte and the mechanisms occurring in porous Cd electrodes such as Cd battery plates. It is apparent that the mechanism of a smooth Cd electrode in bulk electrolyte may differ substantially from the mechanism occurring in the pores of a Cd battery plate. The nonuniform current distribution and changes in the electrolyte concentration in the pores during charging and discharging are expected to give rise to such differences in mechanism. For Cd electrodes covered with electrolyte films of 0.5 to 2 mm thickness, nonuniform current distribution and changes in the electrolyte concentration during charging and discharging have, in fact, been demonstrated to exist.[26]

The present study is aimed at establishing the effect of repeated charging and discharging on the capacity and morphology of Cd electrodes in bulk solutions and in thin films of alkaline electrolyte. The study is further aimed at identifying the mechanism leading to changes in the capacity and morphology. In the bulk electrolyte study, conditions were chosen such as to produce uniform current distribution and to minimize the effects of changes in the electrolyte concentration. In the thin film study, conditions in a

4

single pore of a battery plate were simulated by using a flat minia-
ture Cd electrode covered with a thin film of electrolyte. Such
an electrode may be considered as resulting from unwinding a hollow
cylinder of inner diameter equaling the pore diameter.[26] With
the exception of the nonsignificant electrode width, all dimensions
were chosen to approximate those encountered in actual battery
plates. The counter electrode was positioned side-by-side rather
than opposite to the test electrode. This resulted in a highly
nonuniform current distribution and minimization of electrolyte
convection in vast contrast to the bulk electrolyte case. The
geometry permitted in situ microscopic examination of changes in
the morphology during charging and discharging. Optical microscopy
was supplemented by scanning electron microscopy to identify changes
in the morphology during the initial stages.

PHASE I - BULK ELECTROLYTE

EXPERIMENTAL

Cell Design

The bulk electrolyte experiments were carried out in a two-compartment glass cell which is shown in Figure 1. The main compartment contains a test electrode and a self-contained hydrogen reference electrode with a capillary opening located close to the test electrode. The counter electrode is contained in a second compartment which communicates with the main compartment via a capillary of 1 mm diameter. Both compartments have provisions for introducing gases which are permitted to escape through electrolyte traps. Magnetic stirring of the electrolyte in the main compartment can be applied when needed. Filling of the cell is accomplished under vacuum. Prepurified argon was used in both cell compartments to decrease undesirable effects due to oxygen and carbon dioxide. Residual currents, due to the diffusion of trace amounts of O_2 into the cell, were essentially eliminated by placing the cell in a polyethylene bag, continually flushed with nitrogen. The test electrode can readily be replaced while potentials are being applied between test and reference electrode.

Electronic Instrumentation

Experiments were carried out under conditions of controlled voltage or controlled current. In the former case, an electronic potentiostat was used to apply potentials with a precision of ±1 mV between the test electrode and the reference electrode. In the latter case, an automatic electronic cycling device was used to apply constant currents between test and counter electrode. The voltage-time transients under conditions of constant charge and discharge currents were recorded on a Hewlett Packard strip chart recorder. The voltage limits during charge and discharge could be set to various arbitrary values.
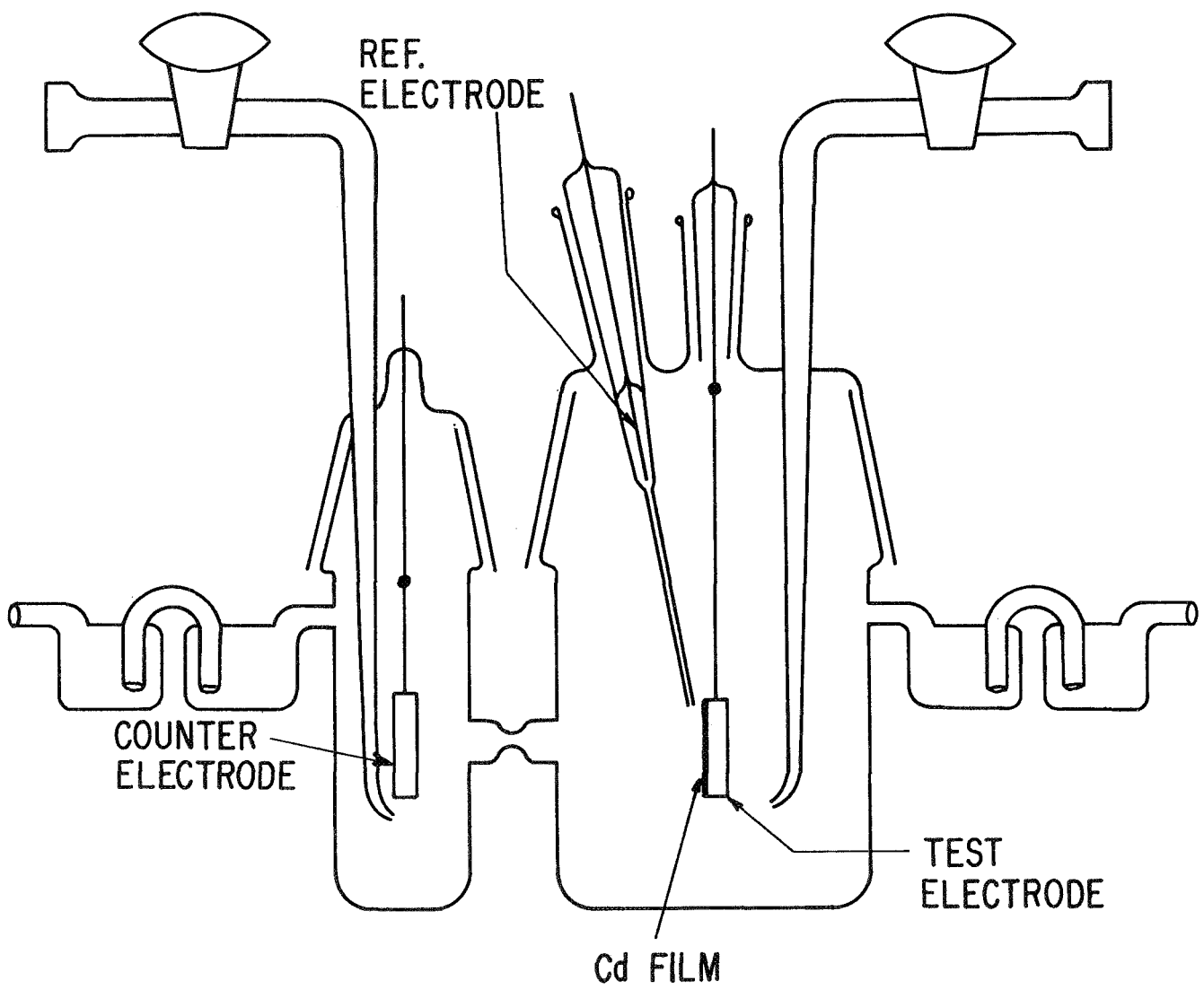
Fig. 1 Cross section of electrolytic cell used for bulk electrolyte experiments.

Electrode Preparation

Test electrodes were prepared by electrodepositing cadmium layers and by evaporating cadmium oxide layers on copper substrate foils. The choice of copper as a substrate material was determined by its relatively high hydrogen overvoltage and complete inertness to alkaline solutions in the potential range of interest. On the standard hydrogen scale, the following potentials at pH 14 are of interest: $H_2/OH^- = -828$ mV, $Cd/Cd(OH)_2 = -809$ mV, $Cu/Cu_2O = -358$ mV and $Cu_2O/Cu(OH)_2 = -80$ mV. Copper is inert to alkaline solutions until oxides or hydroxides of copper are formed. Thus it can be seen that up to potentials of 470 mV positive with respect to the hydrogen reference electrode at pH 14, copper does not dissolve. Hydrogen evolution from the substrate constitutes an undesirable side reaction and has to be minimized. The substrate material should therefore have a high hydrogen overvoltage. In this respect copper is much superior to iron and nickel. The hydrogen overvoltages determined in 6 N NaOH at 25°C for a current density of 1 ma/cm^2 are -140, -260 and -370 mV for iron, nickel and copper, respectively.[27] For comparison, cadmium has a hydrogen overvoltage of -590 mV.

Ideally, the substrate surface should appear structureless in the microscope in order to allow the identification of morphological changes of the cadmium or camdium oxide layers in the initial phases. Copper substrate foils of 5 x 5 cm and 0.5 mm thickness were, therefore, electropolished in an aqueous solution of about 50 volume percent orthophosphoric acid containing 10-15 grams per liter cupric ions. The procedure adopted closely followed that described in the literature.[28] Figure 2 shows an optical micrograph of an electropolished copper surface at a magnification of 1000X. Figure 3 is an electron micrograph of the same surface at a magnification of 30,000X. The surfaces contain relatively few defects and appear mirrorlike to the bare eye. The electropolished foils were then cut to rectangular pieces of dimensions 2 x 0.5 cm and used as substrates for cadmium plating and cadmium oxide evaporation.

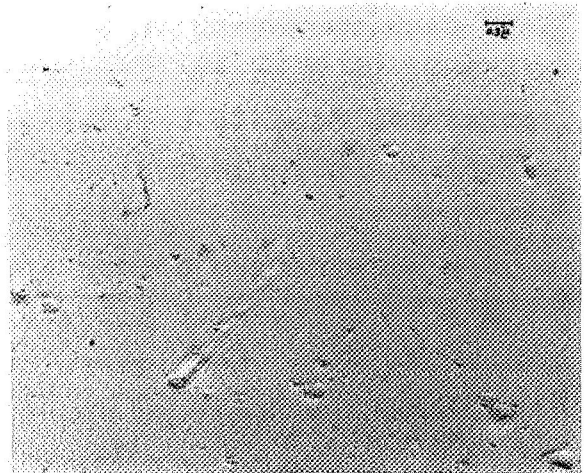Fig. 2. Optical micrograph at 1000X of electro-polished Cu substrate.

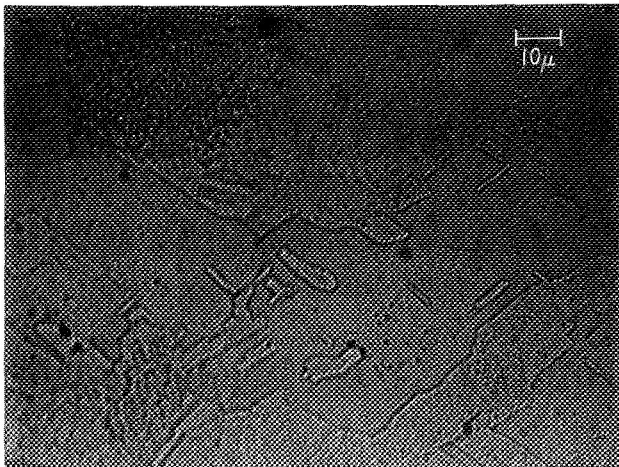Fig. 3. Electron micrograph at 30,000X of electropolished Cu substrate.

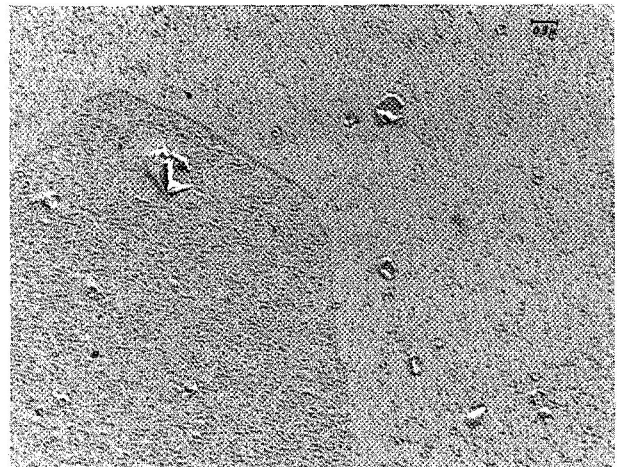Fig. 4. Optical micrograph at 500X of 100Å Cd film as electrodeposited on electropolished Cu substrate.

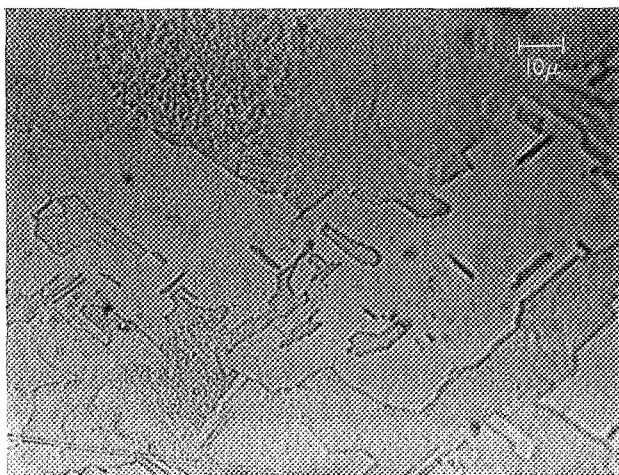Fig. 5. Electron micrograph at 30,000X of 100Å Cd film as electrodeposited.

Fig. 6. Optical micrograph at 500X of same electrode, same area as in Fig. 4, after exposure to 1N KOH for 16 hours with O V applied.
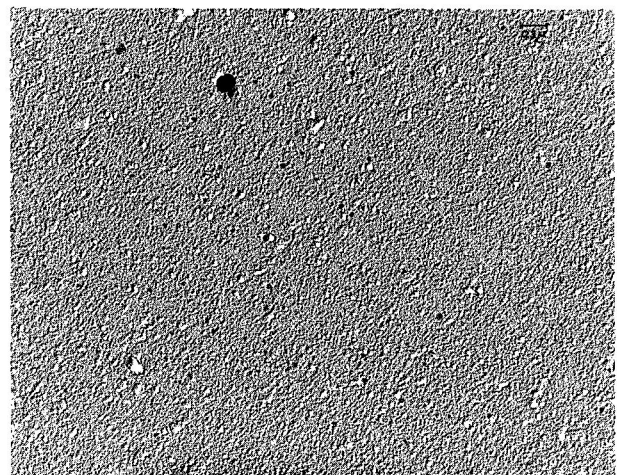

Fig. 7. Electron micrograph at 30,000X of a 100Å Cd film electrode after 190 cycles in 1N KOH.

Cadmium layers in a range of thicknesses from 80 Å to 1μ were produced by electroplating from commercial cadmium cyanide baths containing organic brighteners, from pure cadmium cyanide solutions and from hot concentrated potassium hydroxide solutions containing dissolved cadmium oxide. The cadmium layers were deposited on one side of the copper foils only; the other side was covered with a thin layer of polystyrene. The thinnest coherent layers and those with the highest optical quality were obtained from the commercial plating solutions. Figures 4 and 5 are micrographs of such layers at magnifications of 500 and 30,000X. These layers display a platelet structure and are coherent in thicknesses down to 80Å. They appear silverish and mirrorlike to the bare eye. The morphology of these layers is not affected by exposure to KOH when reducing potentials (negative with respect to the Cd/Cd(OH)$_2$ standard potential) are applied. Figure 6 shows the cadmium film of Figure 4 after exposure to 1 N KOH for 16 hours with 0 volts applied versus the hydrogen reference electrode in 1 N KOH. Both micrographs show virtually the same morphology. Electroplating from pure cadmium cyanide solutions resulted in incoherent layers, and the process was discontinued. However, plating at 86°C from 6 N KOH saturated with cadmium oxide resulted in layers of good quality with a platelet structure resembling that obtained from commercial solutions. The photomicrograph shown in Figure 15 and obtained at a magnification of 500X is an example of such a deposit. The grain size of the deposit is coarser than for the deposits shown in Figures 4 and 5. Results obtained on cadmium layers of this type were found to be identical to those on cadmium layers produced from commercial plating baths.

Cadmium oxide layers were produced by evaporation and by electrophoretic deposition of cadmium oxide or by painting of cadmium oxide-binder compositions. Only the first technique was applied in the bulk electrolyte experiments. In this case AR-grade cadmium oxide powder was heated in an iridium crucible to temperatures of 1500°C in a controlled environment of 0.2 atm oxygen and 0.8 atm argon.[29] The resulting cadmium oxide vapors

were condensed on copper substrate foils of dimensions 2 x 0.5 cm.
Cadmium oxide layers of thicknesses 0.5 to 1μ were thus produced.
However, the adherence of these layers to electropolished copper
surfaces was poor and led to the use of as-rolled copper foils.
Figure 47 shows an optical micrograph of a 1μ cadmium oxide layer
at a magnification of 500X. The drawing lines of the copper foil
are clearly visible through the cadmium oxide layer. Figures 51
and 52 are electron micrographs at 30,000X of cadmium oxide layers
of 0.5 and 1μ thicknesses, respectively. One can clearly recog-
nize many cubic cadmium oxide particles with sizes ranging from
100 to 5000Å. The particles tend to form clusters in the thicker
cadmium oxide layer.

The self-contained hydrogen reference electrode[30] consists
of a platinized platinum wire sealed into a glass tube with one
open end. Filling of the capillary tube is accomplished with a
syringe or in vacuum. Hydrogen is then evolved on the wire such
that about one-half of the wire remains immersed in the electro-
lyte. The emerging part of the wire is covered with a thin film
of electrolyte[31] and allows the hydrogen reaction to occur at
high rates. Electrodes of this type have been used for periods
of weeks without the need for replenishing the hydrogen reservoir.

The counter electrode should fulfill the requirements of
inertness and low electrode impedance. Among the counter elec-
trodes considered and tested were $Cd/Cd(OH)_2$, platinum and palla-
dium-hydrogen counter electrodes. However, excessive dissolution
of the cadmium and trace dissolution of the platinum counter
electrodes led to the elimination of those two electrodes. The
palladium-hydrogen electrode, on the other hand, was found to be
inert and was used in all but the initial experiments in bulk
electrolyte.

Electrode Mounting

Electrical connection to the test electrodes was made by in-
serting a copper wire of 4 cm length through a hole in the copper

11

substrate foil and applying pressure to accomplish a cold weld.
The free end of the copper wire was inserted in a sleeve consisting
of split platinum tubing of 1 cm length. Platinum lead wire was
spot-welded to the platinum tubing and sealed into glass tubing.
The use of a sleeve enabled convenient exchange of test electrodes
as needed. The height of the electrolyte level was chosen such
that the rectangular test electrode was just completely immersed
with the side containing the cadmium layer facing the counter
electrode. The backside was covered with a thin layer of polystyrene.

The counter electrode consisted of a palladium wire of 10 cm
length and 1 mm diameter. It was spot welded to platinum lead
wire which in turn was sealed into glass. Before use, the counter
electrode was "charged" with hydrogen by evolving hydrogen on it
for several hours in an electrolysis cell filled with KOH. During
use such an electrode exhibits a potential of about 0.05 volts
versus the hydrogen reference electrode as long as hydrogen is
occluded by the palladium.

Solution Preparation

All experiments were carried out in KOH solutions from 0.1
to 6 N prepared from AR-grade KOH and doubly quartz-distilled
water. After preparation the solutions were carefully kept in an
oxygen and carbon dioxide free environment. After filling the
cell with fresh electrolyte, preelectrolysis was carried out over-
night with a copper electrode kept at a potential of 0 volts
versus hydrogen reference. All experiments in bulk electrolyte
were carried out at room temperature, that is about 25°C.

Experimental Procedure

After electrodepositing cadmium layers in the plating bath,
the electrodes were immediately rinsed in oxygen-free distilled
water and dried in a stream of nitrogen. After microscopic ex-
amination they were introduced into the cell with a reducing po-
tential applied. Likewise electrodes were always removed from the

cell while the potential of interest was being applied. Again
the electrodes were immediately rinsed in distilled water, dried
in nitrogen and subjected to microscopic examination. When not
in use, electrodes were stored in a dessicator continually purged
with nitrogen.

RESULTS AND DISCUSSION

Effect of Counter Electrode

When a section of a cadmium battery plate was used as the
counter electrode, the capacity of the test electrode was observed
to increase on continued cycling, in some cases beyond the theo-
retical capacity. Figure 8 shows the capacity as a function of
the number of cycles for a 1μ cadmium film in 1 N KOH. The
theoretical capacity of this film is 1.5 asec/cm^2. The initial
capacity amounts to only 2.5% of the theoretical value when cycling
with a current density of ±50 $\mu a/cm^2$ between limits of 300 and
-100 mV. During cycling the capacity decreases at first but then
increases continually. Extensive reduction leads to a doubling
of the discharge capacity and extensive oxidation leads to an
increase in the charge capacity by a factor of five. In contrast
to subsequent experiments, this experiment was performed without
the use of a nitrogen purged polyethylene bag and with non-
electropolished copper substrate foils.

Cycling of a 100Å cadmium layer in 1 N KOH with a cadmium
counter electrode leads to a complete redistribution of the original
layer on cycling. In fact, a part of the electrode surface inten-
tionally left as bare copper became covered with a cadmium layer
during cycling. As shown in Figure 9, the capacity of this elec-
trode decreases from a value close to the theoretical capacity of
15 ma sec/cm^2 to values of 4 ma sec/cm^2. Extensive reduction of
the electrode produces capacities more than three times larger
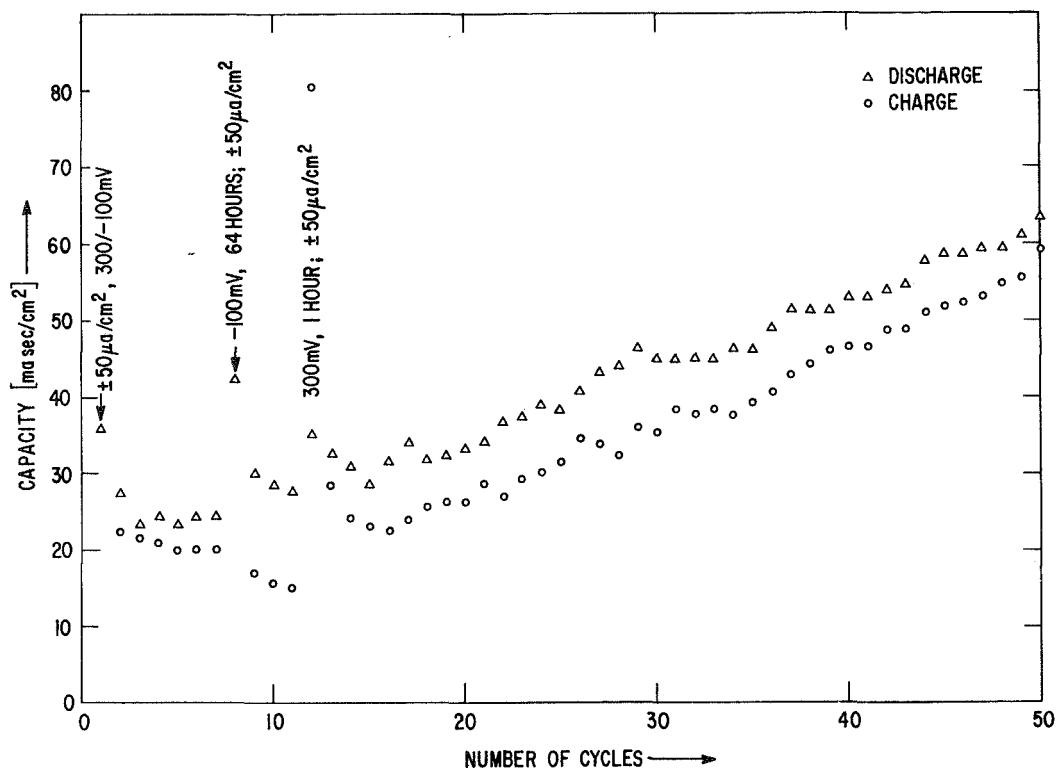than the theoretical value. At the same time the shape of the

13

Fig. 8 Capacity of a 1μ Cd film electrode in 1 N KOH vs. number of cycles, using a Cd counter electrode.
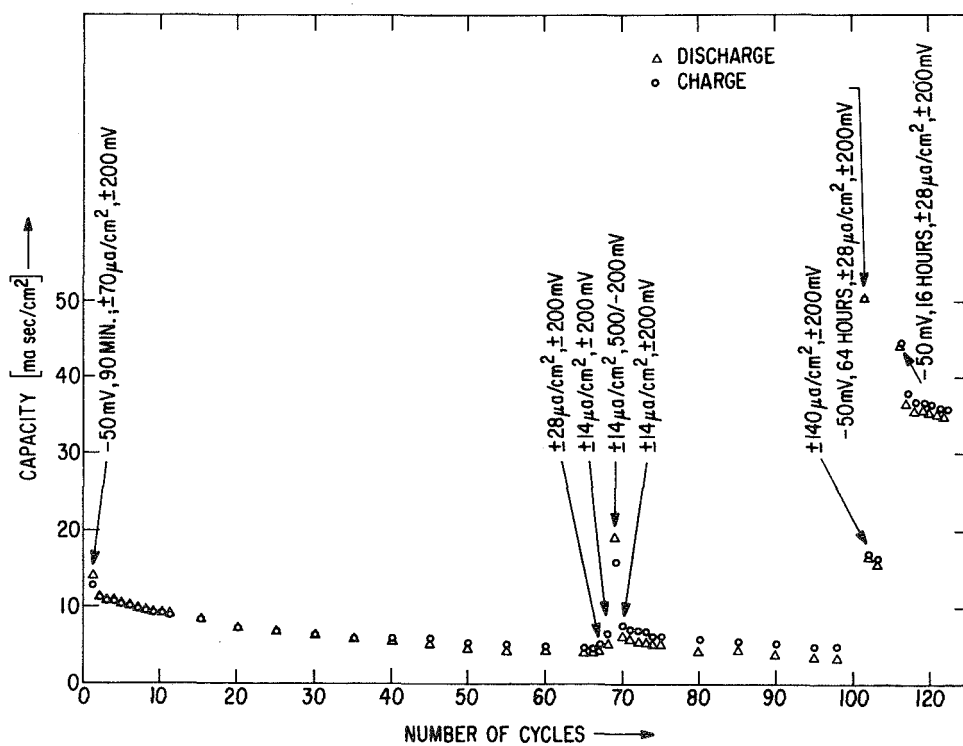

Fig. 9 Capacity of a 100Å Cd film electrode in 1 N KOH vs. number of cycles, using a Cd counter electrode.

14

charge and discharge curves remains essentially unaltered. This indicates that cadmium dissolves from the counter electrode and is deposited on the test electrode.

To prove this migration of soluble cadmium species, a bare copper foil was repeatedly charged and discharged in 1 N KOH against the cadmium counter electrode. The effect of cycling on the capacity of the test electrode is shown in Figure 10. Originally the capacity amounts to values of 0.2 to 0.3 ma sec/ cm^2. The charge and discharge of the double layer capacity of a metal electrode would only require 0.012 ma sec/cm^2 for a voltage swing of ±0.2 volts. Hence, the observed capacity values are too high to be associated with the double layer capacity. Since values of this order were also observed on copper electrodes in KOH solutions free of dissolved cadmiate ions, this capacity is probably a pseudo capacity due to hydrogen reacting with the copper surface. When potentials negative with respect to the $Cd/Cd(OH)_2$ potential are applied for several hours, the capacity rises to values as high as 3.6 ma sec/cm^2. This is undoubtedly due to the deposition of soluble cadmium species from the counter electrode. In fresh KOH and with a platinum counter electrode the effect is totally absent, and the capacity remains at values close to 0.2 ma/cm^2. A typical voltage-time or voltage-charge transient during the initial two cycles is shown in Figure 11. The lack of any voltage arrest close to the reversible $Cd/Cd(OH)_2$ potential is consistent with a copper surface free of cadmium layers during the initial cycle.

Capacity and Morphology on Cycling of Cd Electrodes in 6N KOH

Cycling of cadmium electrodes in 6N KOH leads to a profound decrease in capacity and to a drastic change in their morphology as well as their color. The loss of capacity on cycling is shown in Figure 12 for a cadmium electrode with a theoretical capacity of 80 ma sec/cm^2. Typical charge and discharge curves, obtained at a controlled current density of ±28 $\mu a/cm^2$ after extensive charging at -250 mV, are shown in Figure 13.
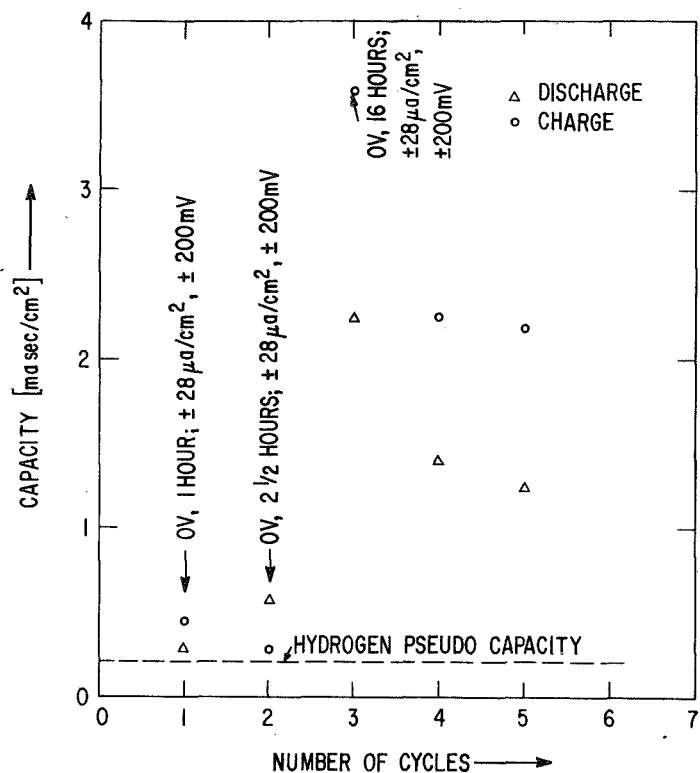
15

Fig. 10 Capacity of a bare Cu electrode in 1 N KOH vs. number of cycles, using a Cd counter electrode.
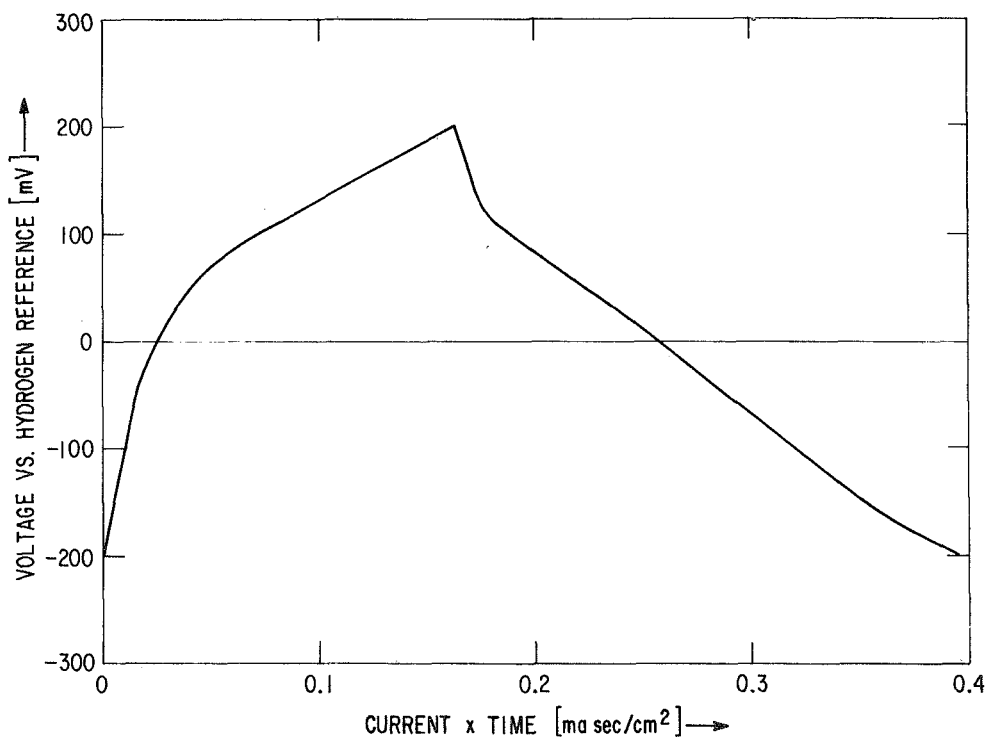

Fig. 11 Recorder trace of discharge (upward trace) and charge curve (downward trace) of same electrode applying ± 28 $\mu a/cm^2$; amount of charge passing through 1 cm^2 electrode area is plotted on abscissa.
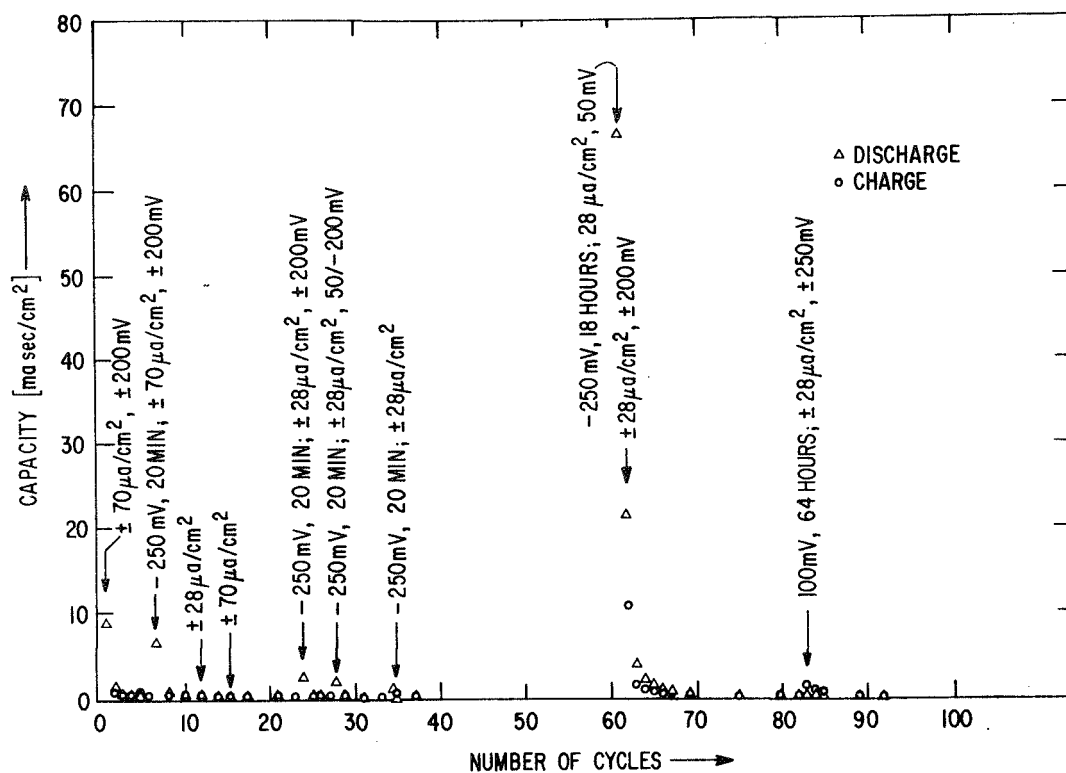
16

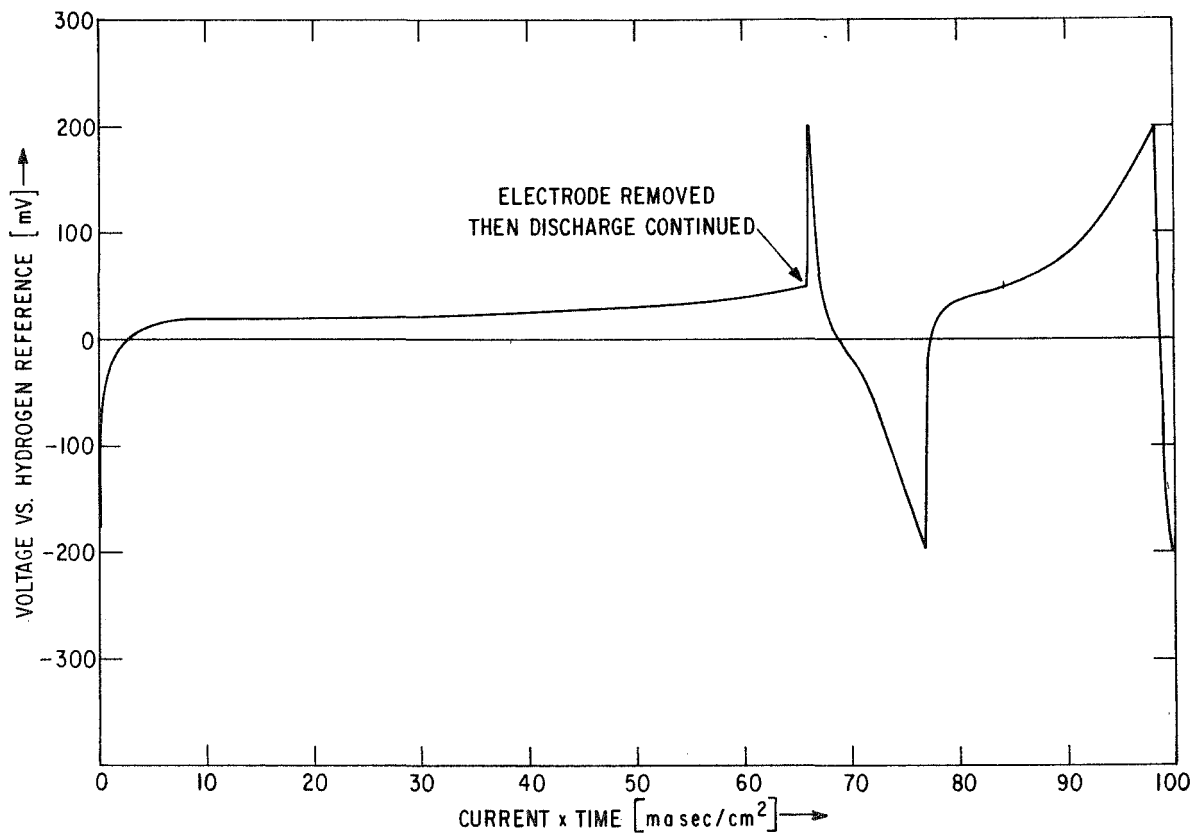Fig. 12 Capacity of a 540Å Cd film electrode (electrode 1) in 6 N KOH vs. number of cycles.

Fig. 13 Discharge and charge curves of 540Å Cd film electrode in 6 N KOH, applying ±28 μa/cm². Curves obtained after applying -250 mV for 18 hours and correspond to cycles 61, 62, and 63 in Fig. 12.

Electrodes were prepared by electroplating cadmium films on copper foils from KOH solution saturated with cadmium oxide at 86°C. The plating of "electrode 1" was performed at a controlled current density of -400 $\mu a/cm^2$ for 200 seconds. The charge equivalent of 80 ma sec/cm^2 corresponds to an average cadmium layer thickness of 540Å. Figures 14 and 15 show optical micrographs of the original copper substrate surface and of the cadmium layer at a magnification of 500X. The cadmium layer exhibits a platelet morphology similar to that obtained when plating from commercial cadmium cyanide baths.

The original discharge capacity of electrode 1 amounts to 9.1 ma sec/cm^2 which constitutes 11% of the theoretical capacity. Figure 12 shows that the capacity decreases to 0.6 ma sec/cm^2 during only 5 cycles with ±70 $\mu a/cm^2$. Prolonged charging, for instance at -250 mv for 20 minutes, produces increased capacity on subsequent discharge. However, within a few cycles very low values are again obtained.

The appearance of the cadmium deposit after plating is uniformly silverish to the bare eye. The low capacity values obtained on cycling are associated with a distinctly copperish appearance of the surface. Microscopic examination reveals isolated particles on an otherwise bare copper surface. The complete change in morphology after 60 cycles is shown in the photomicrograph in Figure 16 at a magnification of 500X.

Charging of the electrode at -250 mV for 18 hours results in a surface which appears silverish again to the bare eye. Microscopic examination shows that the surface is covered with a continuous cadmium film on top of which isolated cadmium particles persist. This is shown in the micrographs in Figures 17 and 18, obtained at magnifications of 500 and 1000X. On subsequent discharging to 50 mV with 28 $\mu a/cm^2$, a capacity of 67 ma sec/cm^2 is recovered which constitutes 84% of the theoretical capacity. The shape of this discharge curve is shown in Figure 13. Most of the discharge occurs at a potential very close to the Cd/Cd(OH)$_2$
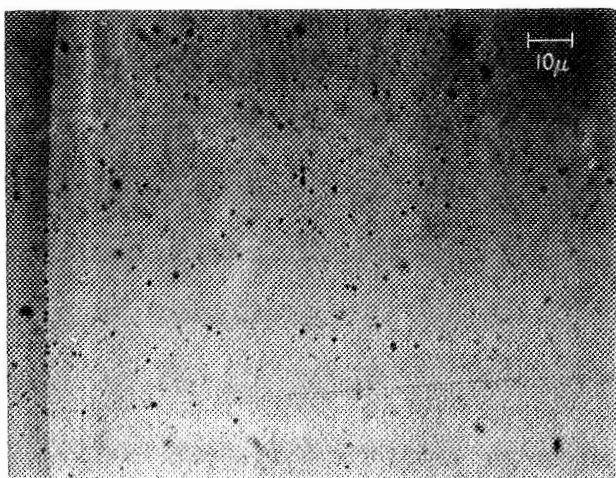
18

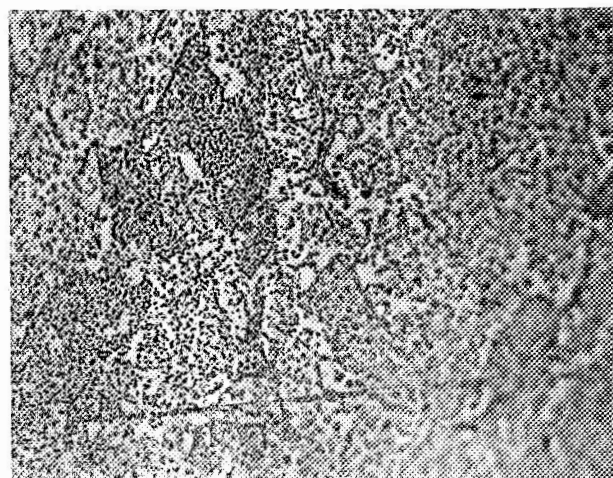Fig. 14. Optical micrograph at 500X of original Cu substrate (electrode 1).

Fig. 15. Optical micrograph at 500X of 540Å Cd film as electrodeposited (electrode 1). Same area as in Figure 14.
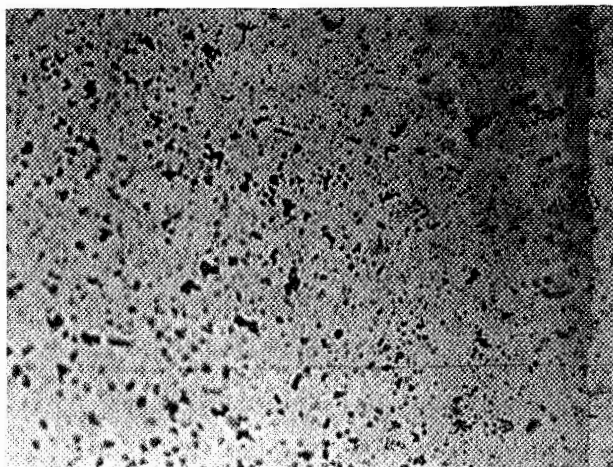

Fig. 16. Optical micrograph at 500X of electrode 1, after 60 cycles in 6N KOH. Same area.
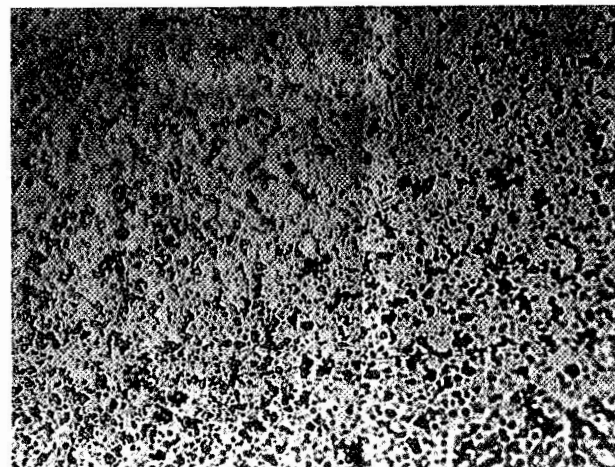

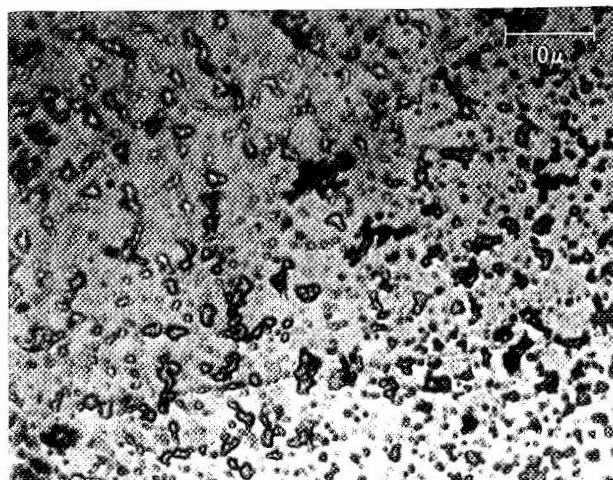Fig. 17. Optical micrograph at 500X of electrode 1, after applying -250 mV for 18 hours. Same area.

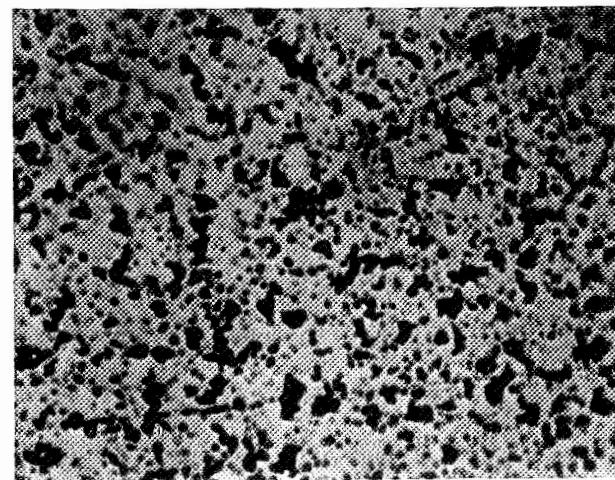Fig. 18. Same as Fig. 17, but at a magnification of 1000X.

Fig. 19. Optical micrograph at 1000X of electrode 1, after discharge with 28 $\mu a/cm^2$ to 50 mV. Same area as in Fig. 18.

19

equilibrium potential (19 mV vs. hydrogen reference electrode).
When a discharge voltage of 50 mV was obtained, the electrode had
a distinctly copperish appearance and was removed for microscopic
examination. Figure 19 shows a photomicrograph of the surface at
1000X. We note the existence of the same particles as after the
18 hour charge. However, these particles are separated by ap-
parently bare copper surface and the color of the particles has
changed from metallic gray to blue and brown. The fast rise in
potential on continued discharge (Figure 13) indicates some loss
of capacity due to oxidation of cadmium on exposure to air during
the microscopic examination.

Further cycling of the electrode leads to a drastic decrease
of the capacity as evidenced by the decreasing charge and discharge
times in Figure 13. After 82 cycles, values as low as 0.5 ma
sec/cm^2 are obtained (Figure 12) and the number and size of the
particles on the surface have decreased (Figure 20). Discharge
at 100 mV for 64 hours has only a small effect on the subsequent
charge capacity (Figure 12), and the number and size of particles
remain approximately the same (Figure 21). The discharge capacity
on continued cycling amounts to only 0.13 ma sec/cm^2. This is
about the same capacity as that of bare copper electrodes and in-
dicates that the particles remaining on the surface are largely
passivated. It is likely that the brown and blue color of the
particles is related to this passivation phenomenon.

Dissolution vs. Solid State Mechanism on Discharge in 6N KOH

The findings that cycling changes the silverish color of the
original cadmium deposit to a copperish appearance and according
to micrographs produces isolated cadmium particles on an other-
wise bare copper substrate, shows that extensive dissolution of
cadmium species must have occurred during cycling. The following
experiments were aimed at establishing how much cadmium dissolves
in the electrolyte during discharge and how much remains at the
surface after undergoing solid state oxidation. The experimental
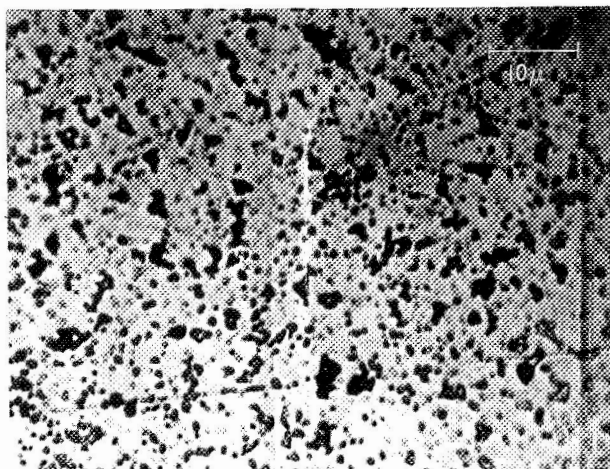procedure is outlined schematically in Figure 26. It consists of

Fig. 20. Optical micrograph at 1000X of electrode 1, after 82 cycles in 6N KOH. Same area.
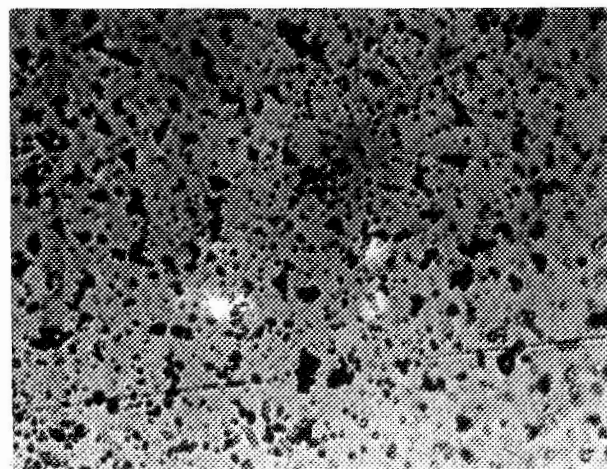

Fig. 21. Optical micrograph at 1000X of electrode 1, after applying 100 mV for 64 hours. Same area.
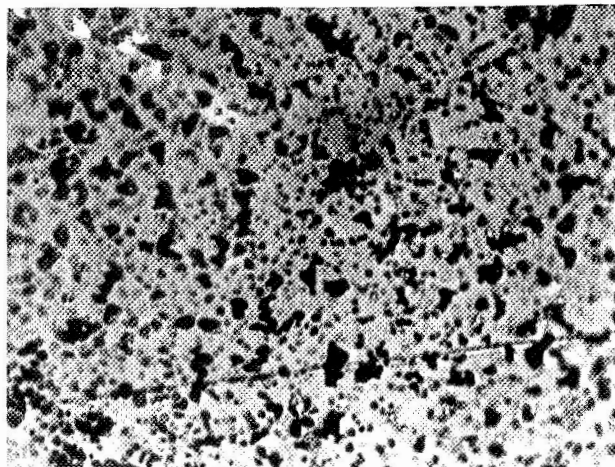

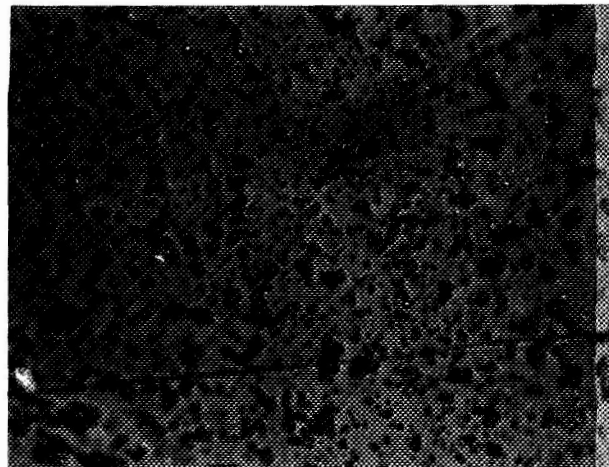Fig. 22. Optical micrograph at 1000X of electrode 1, after applying -250 mV for 4 hours. Same area.

Fig. 23. Optical micrograph at 1000X of electrode 1, after discharge with 28 $\mu a/cm^2$ to 50 mV. Same area.
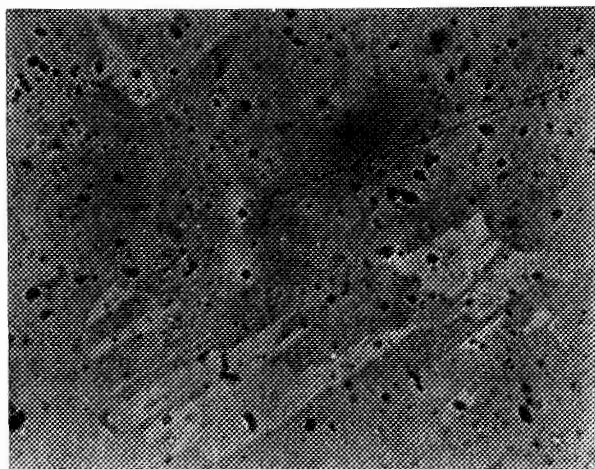

Fig. 24. Optical micrograph at 1000X of electrode 2, after applying -250 mV for 3 hours.
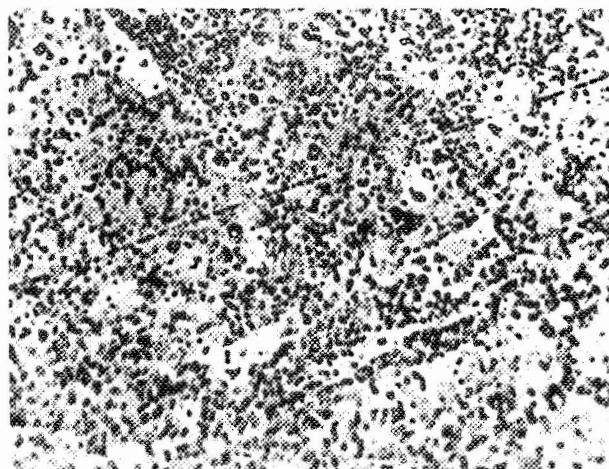

Fig. 25. Optical micrograph at 1000X of electrode 2, after applying -250 mV for 15 hours. Same electrode area as in Fig. 24.

21

the following five major steps:

a. Plate a known amount of cadmium (theoretical capacity) on a copper substrate (electrode 1) and determine its actual capacity on constant current discharge to 50 mV in fresh 6N KOH followed by extensive cycling and discharge at 100 mV.

b. Replace electrode 1 with a bare copper substrate (electrode 2) and plate the dissolved cadmium species by charging at -250 mV for 18 hours.

c. Replace electrode 2 with electrode 1 and reduce the cadmium species remaining on electrode 1 at -250 mV followed by determining its amount by constant current discharge to 50 mV.

d. Replace electrode 1 with electrode 2 and determine the amount of cadmium plated on electrode 2 by constant current discharge to 50 mV.

e. Replace electrode 2 with a bare copper substrate (electrode 3) and plate the cadmium species dissolved during the second discharge of electrode 1 and the discharge of electrode 2 by charging at -250 mV for 16 hours followed by determining the plated amount by constant current discharge to 200 mV.

The first block diagram in Figure 26a shows the total amount of 80 millicoulomb (mC or masec) cadmium originally plated on electrode 1 (signified by the area with the open circles to the left) and the KOH electrolyte, originally free of dissolved cadmium species, next to the electrode (signified by the blank area to the right). The second diagram in Figure 26a shows the amounts of unreacted cadmium, solid oxidized cadmium species ($Cd(OH)_2$, dark area) and dissolved cadmium species ($Cd(OH)_3^-$, area with broken lines) after cycling, extensive charge and finally constant current discharge to 50 mV. The charge equivalents of $Cd(OH)_2$ and $Cd(OH)_3^-$ add up to the measured discharge capacity of 67 mC which constitutes 84% of the theoretical capacity. The amounts of $Cd(OH)_2$ and $Cd(OH)_3^-$ are determined separately from the results obtained in steps d and e. The third diagram in Figure 26a shows the amounts of solid and dissolved oxidized cadmium species after
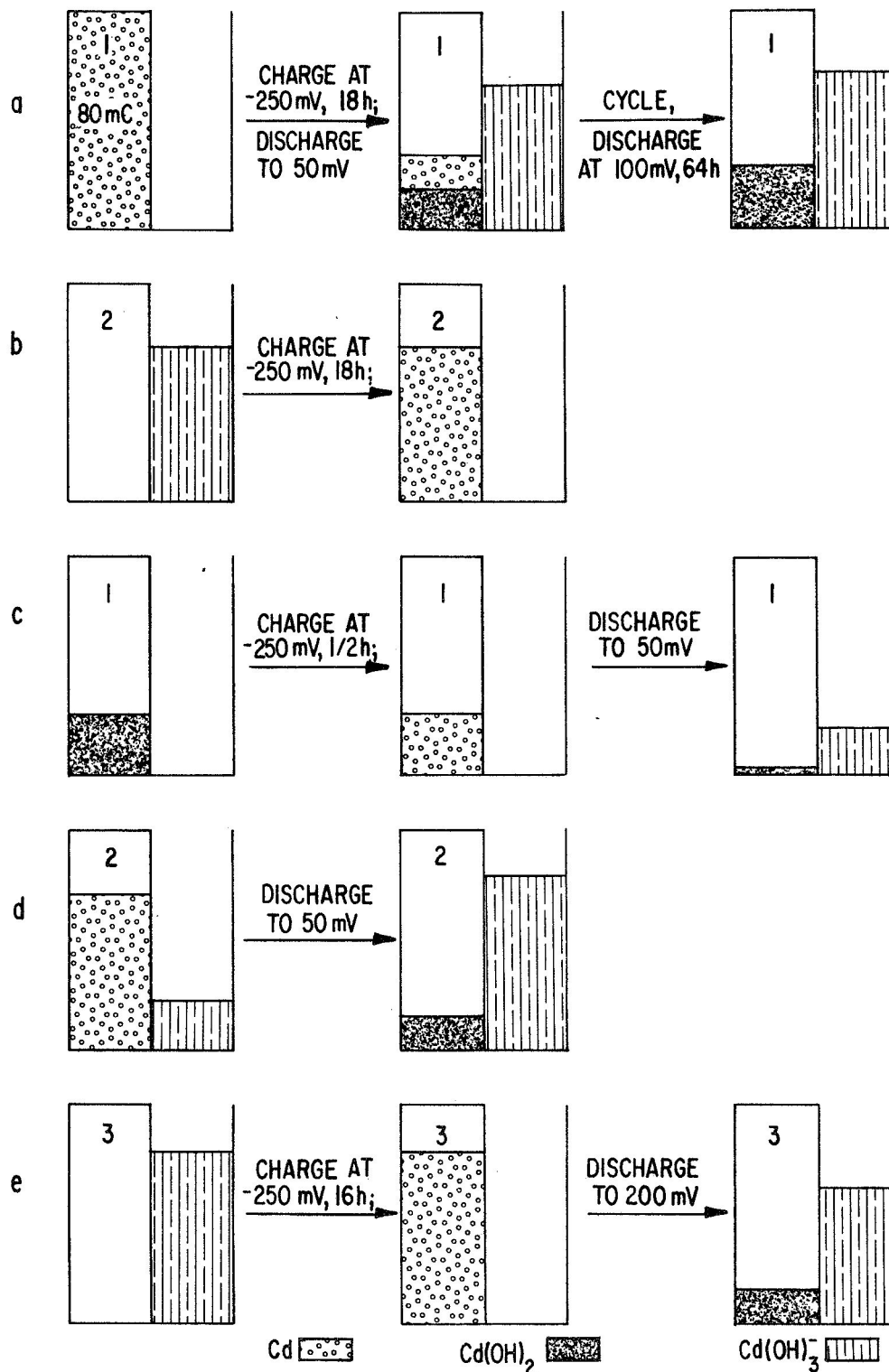
Fig. 26 Schematic of experimental procedure establishing amounts of cadmium species dissolving (Cd(OH)$_3^-$) vs. undergoing solid state oxidation (Cd(OH)$_2$). Height of shaded areas proportional to the charge equivalents (m coulomb) of Cd, Cd(OH)$_2$ and Cd(OH)$_3^-$.

extensive cycling and discharge at 100 mV. These amounts were determined from the measured discharge capacities of 56.9 mC for electrode 2 after plating and discharging (steps b and d) and 19.4 mC for electrode 1 after charging and discharging in cadmium-free KOH (step c). These two amounts add up to 76.3 mC and leave only 3.7 mC unaccounted for. With this maximum error one obtains a range of values of 56.9 to 60.6 mC for the dissolved oxidized cadmium species and 19.4 to 23.1 mC for the solid oxidized cadmium species as formed during the discharge of electrode 1 at 100 mV for 64 hours. These values are equivalent to 71-76% and 24-29% of the theoretical capacity.

The first two diagrams in Figure 26e demonstrate the plating onto electrode 3 of the cadmium species dissolved during the previous discharge of electrodes 1 and 2 (steps c and d). Constant current discharge of electrode 3 to 200 mV leads to a capacity of 60.4 mC. This constitutes 79% of the added capacities of electrodes 1 and 2 and, hence, sets a lower limit of 79% for the formation of dissolved cadmium species and an upper limit of 21% for the solid state oxidation of cadmium on discharge to 50 mV with a current density of 28 $\mu a/cm^2$.

It is of interest to examine the morphology of the cadmium deposits on electrodes 2 and 3. Figures 24 and 25 show the appearance of electrode 2 after applying -250 mV for 3 hours and 15 hours, respectively, at 1000X. The growth of a cadmium layer with platelet morphology is clearly evident. Figures 22 and 23 show the appearance of electrode 1 after reintroducing the electrode into the electrolyte when free of dissolved cadmium species (step c) and charging at -250 mV for 4 hours (Figure 22) followed by discharge to 50 mV (Figure 23). A comparison with Figure 21 shows that the number and size of the particles has changed only slightly. Figures 27 to 30 show optical micrographs at 1000X of electrode 3. Figure 27 shows the original copper substrate, Figure 28 the surface after 3 hours charging at -250 mV and Figure 29 the same area after 16 hours of charging. The plating of a cadmium film with platelet structure (dark areas represent thick cadmium layers, light areas thin cadmium layers) on the
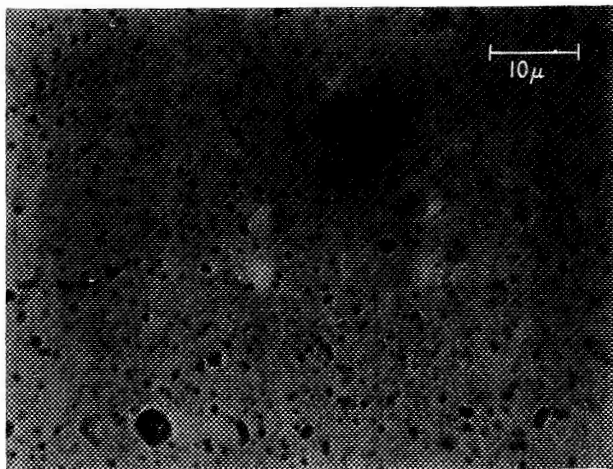
Fig. 27. Optical micrograph at 1000X of original Cu substrate of electrode 3.
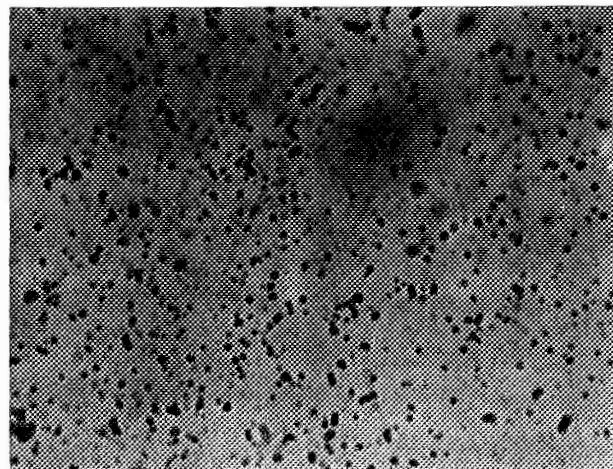

Fig. 28. Optical micrograph at 1000X of electrode 3 after applying -250 mV for 16 hours. Same area as in Fig. 27.
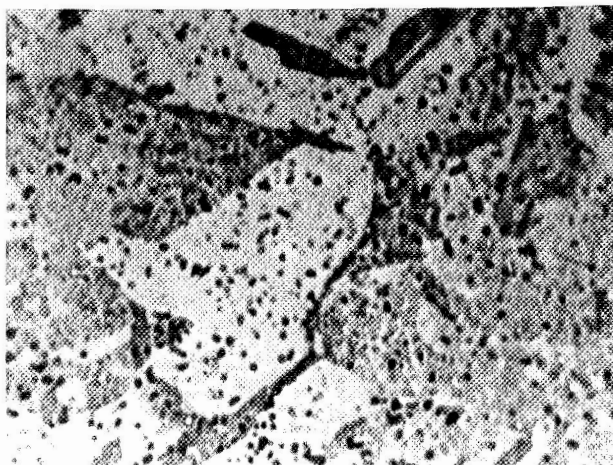

Fig. 29. Optical micrograph at 1000X of electrode 3 after applying -250 mV for 16 hours. Same area.
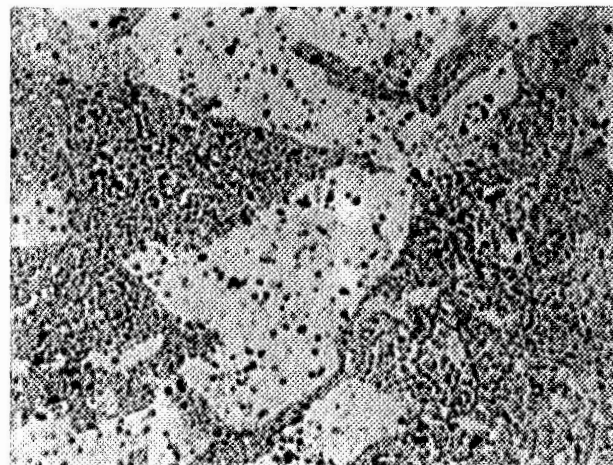

Fig. 30. Optical micrograph at 1000X of electrode 3 after discharge with 28 $\mu a/cm^2$ to 50 mV.
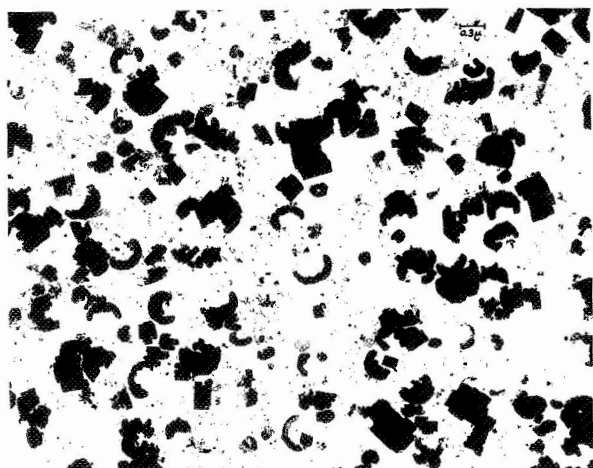

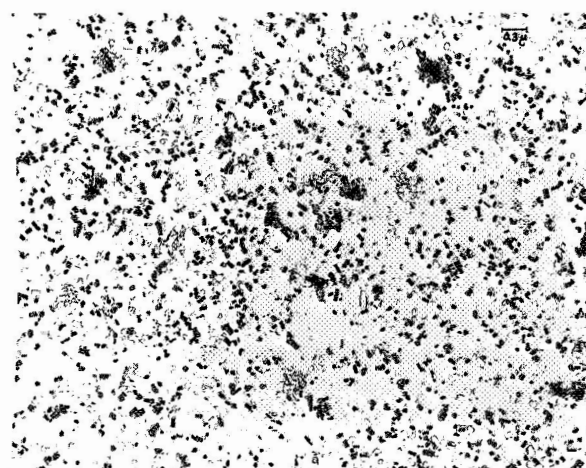Fig. 31. Electron micrograph at 30,000X of electrode 2, after discharge with 28 $\mu a/cm^2$ to 50 mV.

Fig. 32. Electron micrograph at 30,000X of electrode 3, after discharge with 28 $\mu a/cm^2$ to 50 mV.

25

originally bare copper is again clearly evident. Discharge of
this electrode to 50 mV results in the surface as shown in
Figure 30. The light areas now represent bare copper signifying
dissolution of cadmium from these areas.

As observed earlier on electrode 1, discharge and continuous
cycling produces a brown appearance of the particles left on the
surface. Electron micrographs were obtained to examine the crystal
habit of these particles. Figures 31 and 32 show electron micro-
graphs obtained at 30,000X of electrodes 2 and 3 after discharge
to 50 and 200 mV respectively. The existence of cubic crystals
suggests the formation of cadmium oxide which would account for
the observed passivation of the electrode.

Capacity and Morphology of Cd Electrodes in 1N KOH

The capacity of cadmium films on cycling in 1N KOH shows a
quite different behavior from that obtained on cycling in 6N KOH.
Figures 33 to 35 show the typical cycling behavior of three dif-
ferent electrodes with cadmium film thicknesses of 83 and 100Å.
These film thicknesses correspond to theoretical capacities of 12
and 15 ma sec/cm^2, respectively. The initial capacities amount
to 10% of the theoretical values when cycling with 150 mV limits,
to 20% when cycling with 250 mV limits and to 22% when cycling
with 500 mV limits. Loss of the capacity on cycling is found to
be much less pronounced than in 6N KOH. Also in contrast to 6N
KOH, extensive reduction has almost no effect on the capacity,
while oxidation with increasingly large anodic potentials results
in increased capacities on subsequent charge.

The shape of typical charge and discharge curves is shown in
Figure 36. The discharge curves look very much different from the
discharge curve in 6N KOH after extensive reduction but are similar
to the discharge curves on continued cycling in 6N KOH. After
exhibiting a potential arrest at about 40 mV, the curves enter a
straight-line portion. The rate of potential increase, dE/dt,
in this straight-line portion is proportional to the current den-
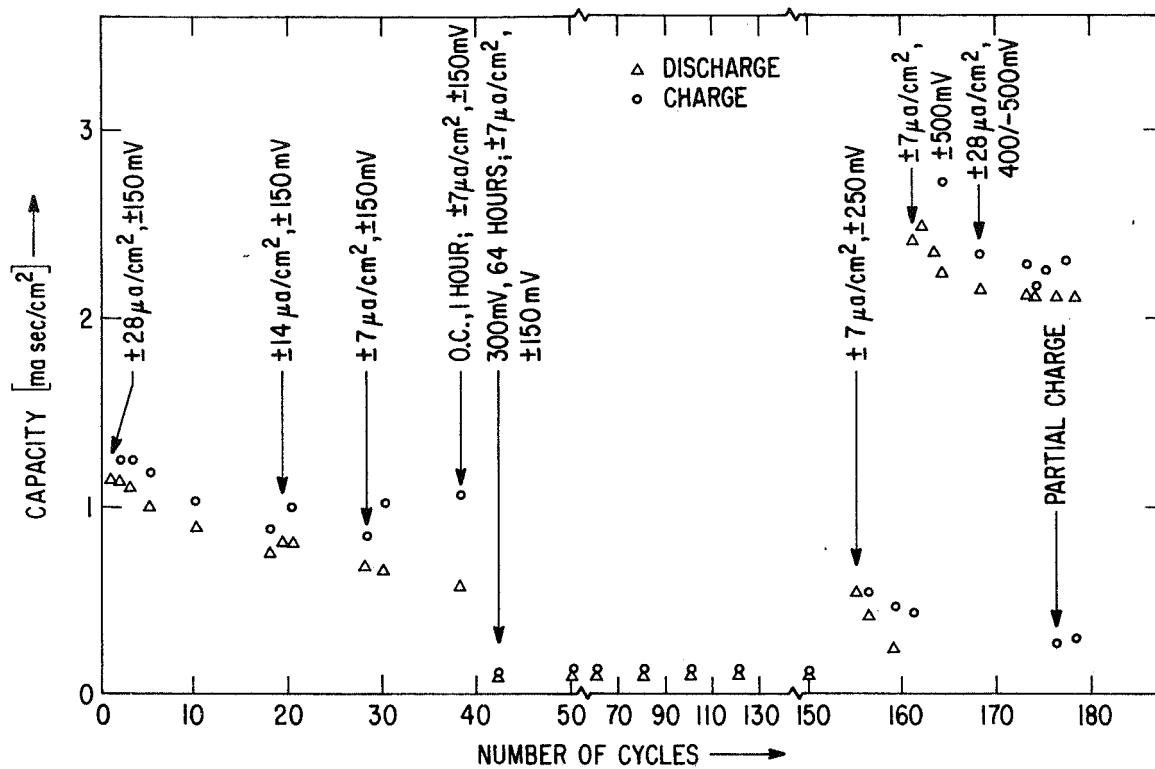sity and the slope dE/dQ is independent of current density. This

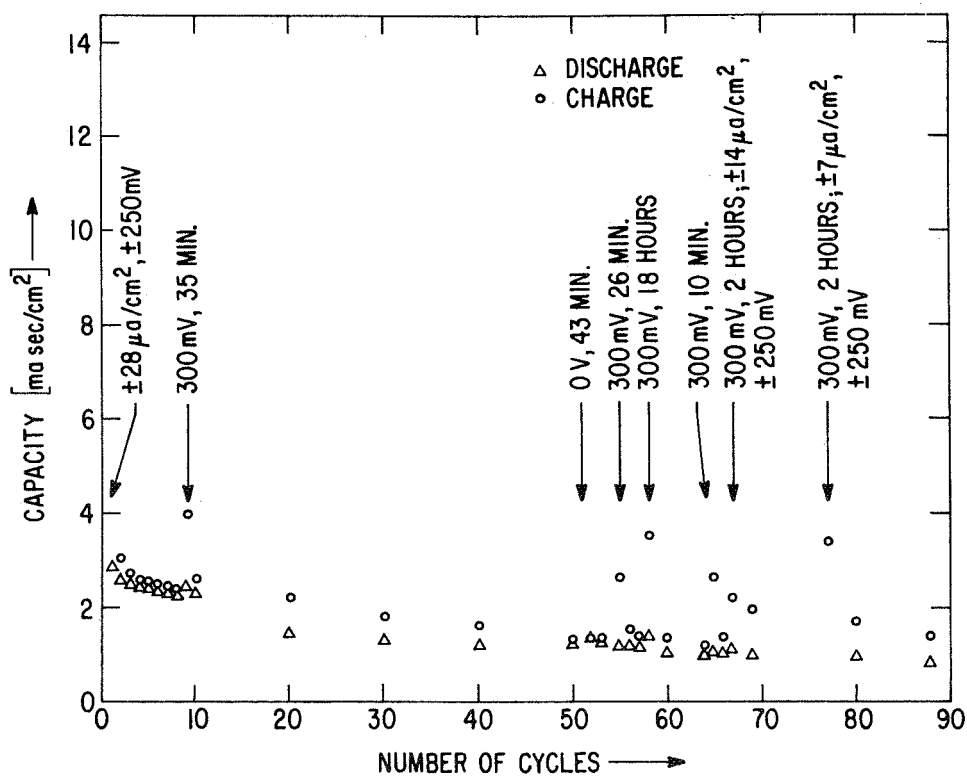Fig. 33 Capacity of a 83Å Cd film electrode in 1 N KOH vs. number of cycles.

Fig. 34 Capacity of a 100Å Cd film electrode in 1 N KOH vs. number of cycles.
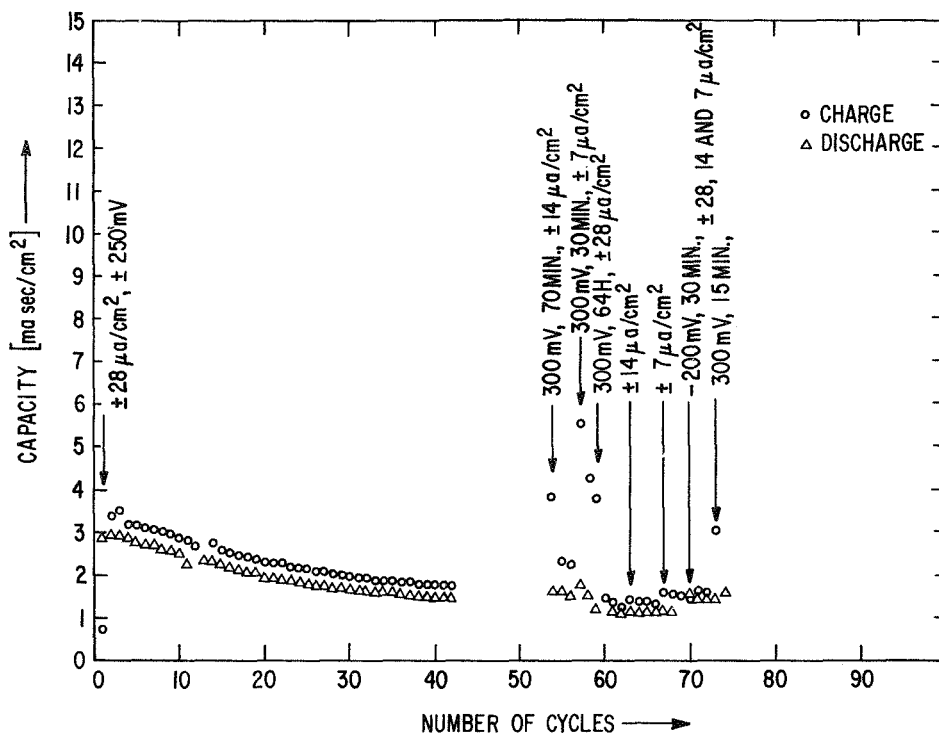
27

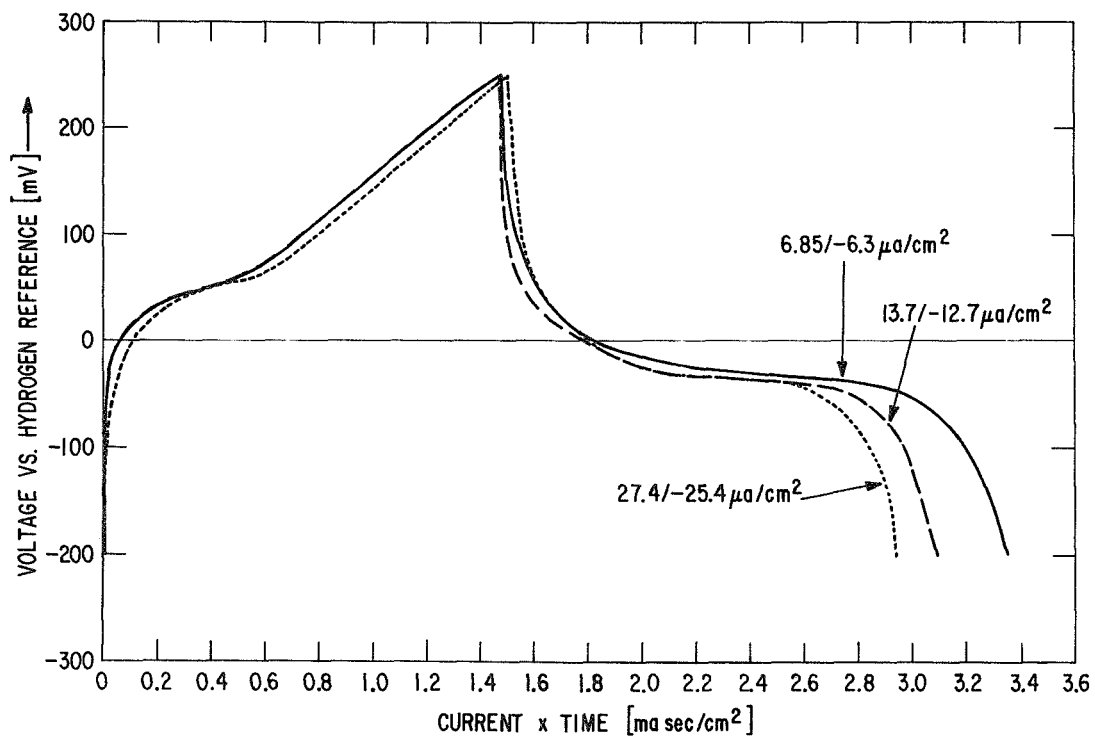Fig. 35 Capacity of a different 100Å Cd film electrode in 1 N KOH vs. number of cycles.

Fig. 36 Recorder traces of discharge and charge curves of a 100Å Cd film electrode in 1 N KOH with different current densities applied. Curves correspond to cycles 70, 71, and 72 of Fig. 35.

is a behavior which is typical for charging a capacitor and has been observed in the formation of monolayers of hydrogen and of oxide layers on noble metal electrodes. Figures 37 and 38 show that small changes in morphology on extensive cycling do, however, occur. Figure 37 shows a 100Å cadmium layer after electrodeposition and Figure 38 the same area of the electrode after 190 cycles, both at a magnification of 500X. Figures 5 and 7 show electron micrographs at 30,000X of a cadmium layer after deposition and of the 100Å cadmium layer, shown in Figure 38, after 190 cycles. It is seen that the pronounced platelet structure of the original cadmium deposit has become diffuse by extensive cycling.

The results obtained on the cycling behavior together with the microscopic observation suggest that in 1N KOH both a dissolution and a passivation mechanism determine the behavior of the cadmium electrode. Due to the smaller solubility of cadmium species in 1N KOH, the dissolution mechanism is much less significant than in 6N KOH.

Capacity and Morphology of Cd Electrodes in 0.1N KOH

The behavior of a 100Å cadmium film electrode on cycling in 0.1N KOH continues the trends observed when decreasing the electrolyte concentration from 6N to 1N. Figure 39 shows the effects of cycling on the capacity. Initially three different current densities are used for cycling, that is 28, 14 and 7 $\mu a/cm^2$. These current densities result in charge capacities of .47, .43 and .37 ma sec/cm^2. These values correspond closely to the charge equivalent of a monolayer of $Cd(OH)_2$, that is .48 ma sec/cm^2. In vast contrast to the case of 6N KOH, the application of cathodic voltages between 0 and -250 mV does not lead to higher discharge capacities, and the capacities during cycling remain essentially constant.

When the voltage limits are changed to +400 and -100 mV, the charge and discharge capacity increases and amounts to the equivalent of 3 to 3 1/2 layers of $Cd(OH)_2$. Within 80 cycles the

capacity decreases from 1.65 to 1.35 ma sec/cm^2. Immediately following discharge at 400 mV for 15 and 30 minutes, the charge capacity increases to values between 2.1 and 3.1 ma sec/cm^2. The latter value corresponds to 21% of the theoretical capacity.

Figure 40 shows recorder traces of charge and discharge curves. The latter do not exhibit any potential arrest, and their shape is independent of current density. This behavior was also observed in 1N KOH and reflects the absence of any significant dissolution of cadmium species.

After 195 cycles, the cadmium film electrode is removed from the cell for microscopic examination. Figure 41 shows a photo-micrograph of the original cadmium layer obtained at a magnifica-tion of 1000X. Figure 42 shows the same area after 195 cycles. To the bare eye the electrode looks identical before and after cycling, that is uniformly shiny and silverish. A comparison between Figures 41 and 42 shows that the major features of the cadmium film have not been changed by the cycling. The lack of changes in morphology and capacity on extensive cycling shows that dissolution of cadmium species is insignificant. This is in agreement with the known low solubility of cadmium species in 0.1N KOH.[6] On the other hand, the increase in charge capacity with increasingly oxidizing potentials suggests the formation of passivating layers and subsequent ionic transport through them.

Further evidence for this mechanism was accumulated by dis-charging the cadmium film electrode at various potentials between 100 and 400 mV for the same length of time. Figure 43 shows charging curves which were obtained with a current density of 14 μa/cm^2 after applying anodic voltages of 100, 200, 300 and 400 mV for 30 minutes. The charge capacities corresponding to these curves are plotted against the discharge voltages in Figure 44. The open circles relate to the curves in Figure 43, the solid circles correspond to another series of experiments obtained earlier on the same electrode. The lower curve in Figure 44 shows a retracing of a single actual discharge curve.
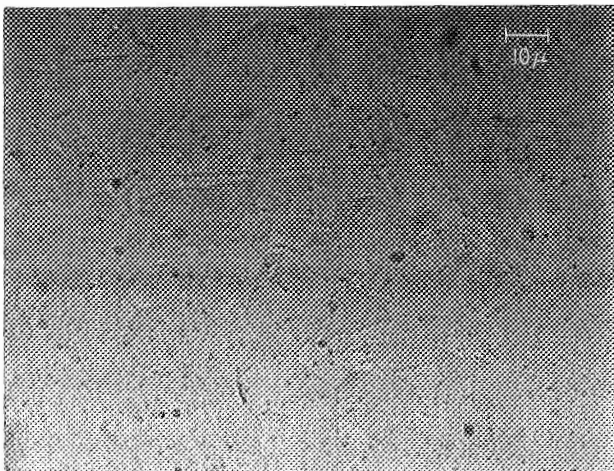
Fig. 37. Optical micrograph at 500X of 100Å Cd film as electrodeposited.
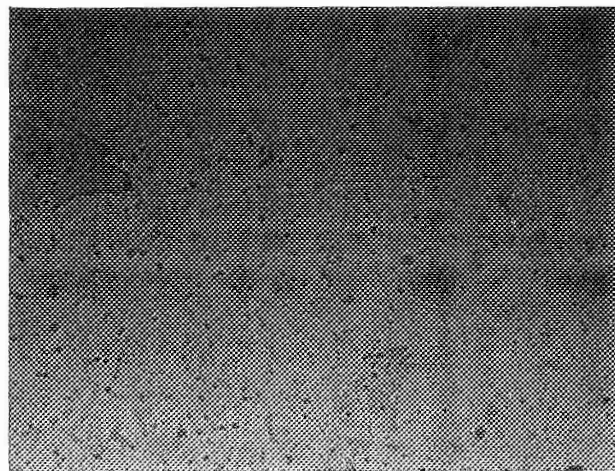

Fig. 38. Optical micrograph at 500X of same 100Å Cd film after 190 cycles in 1N KOH. Same area as in Fig. 37.
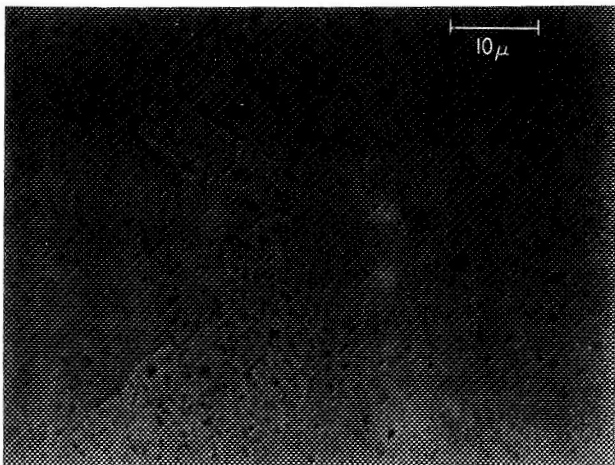

Fig. 41. Optical micrograph at 100X of 100Å Cd film as electrodeposited.
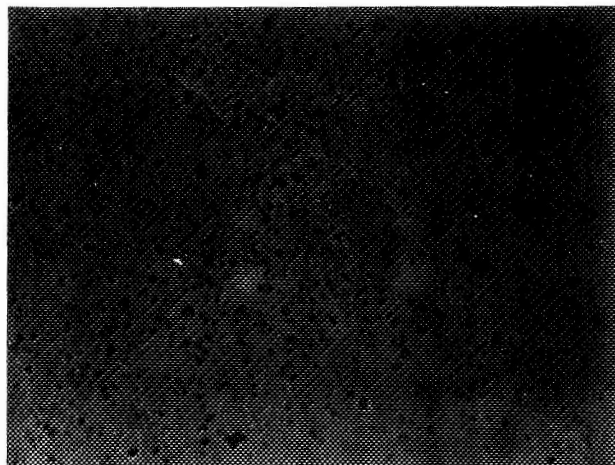

Fig. 42. Optical micrograph at 1000X of same 100Å Cd film after 195 cycles in 0.1N KOH. Same area as in Fig. 41.
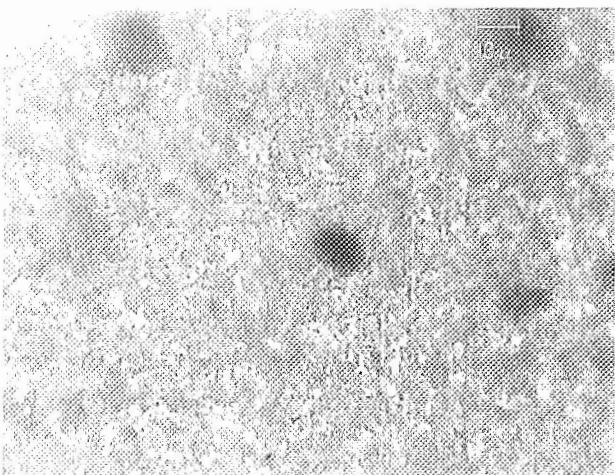

Fig. 47. Optical micrograph at 500X of 1µ CdO film as deposited on as-rolled Cu substrate foil.
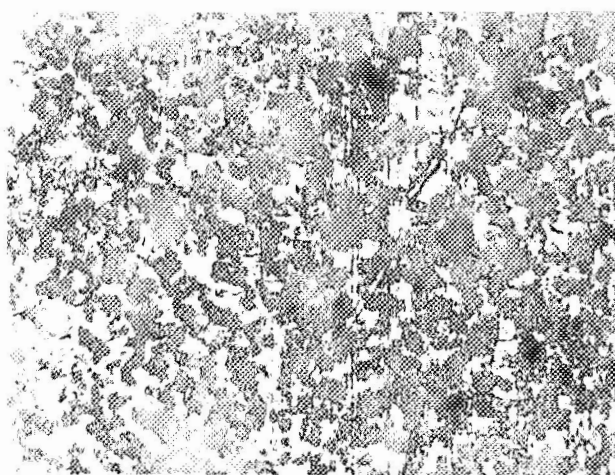

Fig. 48. Optical micrograph at 500X of 1µ CdO film after 1 cycle in 1N KOH. Same area as in Fig. 47.
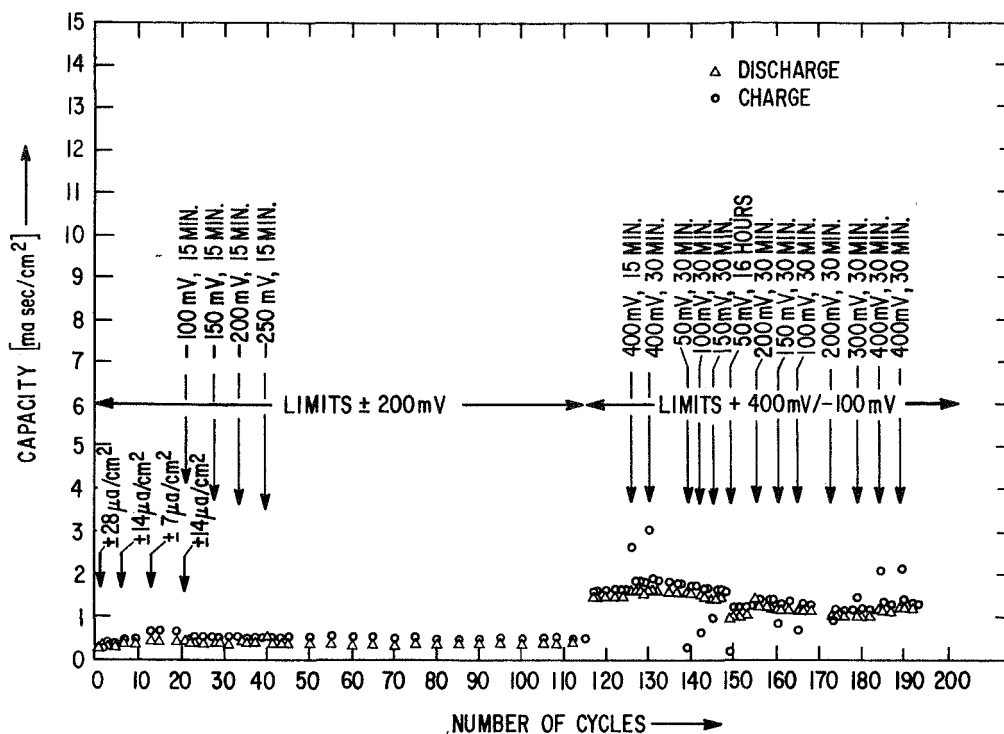
31

Fig. 39 Capacity of 100Å Cd film electrode in 0.1 N KOH vs. number of cycles.
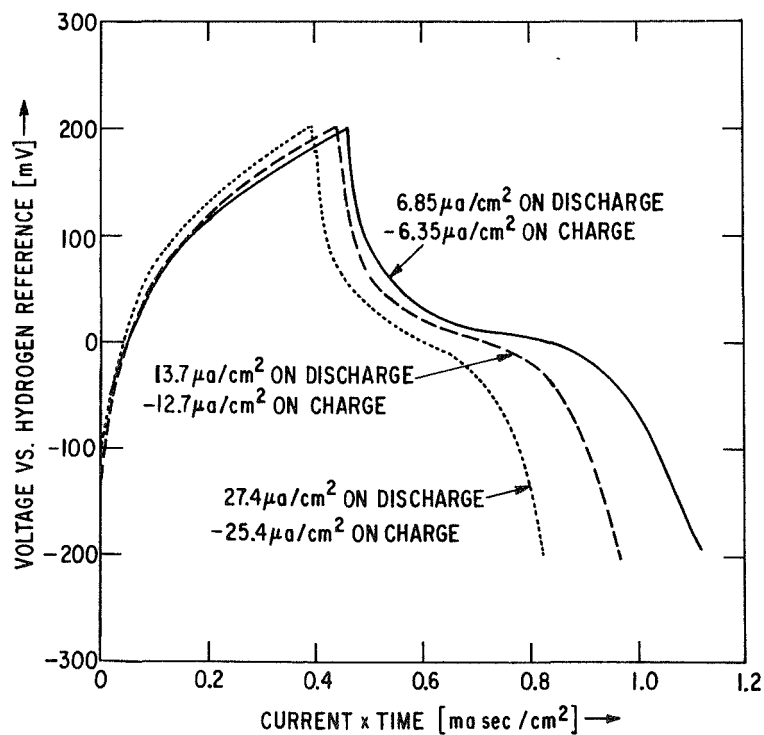
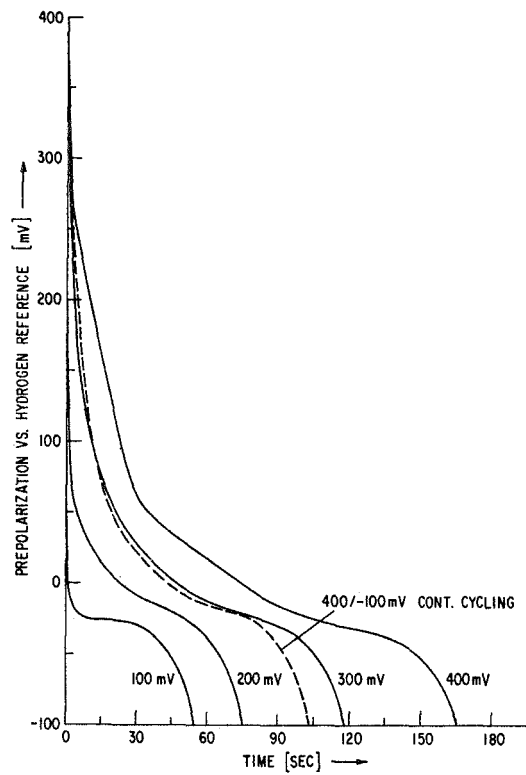Fig. 40 Recorder traces of discharge and charge curves of same electrode with different current densities applied. Curves correspond to cycles 4, 11, and 16 in Fig. 39.

Fig. 43 Voltage-time transients of 100Å Cd film electrode in 0.1 N KOH on charge with -14 μa/cm² after discharging at 100, 200, 300, and 400 mV for 30 minutes.

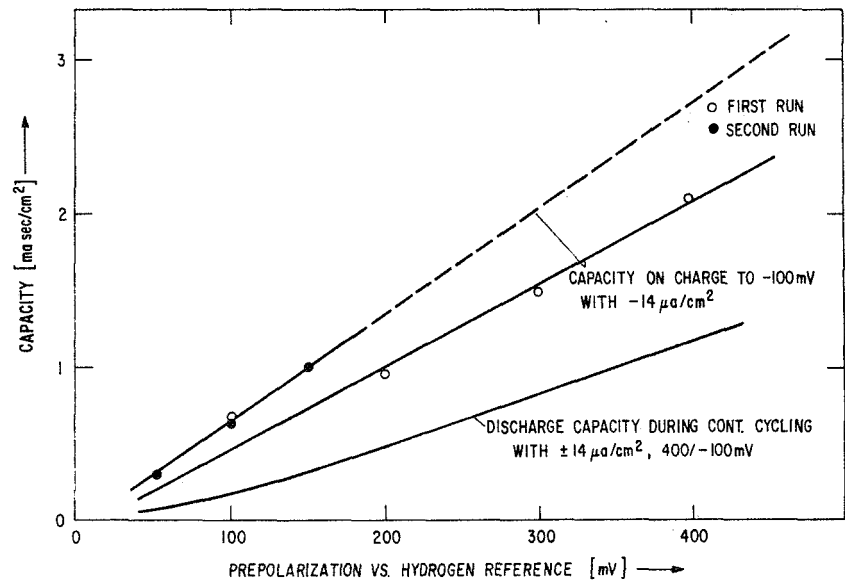Fig. 44 Capacity of 100Å Cd film electrode in 0.1 N KOH on charge with -14 μa/cm² to -100 mV vs. discharge voltage.

33

All three curves can be quite well represented by straight lines. This behavior is actually that expected for a solid state transport mechanism. The charge capacity is proportional to the film thickness, and a passivating film with constant conductivity throughout requires a constant electric field (volts/cm thickness) for its growth at constant current. The fact that the individual discharge curve in Figure 44 lies below the two charging curves is due to the much shorter time (only 100 seconds) available for the formation of the passivating film. In additional experiments it was shown that extending the time of discharge beyond 30 minutes increases the layer thickness but slightly. Thus, the charge capacities shown in Figure 44 represent values close to the equilibrium thickness of the passivating layer.

Figure 43 shows that the shape of the charging curves changes gradually as the discharge voltage increases. The charging curve following a discharge at 100 mV for 30 minutes indicates that only one species, probably $Cd(OH)_2$, is being reduced. However, the charging curve obtained after discharge at 400 mV for 30 minutes consists of several distinct parts. This indicates that more than one cadmium species is being reduced.

Capacity and Morphology of CdO Electrodes in 1N KOH

The cycling behavior of electrodes consisting of evaporated cadmium oxide layers on copper in 1N KOH was found to be quite different from that of cadmium layers in 1N KOH. The capacities on cycling for two electrodes with 1μ cadmium oxide layers are shown in Figure 45. The initial capacities of these two electrodes amount to only 3 and 5% of the theoretical value (calculated under the assumption of a 50% dense layer). In contrast to the behavior of cadmium films in 1N KOH, a drastic loss of capacity is observed during the initial ten cycles. Also in contrast to cadmium films in 1N KOH, the discharge capacities increase by one order of magnitude when reduced at 0 volts versus hydrogen reference for short periods of time. This different behavior is probably due to the much larger surface area of the cadmium oxide electrodes
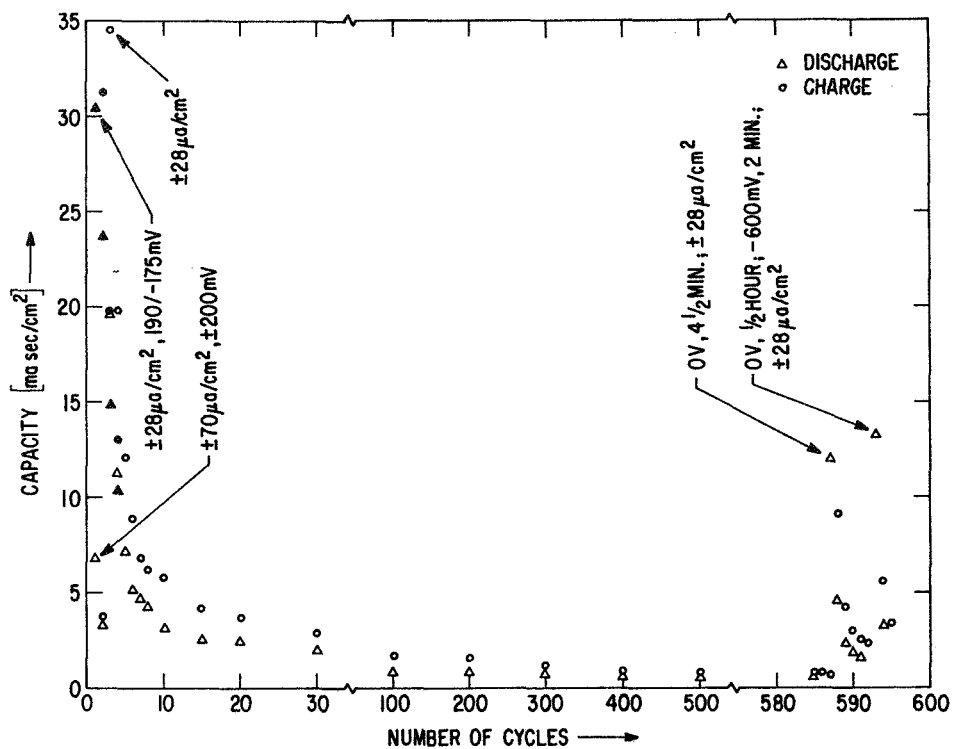
Fig. 45 Capacities of two 1μ CdO film electrodes (filled-in and open symbols) in 1 N KOH vs. number of cycles.
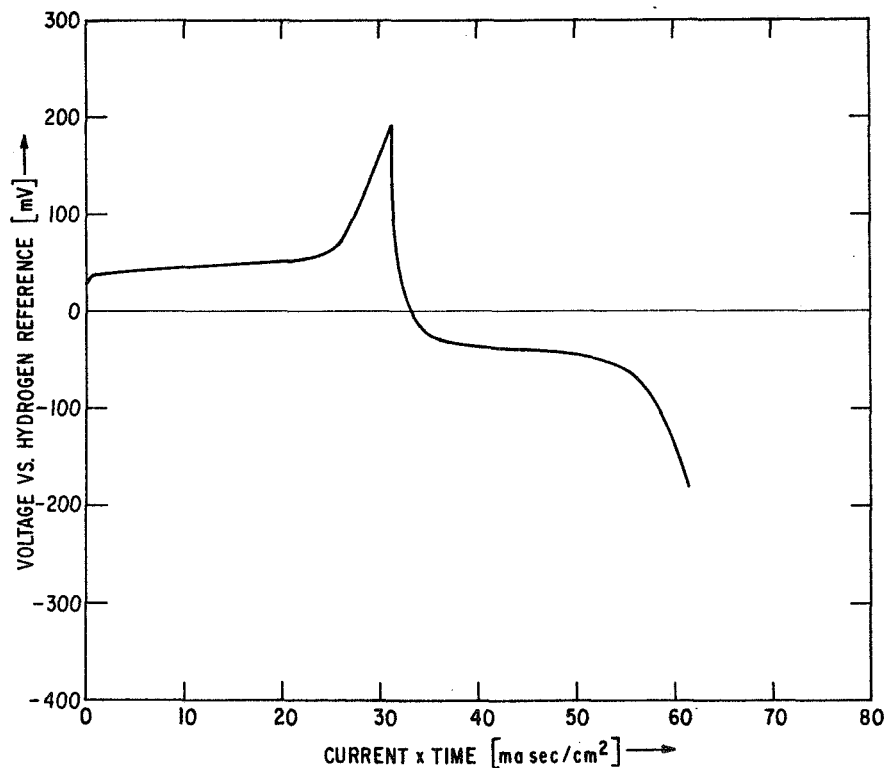

Fig. 46 Recorder trace of discharge and charge curve of 1μ CdO film electrode, applying current density of ±28 μa/cm². Curves correspond to 1st discharge and 2nd charge of electrode with filled-in symbols in Fig. 45.

which enhances dissolution. In this respect the results are there-
fore similar to those obtained on cadmium films in 6N KOH. The
charge and discharge curves exhibit well defined potential arrests.
Figure 46 shows the first constant current discharge and charge
of the electrode characterized by the filled-in symbols in
Figure 45. It is seen that charge and discharge proceed to the
largest extent at voltages of $\pm$50 mV versus hydrogen reference,
that is, near the $Cd/Cd(OH)_2$ equilibrium potential.

The drastic change in capacity on cycling is accompanied by
a pronounced change in the morphology. Figure 47 shows a photo-
micrograph of the cadmium oxide after deposition on the copper
substrate foil at a magnification of 500X. Figures 48, 49, and
50 were obtained on the same electrode after 1, 50 and 500 cycles,
respectively. The dramatic loss of active material from the
electrode is evident. However, the resolution of the photomicro-
graphs is insufficient to resolve the shape and size of individual
particles. Hence electron micrographs of particles stripped from
the surface were obtained. Figures 51 and 52 show electron micro-
graphs of cadmium oxide particles stripped from the as-prepared
cadmium oxide electrode at a magnification of 30,000X. The cubic
cadmium oxide particles range in size from 100 to 2000Å and are
slightly larger for the cadmium oxide layer shown in Figure 52
which was obtained after longer times of evaporation. Figure 53
shows a micrograph of particles stripped from the surface after
the electrode had been oxidized at 300 mV for one hour. As com-
pared to Figures 51 and 52, there is no dramatic increase in
average particle size. However, as expected, a large number of
hexagonal $Cd(OH)_2$ particles are evident from comparing Figure 54
with Figures 51 to 53. The electron micrograph in Figure 54 cor-
responds to the photomicrograph in Figure 48. The pronounced loss
of capacity during the very first cycle is undoubtedly caused by
the observed increase in particle size. The loss of capacity during
later cycles is most likely caused by the gradual loss of active
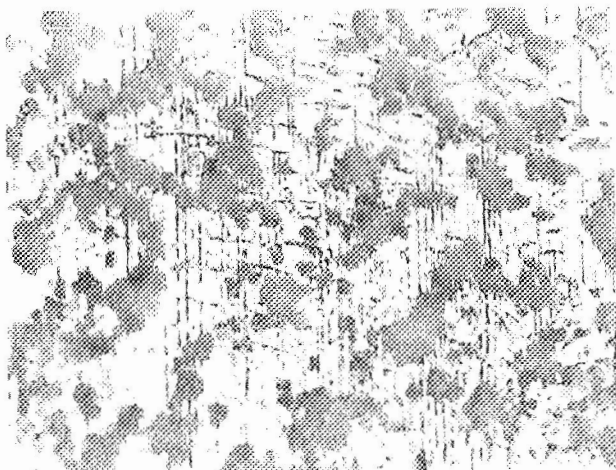material from the electrode evidenced by Figures 49 and 50.

36

Fig. 49. Optical micrograph at 500X of 1μ CdO film after 50 cycles in 1N KOH.
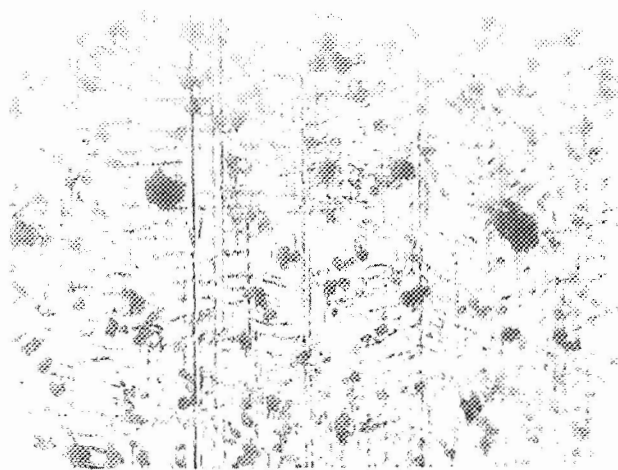
Fig. 50. Optical micrograph at 500X of 1μ CdO film after 500 cycles in 1N KOH.

Fig. 51. Electron micrograph at 30,000X of particles stripped from surface of as-deposited 0.5μ CdO film.

Fig. 52. Electron micrograph at 30,000X of particles stripped from surface of as-deposited 1μ CdO film.

Fig. 53. Electron micrograph at 30,000X of particles stripped from surface of CdO film electrode after exposure to 1N KOH at 300 mV.
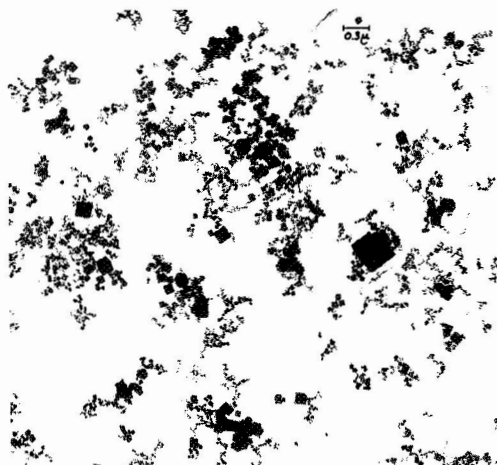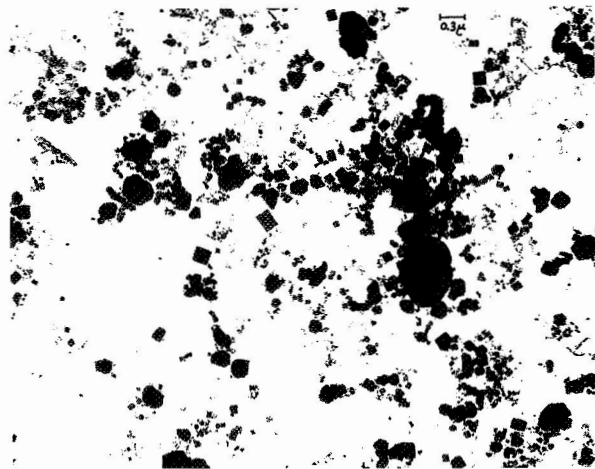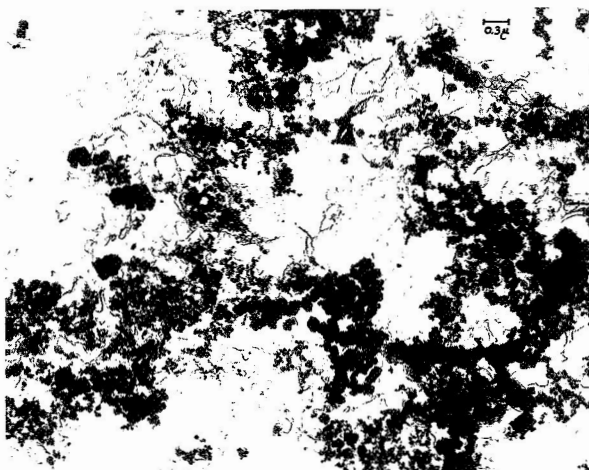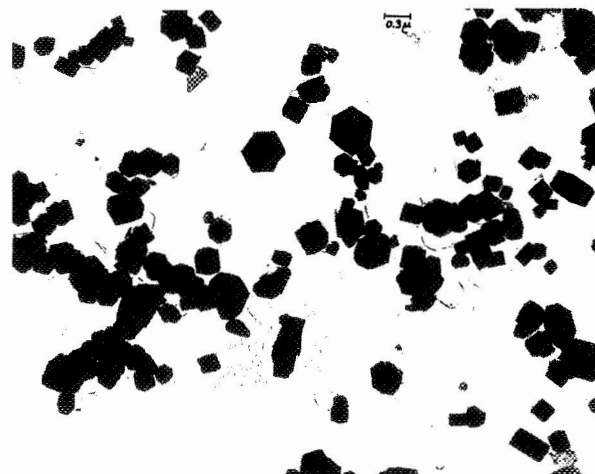

Fig. 54. Electron micrograph at 30,000X of particles stripped from surface of CdO film electrode after 1 cycle in 1N KOH.

EXPERIMENTAL

Overall Arrangement

The film electrolyte experiments were carried out in a cell positioned on the stage of a Leitz Ortholux microscope to allow examining changes in the electrode morphology during charge and discharge. Figure 55 shows an overall view of the experimental arrangement. The microscope stage is enclosed in a polyethylene bag, continually flushed with nitrogen, to reduce effects due to the diffusion of oxygen and carbon dioxide into the cell. The carbonate concentration accumulating in the cell during the maximum duration of an experiment was determined by analysis as 0.13 moles of K_2CO_3 per liter of 6N KOH. The in-situ microscopic studies were performed with dark field lenses to eliminate unwanted reflections from the glass plate covering the cell. Dark field viewing was complemented by bright field examinations of the electrode surface before and after experimental runs. A Polaroid camera was used to obtain optical micrographs.

The electronic instrumentation was essentially identical to that used in the bulk electrolyte studies. Special attention had to be paid to minimizing the electronic noise in the system by proper grounding and shielding because of the low level of the currents to be measured. The small currents also necessitated the use of a high impedance voltmeter between the recorder and the cell terminals.

Cell Design

The experiments were performed in a Lucite cell of outer dimensions 3 x 3 cm by 0.6 cm thick. A photograph of the cell is shown in Figure 56 and a cross section of the cell in Figure 57. The counter electrode is contained in a well of dimensions 2 x 2 cm by 0.3 cm deep. It consists either of a palladium foil or of a
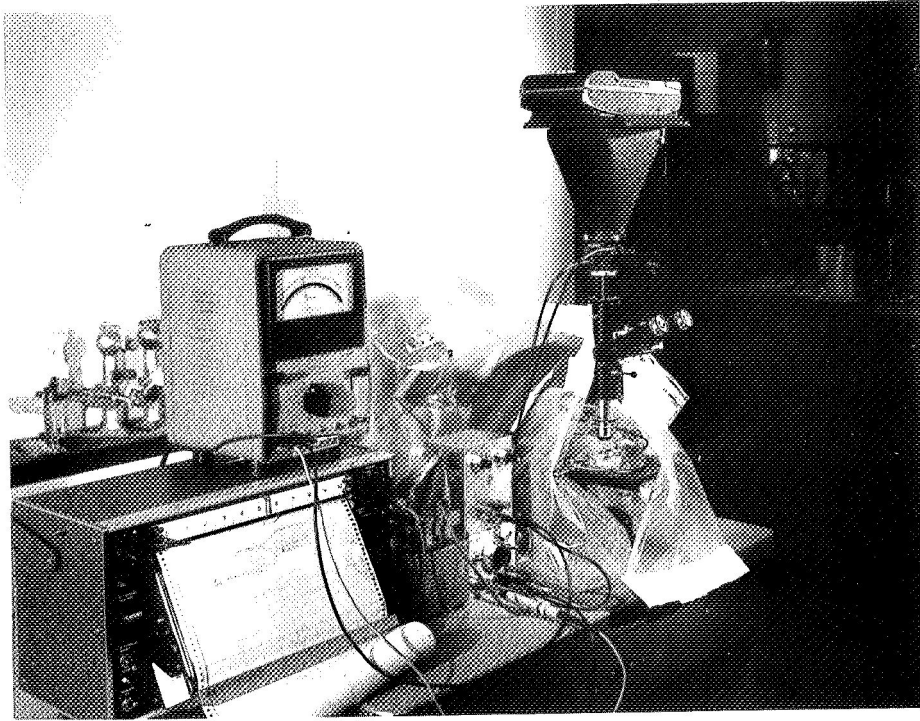
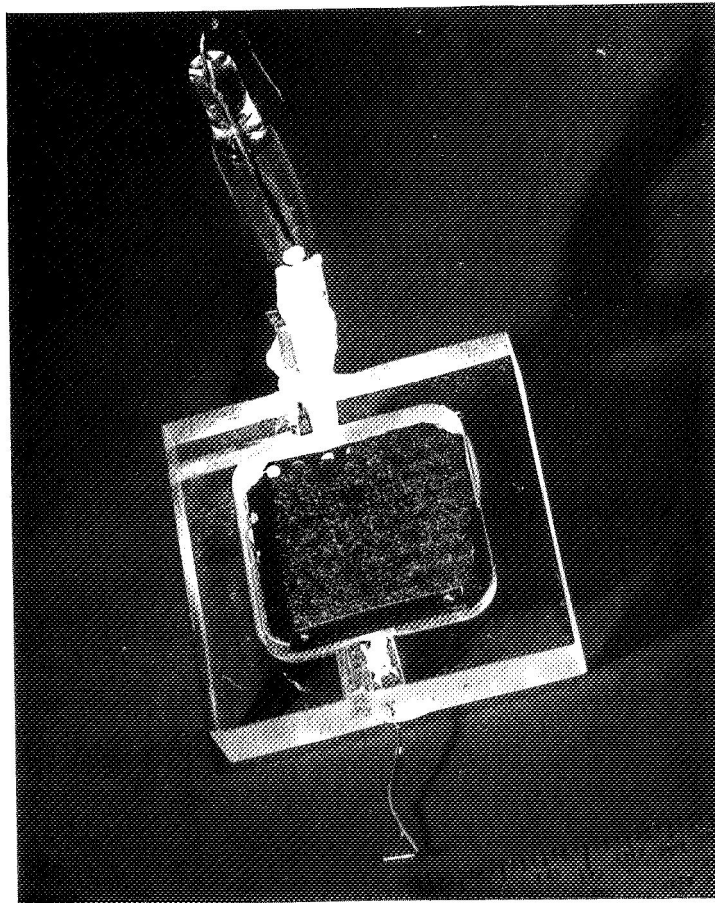Fig. 55. Overall view of arrangement for film electrolyte study.

Fig. 56. Electrolytic cell used for film electrolyte study.

section of a nickel hydroxide battery plate. The reference electrode is a self-contained hydrogen electrode as described earlier. It communicates with the electrolyte in the well via a capillary with a 1 mm opening. The opening is located at a distance of 1-2 mm from the test electrode. The latter consists of a copper strip of 1 mm width, 10 mm length and 0.13 mm thickness. A cadmium oxide layer of dimensions 1 x 1 mm and a few micron thickness is deposited on the end of the copper strip adjoining the well. Epoxy resin (Shell Epon 828) is used to cement the test electrode into the cell housing in such a way that its upper surface is flush with the top of the Lucite cell housing. A spacer of silicone rubber or polyethylene covers the entire rim of the cell housing except for the 1 x 1 mm layer of cadmium oxide on the copper strip. A glass cover consisting of a microscope slide with 0.25 mm thickness is placed upon the spacer. Thus the spacer thickness determines the thickness of the electrolyte film covering the test electrode.

Electrode Preparation

In all but a few cases, test electrodes were prepared by electrophoretically depositing a cadmium oxide-binder composition on the copper substrate strips. The copper strips were cut from large specimens of electropolished copper foil. The strips were then amalgamated to further reduce the evolution of hydrogen during cathodic experiments. The evolution of even small amounts of hydrogen interferes with the microscopic examinations due to entrapment of bubbles between the test electrode and the glass cover. Electrophoretic deposition resulted in cadmium oxide layers which were even and uniform down to thicknesses of a few microns. In the few cases where cadmium oxide layers much thicker than 10μ were required, a cadmium oxide-binder composition was brushed on the copper strip. Finally, electrodes were prepared for a few experiments by electrodepositing cadmium layers from a commercial plating bath in the same way as in the bulk electrolyte studies.

REF. ELECTRODE

TEST ELECTRODE

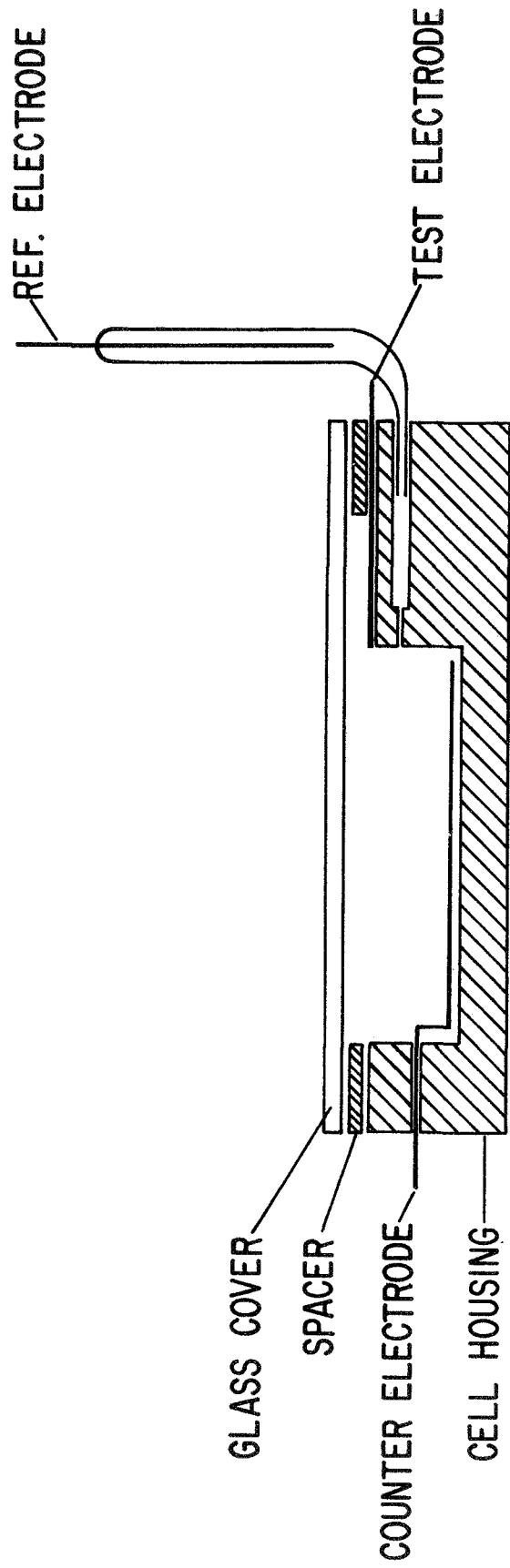GLASS COVER

SPACER

COUNTER ELECTRODE

CELL HOUSING

Fig. 57 Cross section of electrolytic cell.

The cadmium oxide-binder compositions were prepared by ball-milling a mixture of cadmium oxide, polyvinylidene fluoride binder (PVF) and dimethyl acetamide solvent (DMA). For the brushing technique, a mixture of 12 parts CdO, 1 part PVF and 11 parts DMA by weight was applied. For the electrophoretic deposition, a mixture of 4 parts CdO, 0.33 parts PVF and 21 parts DMA by weight was ball-milled and 10 parts DMA and 0.1 part $Cd(NO_3)_2 \cdot 4H_2O$ added subsequently. Electrophoretic deposition of cadmium oxide was accomplished at room temperature in a cell containing a platinum anode and the copper substrate foil as the cathode. It was found that magnetic stirring of the bath before plating resulted in layers of the best quality. Typically the application of a voltage of 100 volts for 20 seconds led to a cadmium oxide layer thickness of about 5μ. After deposition of the cadmium oxide layer, the test electrode was removed from the bath and immediately dried in a stream of nitrogen. The test electrodes were then cemented into the cell housing using epoxy in the way described above.

The porosity and the theoretical capacity of the cadmium oxide layers were calculated from experimental determinations of the film thickness and the weight of the cadmium oxide (+ binder) deposit. The former was done microscopically at a magnification of 500X with an error of ±0.3 to 0.4μ. The latter was done by weighing a copper strip with the cadmium oxide layer and weighing again after removing the layer by a 20-second immersion in 0.1 N HNO_3. This treatment did not result in an attack of the copper substrate. The weights were determined on a electro balance (Cahn) with a precision of ± 0.5μg which is equivalent to ±2.5% of the weight of a 5μ cadmium oxide layer. The mean of the densities of crystalline (8.15 g/cm^3) and amorphous cadmium oxide (6.95 g/cm^3) was used in the calculations. Thus the porosities may be in error by 10% total. Porosities of 46 to 50% were calculated for cadmium oxide layers of 5 to 7μ thickness. The theoretical capacity referred to an area of 1 cm^2 and a thickness of 1μ was calculated as 0.55 asec/cm^2/μ.

Palladium counter electrodes were used in the initial experiments. The need for occasionally recharging them, accompanied by unwanted evolution of hydrogen, led to the use of $NiOOH/Ni(OH)_2$ counter electrodes. These were simply cut from sintered battery plates as used in commercial nickel-cadmium batteries. They were charged just prior to use, avoiding full charge and unwanted oxygen evolution.

Experimental Procedure

After filling the self-contained hydrogen electrode with electrolyte and forming a sufficient amount of hydrogen in the glass capillary, the cell was placed on the microscope stage and the well filled with electrolyte while a reducing potential of -150 mV was applied between the test-and the hydrogen reference electrode. The spacer and the glass cover were then placed on the cell housing. With nitrogen flowing through the polyethylene bag, the residual current transient was recorded. When the residual current had decayed to only a few percent of the cycling currents, typically after one hour, the cycling experiments were started. Experimental runs were terminated by using either of two procedures: 1. The KOH electrolyte was substantially diluted with distilled water with a constant potential applied, followed by rinsing with water and drying with nitrogen. 2. The cell was disconnected from the electric circuit, the KOH solution immediately discarded and the cell rinsed with distilled water and dried with nitrogen. No discernible differences in morphology between these two procedures could be detected in micrographs at magnifications up to 20,000X.

Most of the experiments were carried out in 6N KOH at either room temperature or at 75°C. In the latter case, the cell was placed on a miniature hot plate which in turn was mounted on the microscope stage. Difficulties arose in long-term experiments at elevated temperatures due to the enhanced evaporation of electrolyte.

RESULTS AND DISCUSSION

Effect of Cycling on Capacity and Morphology of Cd Films

Electrodes with electrodeposited cadmium layers from 200 to
640Å thick were cycled in 1N and 6N KOH. The electrolyte film
thicknesses in these experiments amounted to between 300 and
360μ. In the initial experiments in 1N and 6N KOH the nitrogen-
purged polyethylene bag was not used. The oxidation of cadmium
by molecular oxygen resulted in a premature discharge of the cad-
mium electrode. Only the results in 6N KOH obtained under care-
ful exclusion of oxygen and carbon dioxide are reported here.

A cadmium film electrode with 200Å film thickness or the
equivalent of 30 ma sec/cm^2 theoretical capacity was cycled ex-
tensively using a 350μ film of 6N KOH. Residual currents due to
hydrogen evolution and oxygen reduction as low as 1 μa/cm^2 were
observed at O volts. When cycling with a current density of
±0.28 ma/cm^2 between voltage limits of 400 and -100 mV, an initial
capacity of 10 ma sec/cm^2 is obtained which constitutes 30% of
the theoretical value (Figure 58). A recorder trace of one of
the initial charge and discharge curves is shown in Figure 59.
The product of the constant current density and the time of charge
and discharge is plotted on the abscissa which is equivalent to
the amount of charge passing through the electrode during charge
and discharge. The trace does not exhibit any potential arrest
near the Cd/Cd(OH)$_2$ equilibrium potential in contrast to the
curves observed on cycling in 1N and 6N KOH bulk electrolyte.
The trace looks similar to the curves obtained on cadmium elec-
trodes in 0.1N KOH bulk electrolyte (compare Figure 40).

The value of the capacity depends strongly on the current
density used during cycling. Figure 58 shows that a capacity
of 31 ma sec/cm^2 is recovered in the tenth discharge as the cur-
rent density is reduced to 0.028 ma/cm^2. This is equal to the
theoretical capacity within the limits of error. Continued
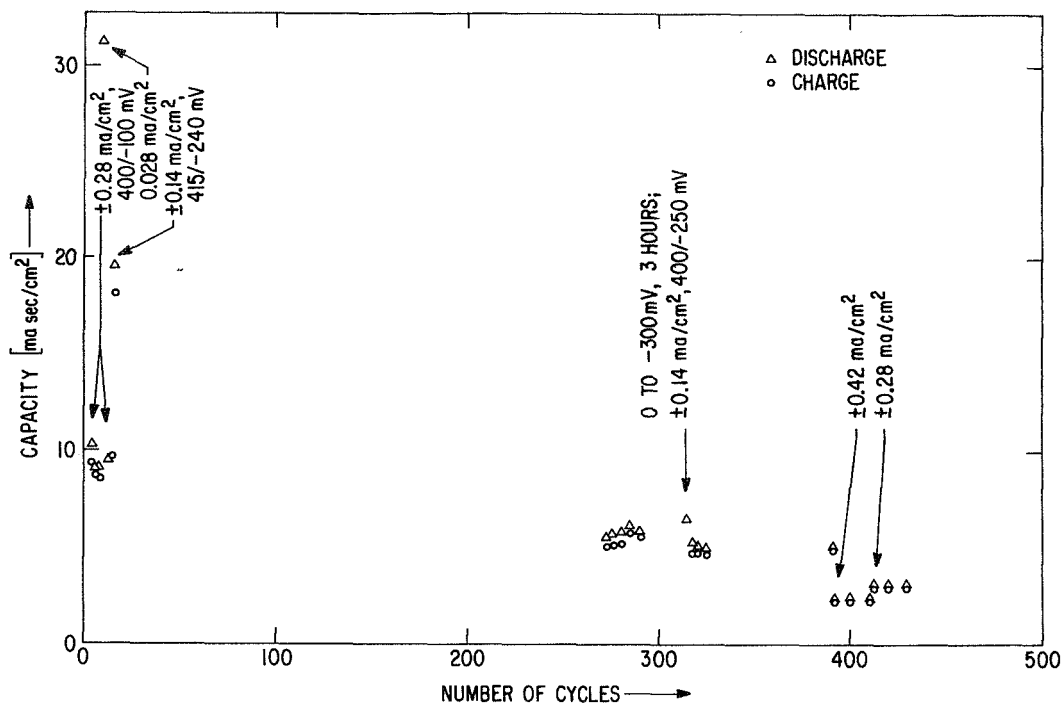cycling with ±0.14 ma/cm^2 leads to a pronounced decrease in the

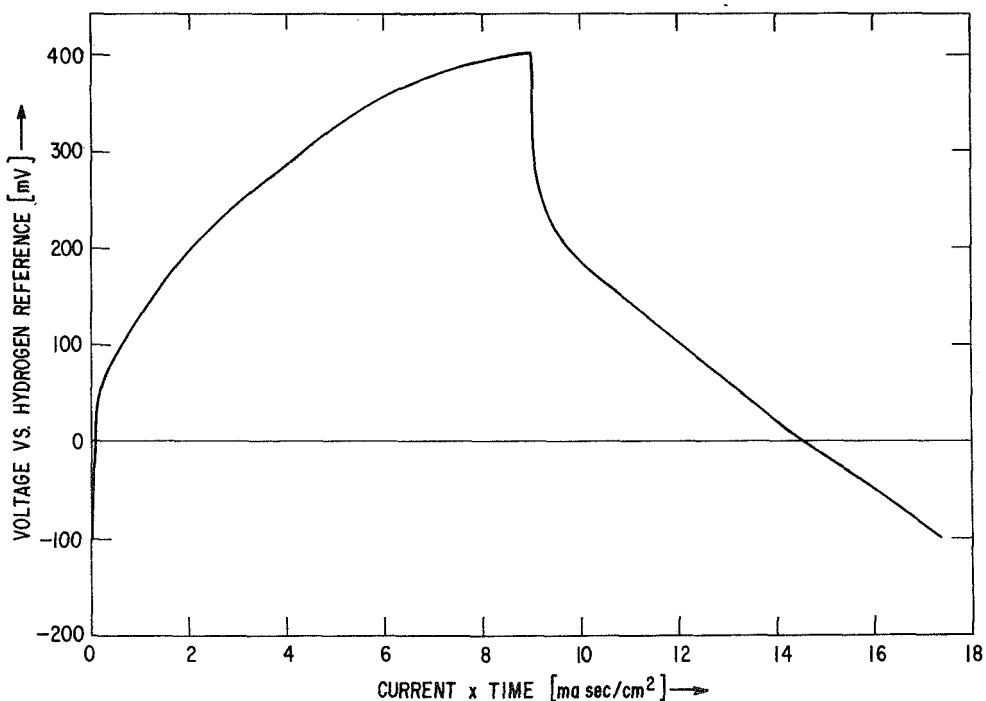Fig. 58 Capacity of a 200Å Cd film electrode vs. number of cycles, using 350μ electrolyte film of 6 N KOH.

Fig. 59 Recorder trace of discharge and charge curve of same electrode, using current density of ±0.28 ma/cm². Curves correspond to cycles 6 and 7 in Fig. 58.

capacity. After 270 cycles, the capacity has decreased to 18% of the theoretical value.

Changes in the morphology of the electrode as observed at a magnification of 220X occur very gradually during cycling. After 10 or 20 cycles , hardly any changes are perceptible. The formation and subsequent growth of particles and the formation of a brownish, cloud-like film take place eventually, however. The series of micrographs reproduced in Figures 60 to 65 document these changes. Figure 60 shows the cadmium layer as deposited in dry condition in bright field at a magnification of 200X, while picture 61 shows the same part of the surface in dark field. A completely black micrograph in dark field would represent an optically flat surface. Figures 62 and 63 show the appearance of the surface after 270 cycles in dark field at a magnification of 220X near the far edge (Figure 62) and near the solution edge (Figure 63). Both pictures were obtained during cycling. The formation of a large number of light particles and the formation of cloud-like film near the solution edge are evident from the micrographs. In some cases small brown particles can be clearly identified. The substrate surface is visible beneath the cloud-like film. The particles and the film persist during continued cycling. However, reduction at voltages of 0, -100, -200, and -300 mV for a total of three hours leads to the disappearance of the brown cloud-like film and to the formation of needle-like transparent crystals. This is shown in Figure 64 representing a section of the electrode close to the solution edge identical to that in Figure 63. Some of these crystals do not adhere to the substrate surface too well as evidenced by their vibrations caused by mechanical shock and by the fact that they can be moved across the substrate surface by moving the cover glass. The large light particles near the far edge, shown in Figure 62, are unaffected by the reduction.

The extensive reduction that leads to the disappearance of the brown film also causes a slight transient increase of the discharge capacity (see Figure 58). However, continued cycling

46

Fig. 60. Optical micrograph at 200X (bright field) of 200Å Cd film as deposited.
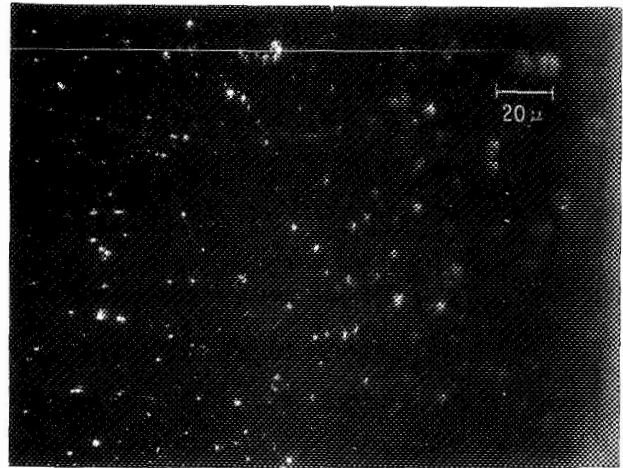

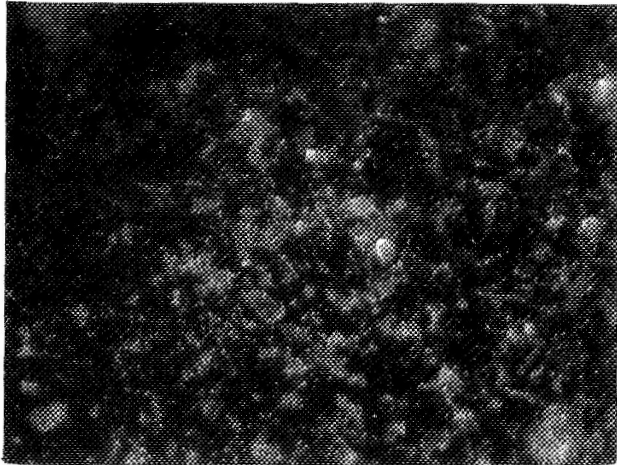Fig. 61. Optical micrograph at 220X (dark field) of 200Å Cd film as deposited.

Fig. 62. Optical micrograph at 220X (dark field) of 200Å Cd film electrode near far edge after 270 cycles, using 350μ film of 6N KOH.
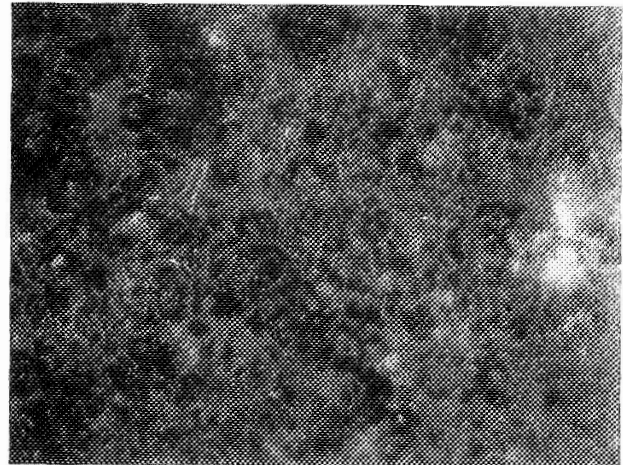

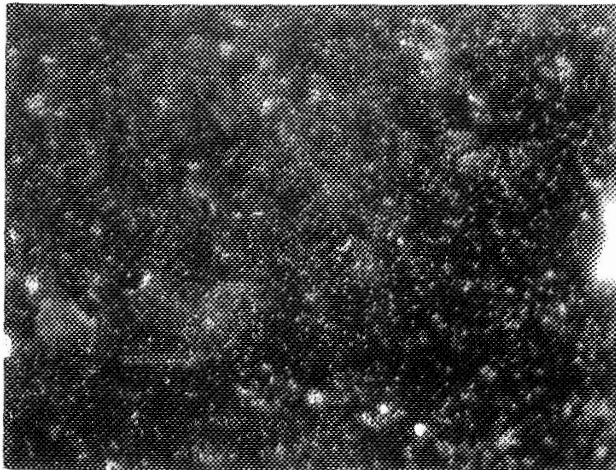Fig. 63. Same as Fig. 62, but near solution edge of electrode.

Fig. 64. Same as Fig. 63, but after applying cathodic potentials for 3 hours.

Fig. 65. Same as Fig. 62, but after 440 cycles.

47

reduces the capacity to 3 ma sec/cm^2 or 10% of the theoretical value (Figure 58). At the same time, a brown cloud-like film reappears on the surface. This is shown in the micrograph in Figure 65 which was obtained near the far edge. The micrograph also reveals a large number of isolated brown particles, some of them protruding from the substrate surface as far as 20μ.

It appears that the observed gradual formation of large particles, probably Cd(OH)$_2$, during continued cycling is to the largest extent responsible for the observed loss in capacity. The formation and disappearance of the brown film (CdO?) has a relatively small effect on the capacity. The lack of any pro-found changes in morphology during the first 10 or 20 cycles to-gether with the similarity between the curves in 6N KOH films and 0.1N bulk KOH suggest that charge and discharge occur mainly by a solid state transport mechanism. Superimposed is a dis-solution mechanism which leads to a gradual increase in particle size and loss in capacity as the larger particles cannot be com-pletely oxidized or lose contact with the substrate surface.

Effect of Cycling on Capacity and Morphology of CdO Films

Changes in the capacity and morphology of cadmium oxide films during the initial ten cycles in 6N KOH were studied in de-tail, using scanning electron microscopy for increased resolution in addition to the in situ microscopic examination. After a given number of cycles, the electrode was removed from the cell, washed, dried and kept in a dessicator until examined in the scanning electron microscope. A new experiment was always started with a freshly prepared cadmium oxide film. Uniform layers of cadmium oxide on copper strips with thicknesses between 4 and 8μ were prepared by electrophoretic deposition as outlined in the experi-mental section. The experiments were carried out with a con-stant electrolyte film thickness of 12.5μ.

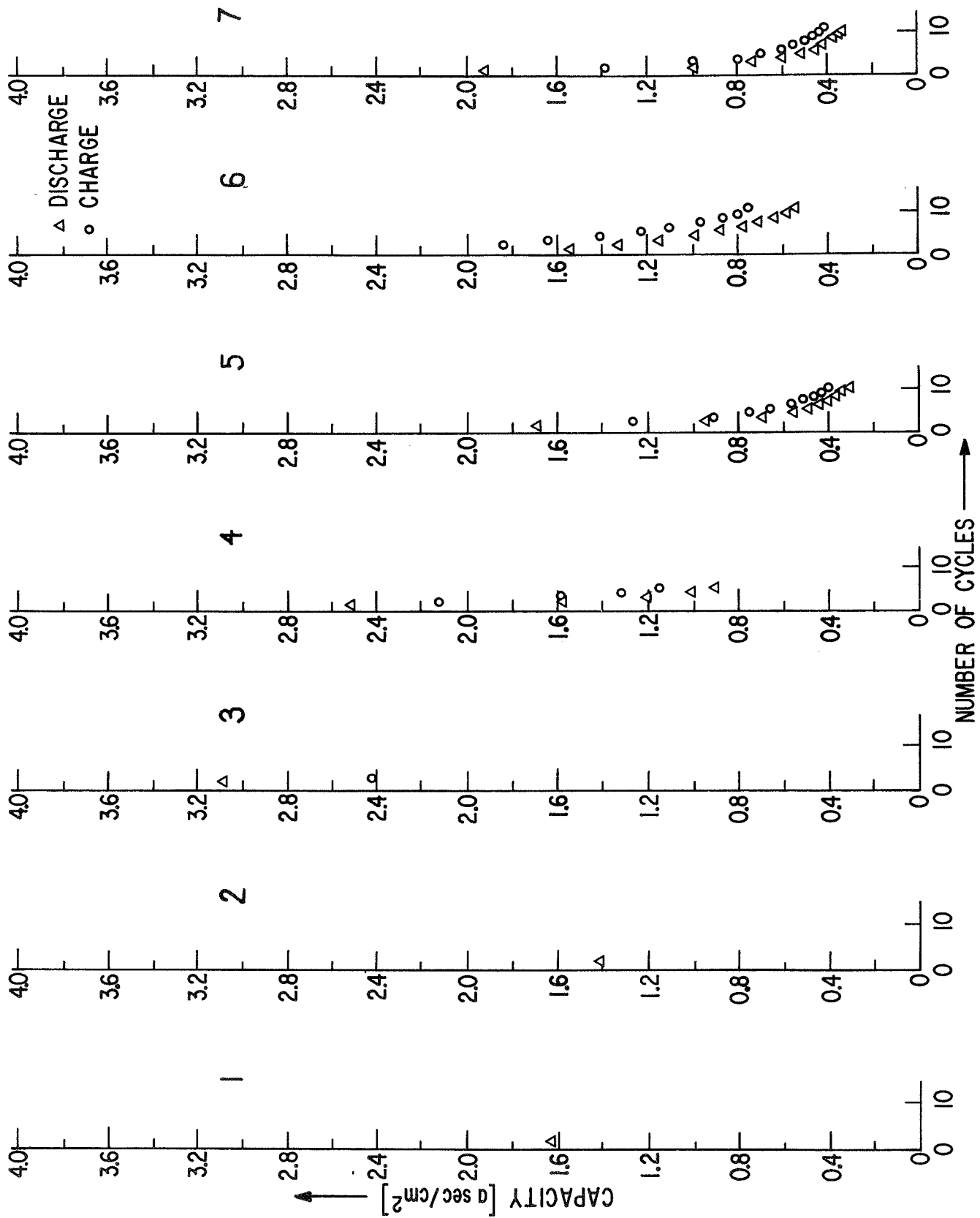Figure 66 shows the capacity vs. the number of cycles for seven different electrodes from the first discharge to the

48

Fig. 66 Capacities of 7 different CdO film electrodes vs. number of cycles, using a constant 6 N KOH film thickness of 12.5μ, applying ±1.5 μa/cm² between limits 300/-200 mV.

49

eleventh charge. The first charge, resulting in the reduction of cadmium oxide to cadmium, is always accomplished at a constant potential of -150 mV. A determination of the amount of charge from an integration of the current-time transient is unfeasible because of the simultaneous reduction of oxygen and evolution of hydrogen immediately following the filling of the cell with KOH. Subsequent charges and discharges are performed with a constant current density of 1.4 ma/cm^2 to cutoff voltages of -200 and 300 mV, respectively. The first discharge results in capacities between 1.4 and 3.1 asec/cm^2. When correction is made for variations in the cadmium oxide film thickness, d_{CdO}, of these electrodes, the discrepancies between the initial capacity values per unit area, C_1/A, of the seven electrodes are much reduced. Table I presents a summary of the initial capacities per unit area, C_1/A, the capacities referred to 1μ cadmium oxide film thickness and 1 cm^2 area, C_1/Ad_{CdO}, and the ratios of subsequent discharge capacities to the initial capacities, C_n/C_1. The table also shows the ratios of the initial capacities to the theoretical values, C_1/C_{theor} and, in addition to the data obtained on electrodes 1-7 of Figure 66, data obtained on an eighth electrode which was cycled more than 4000 times (see Figure 67).

As evidenced by Figure 66 and Table I, a drastic loss in capacity occurs during the first ten cycles. Typically the capacities decrease to one-third of the initial values within five cycles and to one-fifth within ten cycles. Loss of capacity continues on further cycling, but at a smaller rate, as shown in Figure 67 for up to 4700 cycles. The shape of the charge and discharge curves remains approximately the same during the initial ten cycles. This is shown in Figure 68 for the first and tenth cycles. The product of chart speed and time is plotted on the abscissa which is equivalent to the actual length of the curves on the recorder chart. The chart speed during the first cycle was 0.25 inch/min as compared to 1 inch/min for the tenth cycle. Hence the curves reflect the large loss of capacity during the first ten cycles as also evidenced by Figure 67. While the

discharge curves for the first and tenth cycles show a pronounced potential arrest near the $Cd/Cd(OH)_2$ equilibrium potential, such a potential arrest is virtually absent in the discharge curve after 4000 cycles, obtained at a chart speed of 20 inches/min. The voltage rises continually during the entire discharge which means that higher overvoltages are required for oxidation and reduction of the electrode. This suggests the formation of passivating layers which were apparently not formed to any large extent during the first ten cycles. A different cause for the pronounced loss of capacity during the first ten cycles must therefore exist, and a careful study of the changes in morphology during the first ten cycles was undertaken.

TABLE I

Capacity of Cadmium Oxide Film Electrodes During First Ten Discharges

Electrode No.	1	2	3	4	5	6	7	8
$d_{CdO}[\mu]$	5	5	8	8	5.5	5	5.5	6
$C_1/A\,[asec/cm^2]$	1.63	1.40	3.08	2.53	1.70	1.56	1.93	1.85
$C_1/Ad_{CdO}\,[asec/cm^2\mu]$	0.33	0.28	0.38	0.32	0.31	0.31	0.35	0.31
C_1/C_{theor}	0.60	0.51	0.69	0.58	0.56	0.56	0.64	0.56
C_2/C_1				0.63	0.56	0.86	0.52	0.53
C_5/C_1				0.36	0.29	0.56	0.27	0.33
C_{10}/C_1					0.18	0.35	0.18	0.17

d_{CdO} = thickness, A = area of cadmium oxide films
C_1, C_2, C_5, C_{10} = capacities during 1., 2., 5. and 10. discharge
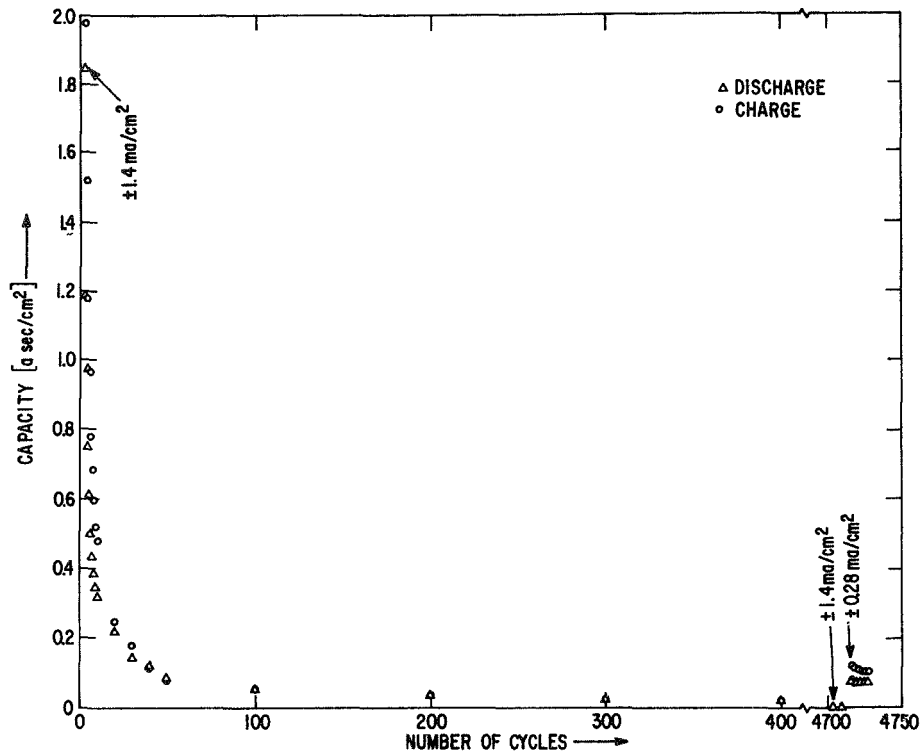C_{theor} = theoretical capacity

51

Fig. 67 Capacity of 6μ CdO film electrode (electrode 8) vs. number of cycles, using 12. 5μ film of 6 N KOH and voltage limits 300/-200 mV.
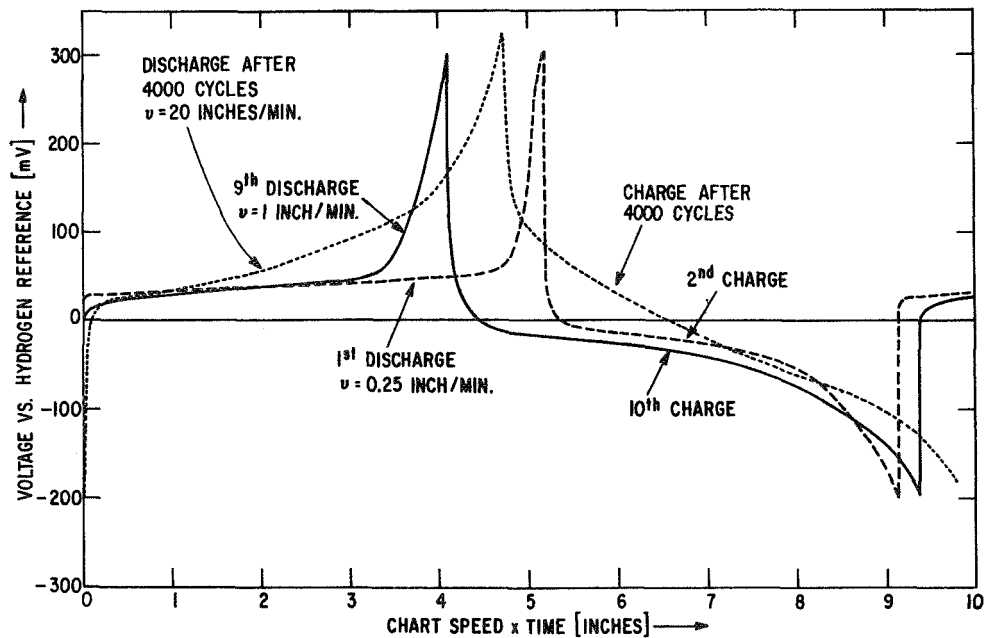

Fig. 68 Recorder traces of discharge and charge curves of electrode 8 after 1, 10, and 4000 cycles, applying ±1. 4 ma/cm². Product of chart speed and time (identical to length on recorder chart) is plotted on abscissa.

Figure 69 shows an optical micrograph of a cadmium oxide layer in dry condition immediately after electrophoretic deposition, obtained in dark field at a magnification of 220X.*
Figures 70 and 71 are scanning electron micrographs (SEM) of the same surface obtained at magnifications of 2000X and 10,000X. The layer is uniformly brown, and the SEMs show a large number of well-developed cubic particles of sizes 0.1 to 1μ. Many of these particles are covered with what appears to be the binder. Exposure of a cadmium oxide layer to a 6N KOH film for ten minutes on open circuit turns the brown color of the deposit into a bright white color. This is shown in the optical micrograph in Figure 72. Only a few brown particles remain at the surface after this exposure. The SEMs in Figures 73 and 74 resolve the changes in the particle shapes caused by the exposure of the electrode to KOH. The formation of a large number of platelets, many of them with hexagonal shapes, is evident. The lateral dimensions lie in the range 3000 to 5000Å. Undoubtedly these particles are β-Cd(OH)$_2$.[25]

Figure 75-77 show the morphology of a surface which results when exposing a cadmium oxide film to 6N KOH with a reducing potential of -150 mV applied for three hours. After this reduction, the surface appears uniformly gray in the microscope (Figure 75). A large number of small, highly reflecting particles are present, but their shapes cannot be resolved in the microscope. The SEMs in Figures 76 and 77 show that the crystal habit has changed but the particle sizes have not (compare Figures 70 and 71). The cubic particles in Figure 71 are no longer visible in Figure 77. Most of the cadmium particles in Figure 77 have sizes between 2000 and 3000Å.

During the first discharge, which results in the formation of Cd(OH)$_2$, microscopic examination reveals the formation of dark areas on the surface which ultimately grow together. The distinct darkening of the surface is the only effect of discharge which

---

*Unless otherwise stated, the following photomicrographs were all obtained in dark field at a magnification of 220X.
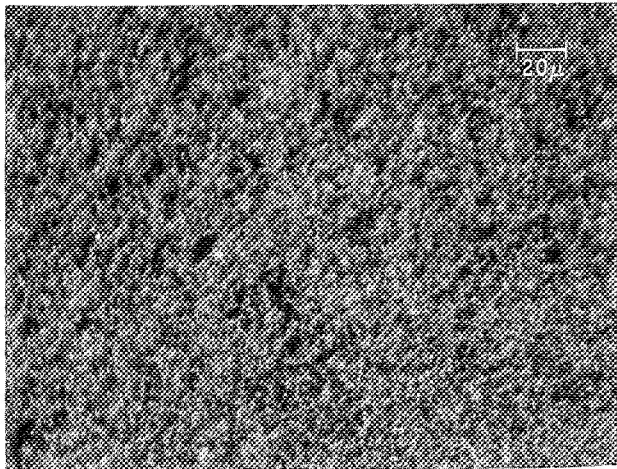
Fig. 69. Optical micrograph of CdO film as deposited by electrophoresis (220X, dark field, dry).
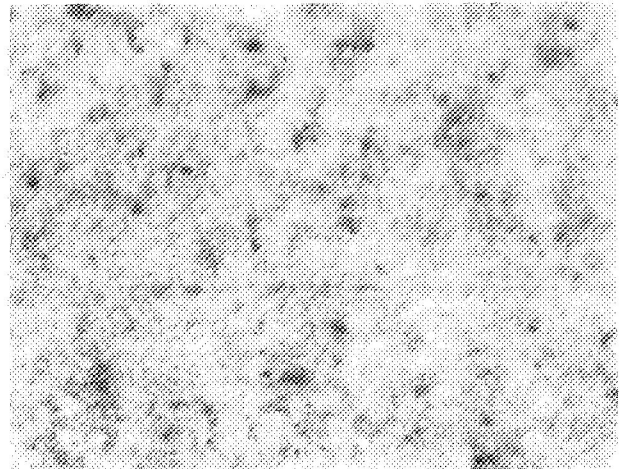

Fig. 72. Optical micrograph of CdO film after exposure to 12.5μ film of 6N KOH on open circuit for 10 min. (220X, dark field, wet).
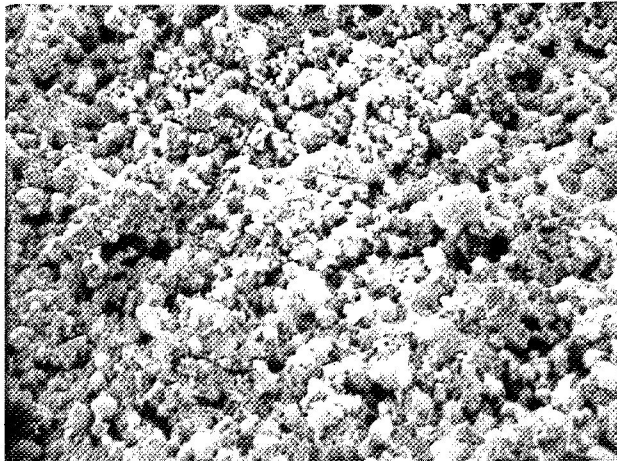

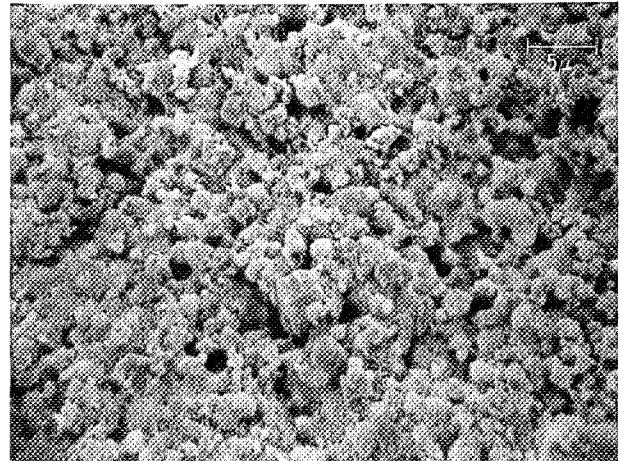Fig. 70. Scanning electron micrograph (SEM) of same CdO film at 2000X.

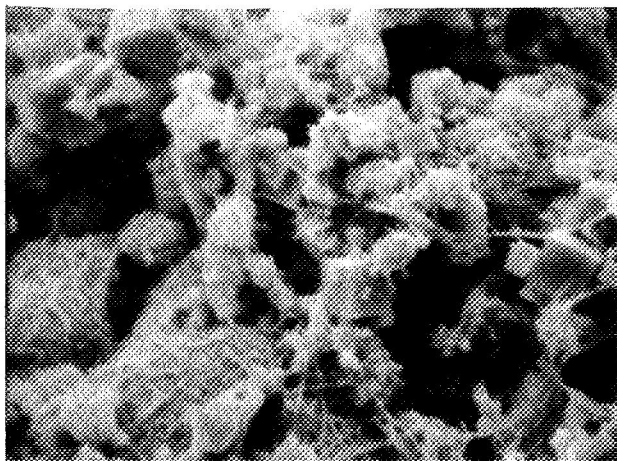Fig. 73. SEM of same surface at 2000X.
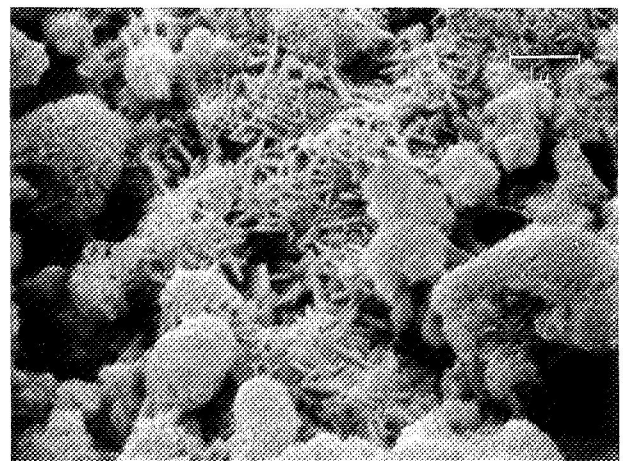

Fig. 71. SEM of same CdO film at 10,000X.

Fig. 74. SEM of same surface at 10,000X.
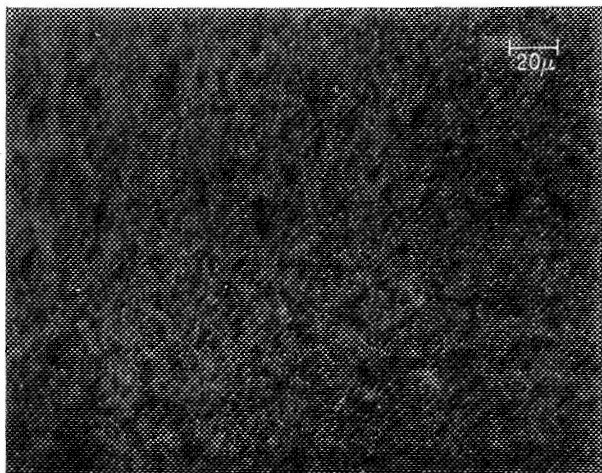
Fig. 75. Optical micrograph of CdO electrode after reducing with -150 mV for 3 hours with 12.5μ film of 6N KOH.
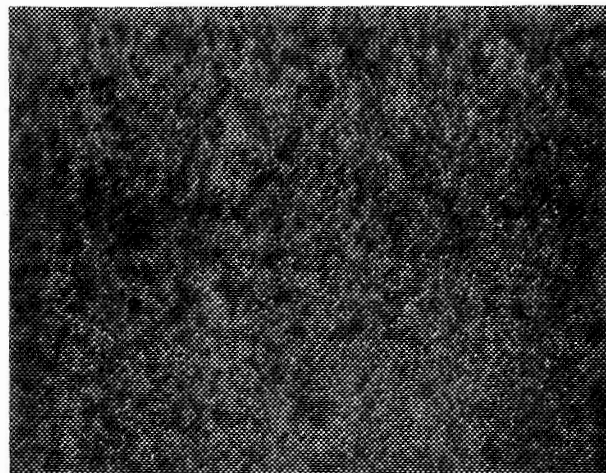

Fig. 78. Optical micrograph of electrode 1 after 1st discharge with 1.4 ma/cm^2 to 300 mV.
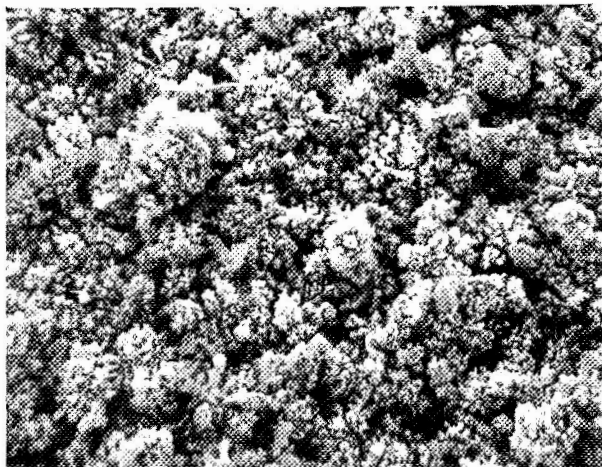

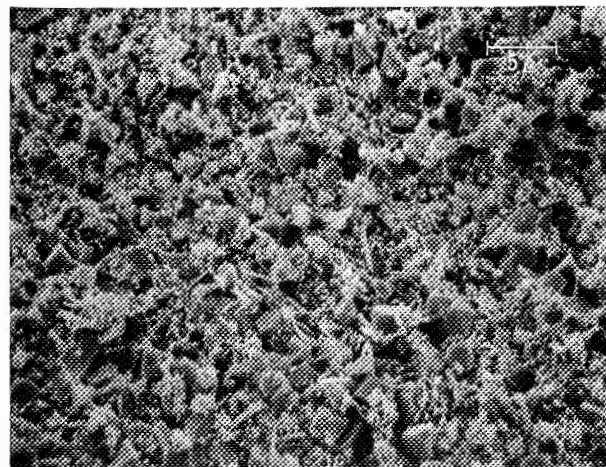Fig. 76. SEM of same surface at 2000X.

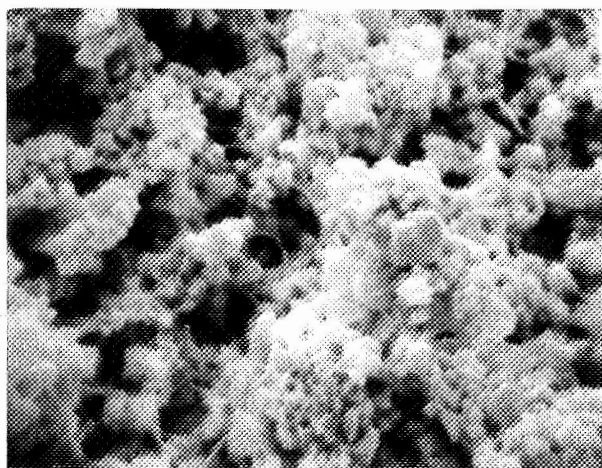Fig. 79. SEM of electrode 1 at 2000X.
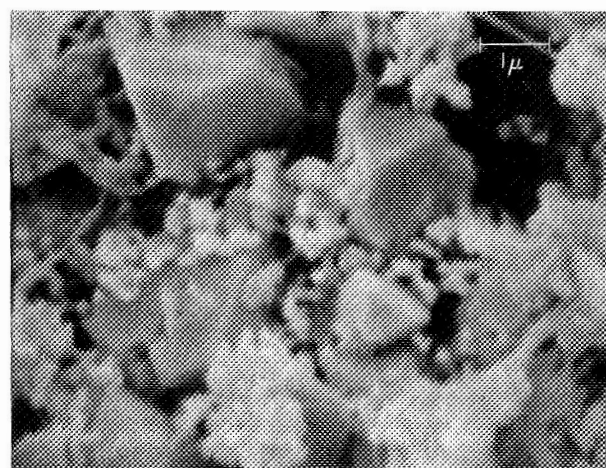

Fig. 77. SEM of same surface at 10,000X.

Fig. 80. SEM of electrode 1 at 10,000X.

55

can be observed in the microscope. Figure 78 shows the surface after complete discharge at a magnification of 220X.

The SEMs in Figures 70 and 80 show that a large number of well-defined crystals, mostly of sizes 1-2μ, have been formed. The hexagonal shape of these crystals identifies them as β-Cd(OH)$_2$.[25] In addition, a few needle-like crystals, most likely γ-Cd(OH)$_2$[25], and distinctly shaped particles with sizes one order of magnitude smaller are visible. It is suggested that the crystals of β- and γ-Cd(OH)$_2$ are precipitated from the super-saturated electrolyte and that the small particles are Cd(OH)$_2$ formed by solid state oxidation of the cadmium particles of identical size as in Figure 77. The micrographs in Figures 78-80 were obtained on electrode 1 of Figure 66 which was removed from the cell on open circuit after discharge at constant current to 300 mV. Electrode 2 in Figure 66 was removed from the cell after the first discharge, while a potential of 300 mV was being applied. The morphology of this electrode was found to be identical to that of electrode 1.

Electrode 3 was removed from the cell after the second charge while a potential of -150 mV was being applied. According to Figure 66 the second charge leads to a capacity which is 20% smaller than that recovered on the first discharge. Simultaneously the microscope reveals a distinct brightening of the surface, and the particle size appears to have grown (Figure 81). The SEMs in Figures 82 and 83 show the formation of whisker-like crystals of lengths up to 10μ and widths up to 1μ. The formation of whisker-like crystals on charge has apparently never been de-scribed before. The nature of these crystals was not identified in the present study. It is also evident from Figures 82 and 83 that many of the hexagonal particles formed during the first dis-charge (compare Figure 70) have remained unchanged during the charge. A great number of the small particles of sizes 2000 to 3000Å have also persisted.
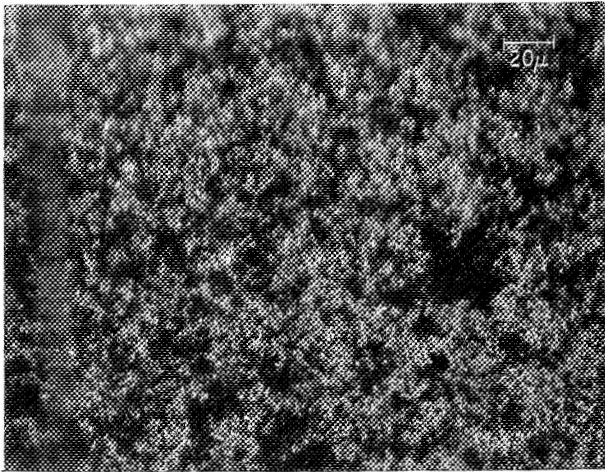
Fig. 81. Optical micrograph of electrode 3 after 2nd charge to -200 mV.
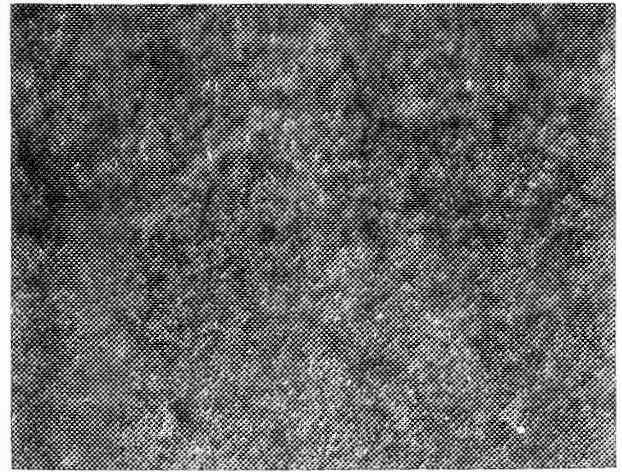

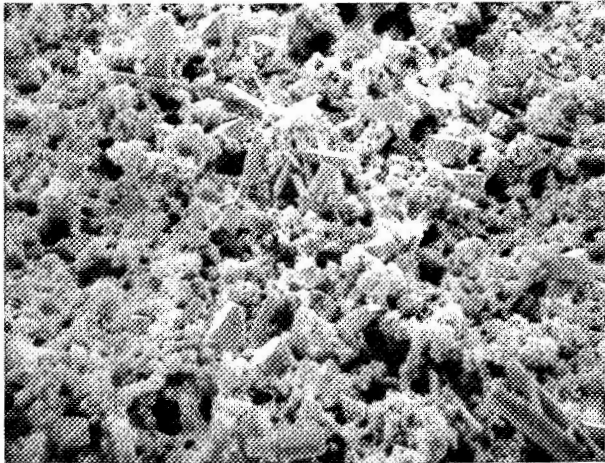Fig. 84. Optical micrograph of electrode 4 after 5th discharge to 300 mV.

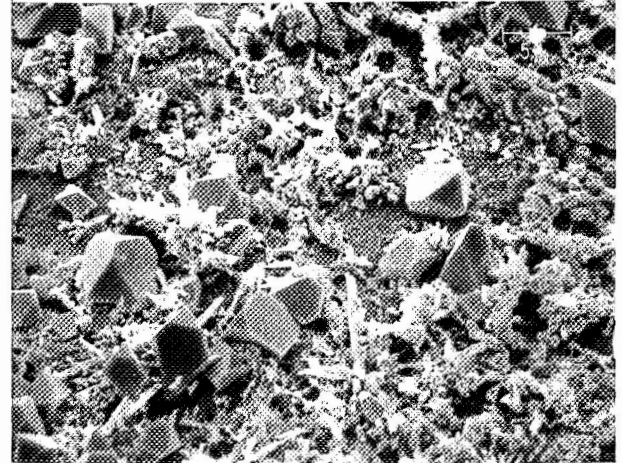Fig. 82. SEM of electrode 3 at 2000X.
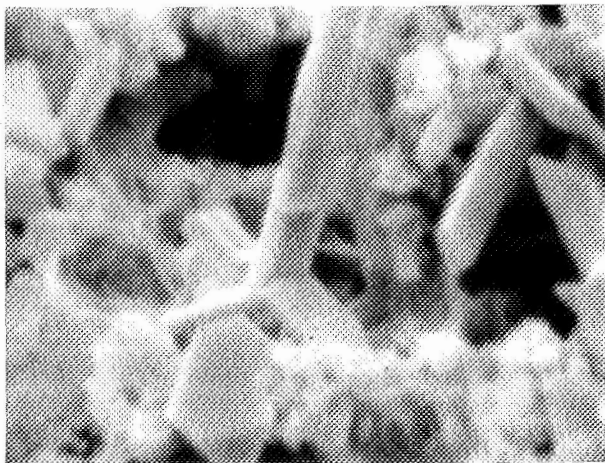

Fig. 85. SEM of electrode 4 at 2000X.
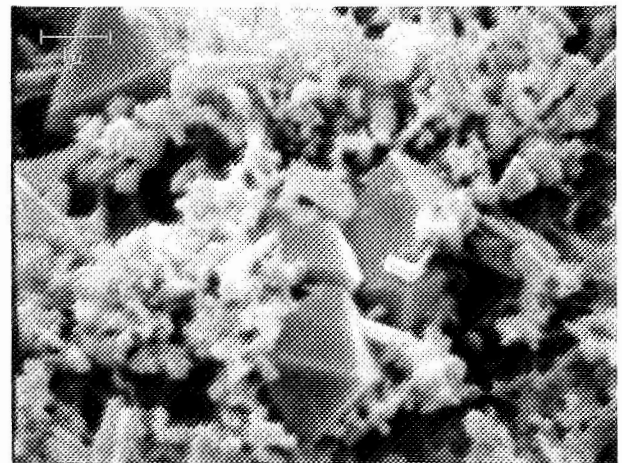

Fig. 83. SEM of electrode 3 at 10,000X.

Fig. 86. SEM of electrode 4 at 10,000X.

Electrode 4 was removed on open circuit from the cell after completing the fifth discharge to 300 mV. Figure 66 shows that the capacity during 5 discharges has decreased to 36% of its original value. The photomicrograph in Figure 84 reveals a coarsening of the surface compared to the appearance of the surface after the first discharge shown in Figure 78. In the higher resolution of the scanning electron microscope a great number of hexagonal crystals of sizes 2-4μ are clearly visible (Figures 85 and 86). Needle-like crystals can also be seen in these micrographs. Electrodes 5 and 6 were each cycled ten times. Electrode 5 was removed from the cell on open circuit, electrode 6 after keeping the electrode at 300 mV for 16 hours following the ten cycles. Further coarsening of the surface of electrode 6 is evident from Figures 87 to 89. Figures 88 and 89 show that the number of well-crystallized particles of sizes 2-4μ have increased compared to Figures 85 and 86. Extensive oxidation at 300 mV leads to a brownish appearance of the surface, as seen in the microscope, and to a disappearance of many crystals (Figures 91 and 92). At the same time, an erosion of the remaining crystals is evident in Figure 91 in that a distinct layer structure of the crystals has developed which was completely absent before the extensive oxidation at 300 mV (Figure 88). No particular features in the SEMs can be associated with the brown color clearly observed in the microscope.

Figures 93-95 show the effects of extensive reduction of the electrode. Electrode 7 was kept at -150 mV for 16 hours after the 11th charge. The extensive charging leads to a considerable brightening of the surface (Figure 93). As evidenced by the SEMs in Figures 94 and 95, the large crystals formed during the 10 preceding cycles (Figures 80-92) have disappeared. The particles remaining on the surface have much less distinct shapes, and most of them have sizes between 2000 and 3000Å. In fact, the SEM in Figure 95 looks very similar to that in Figure 77 which was obtained after the first charge.
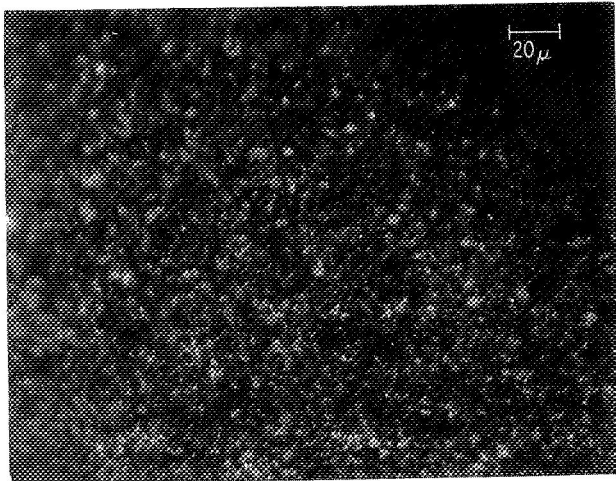
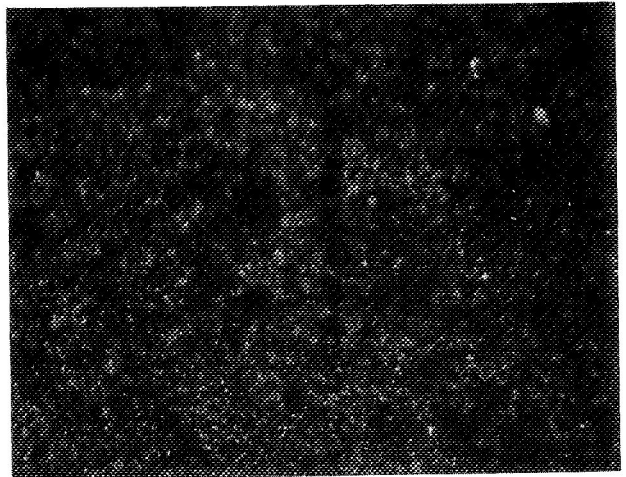Fig. 87. Optical micrograph of electrode 5 after 10th discharge to 300 mV.

Fig. 90. Optical micrograph of electrode 6 after 10th discharge and anodic polarization at 300 mV for 13 hours.
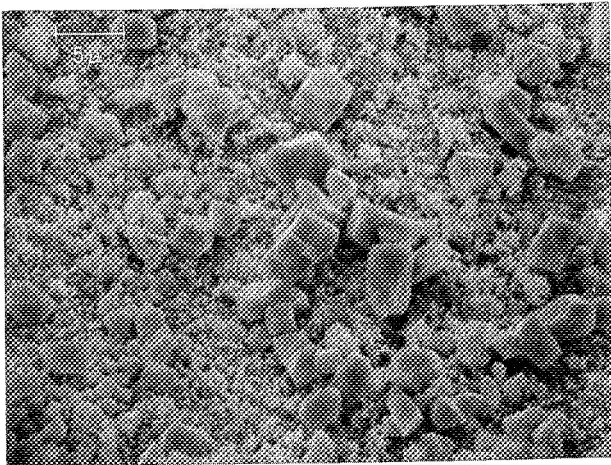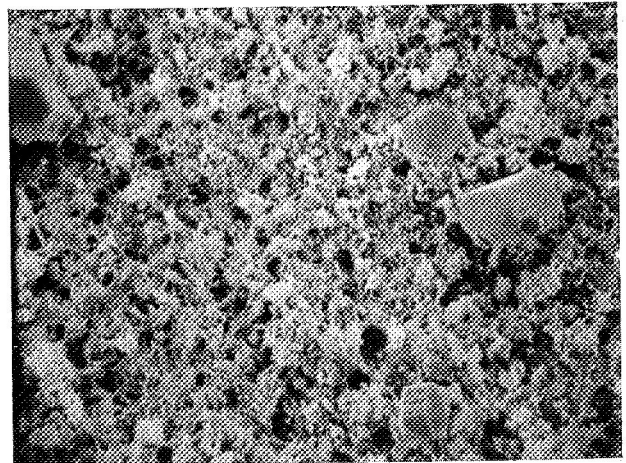

Fig. 88. SEM of electrode 5 at 2000X.

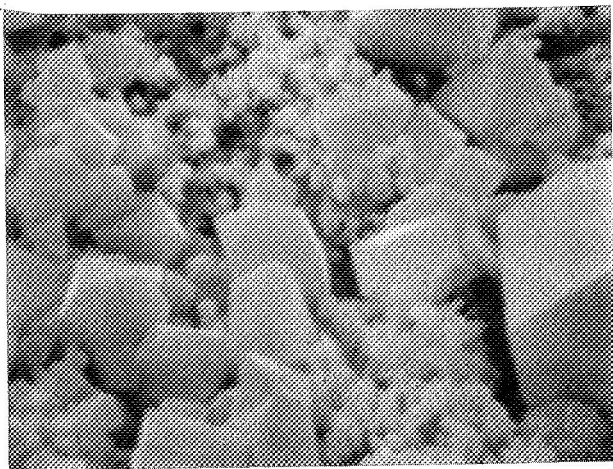Fig. 91. SEM of electrode 6 at 2000X.
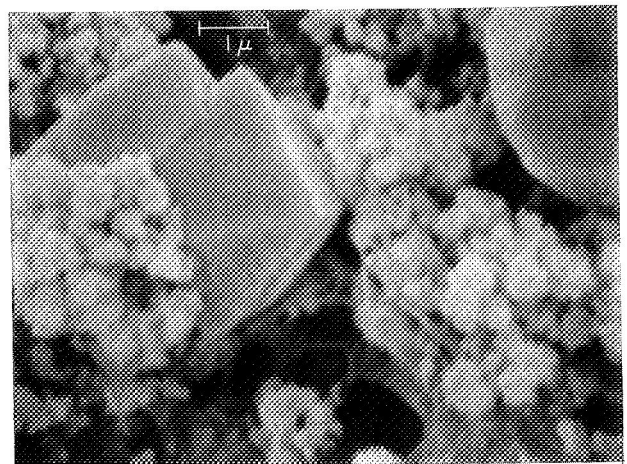

Fig. 89. SEM of electrode 5 at 10,000X.

Fig. 92. SEM of electrode 6 at 10,000X.

59

Electrode 8 was cycled more than 4000 times with current densities of 0.28 and 1.4 ma/cm^2. Figure 67 shows that the capacity on cycling decreases continually to values as low as 10 ma sec/cm^2. The micrographs in Figures 96-98 were obtained after more than 4000 cycles. In this case the magnification of 220X is sufficient to resolve the shapes of a few very large particles (Figure 96). The SEMs in Figures 97 and 98 show the very large crystals which have formed in greater detail. Their sizes range up to 7μ. The hexagonal layer structure already seen in Figure 91 is strikingly evident in Figure 98. As in the case of extensive oxidation, the electrode turns brown on extensive cycling.

Another electrode, instead of being cycled continually with constant voltage limits, was, in addition to cycling, subjected to periods of extensive reduction and oxidation (Figure 105). After more than 8000 cycles, this electrode displayed a morphology quite different from that shown in Figures 96-98. Figures 99-101 show the formation of a large number of hexagonal platelets, many of them with diameters of 2μ and thicknesses of 0.2μ. These platelets are transparent immediately after removing the electrode from the cell. This is shown in the photomicrograph in Figure 102 obtained at a magnification of 500X after washing and drying the electrode. With time these crystals become less transparent. For reference purposes Figures 103 and 104 show the appearance of a cadmium oxide surface in dry condition immediately after deposition, at magnifications of 220 and 500X. The considerable increase in particle size is evident from a comparison of Figures 99 and 102 with Figures 103 and 104.

The initial capacities of electrodes 1 to 8 in Table 1 amount to between 50 and 70% of the theoretical values and are somewhat lower than the values obtained on pasted battery plates. This is most likely due to the much looser and more porous nature of the layer resulting from electrophoretic deposition as compared to pasting. Loss of contact between the particles and the substrate is thus expected to be a larger problem and would account for the relatively small initial capacities.

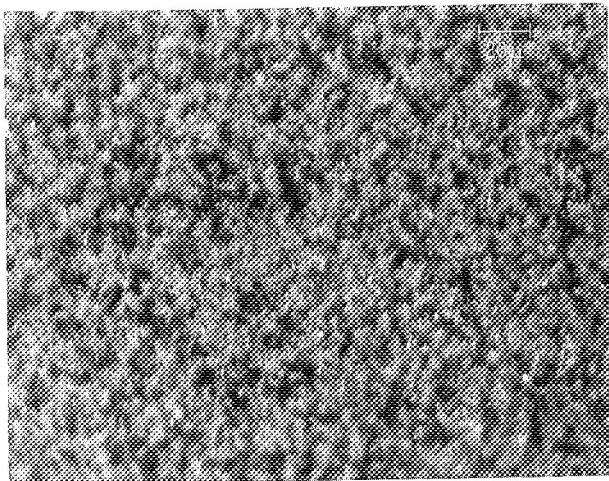Fig. 93. Optical micrograph of electrode 7 after 11th charge and cathodic polarization at -150 mV for 16 hours.
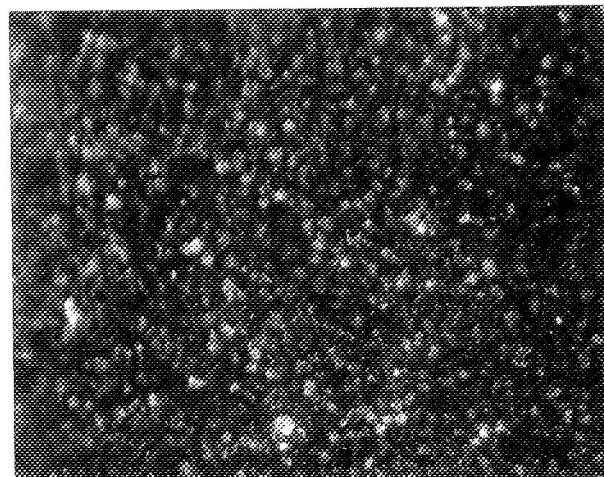

Fig. 96. Optical micrograph of electrode 8 after 4700 cycles with ± 1.4 ma/cm^2 and 0.28 ma/cm^2 between limits 300/-200 mV.
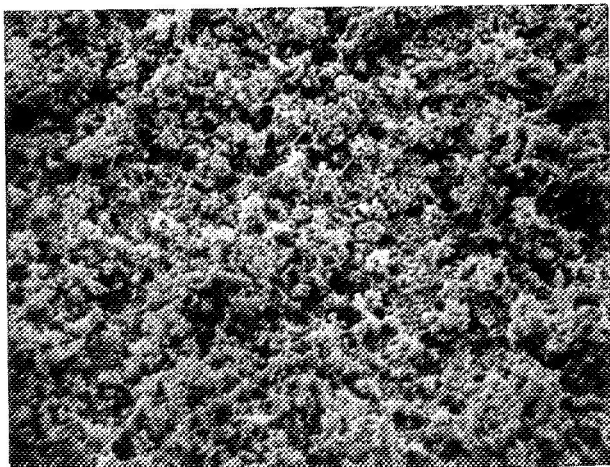

Fig. 94. SEM of electrode 7 at 2000X.
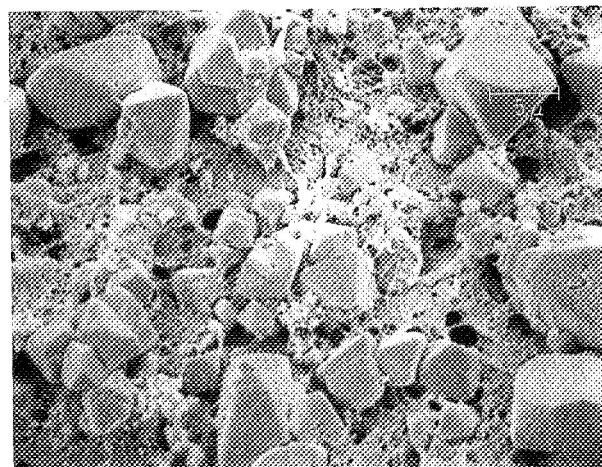
Fig. 97. SEM of electrode 8 at 2000X.
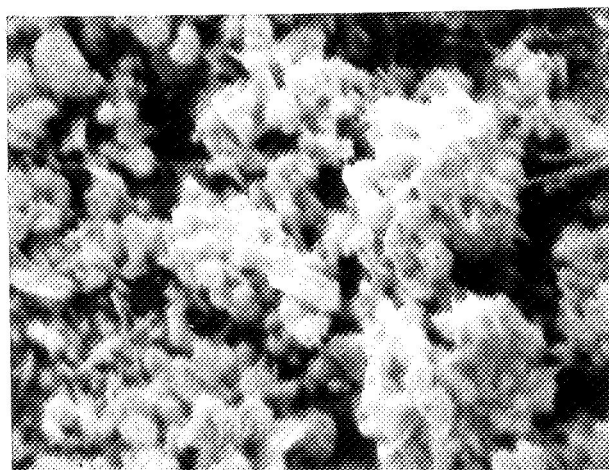
Fig. 95. SEM of electrode 7 at 10,000X.
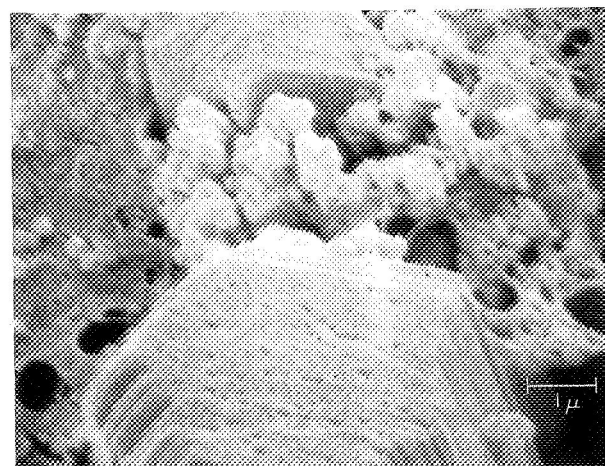
Fig. 98. SEM of electrode 8 at 10,000X.

61

From the preceding detailed studies of the changes in the morphology during the first ten cycles, it is evident that the pronounced decrease of the capacity during these cycles (compare Figure 66) is due to the observed formation of large $Cd(OH)_2$ crystals, probably caused by precipitation from the supersaturated KOH film during discharge. The supersaturation is favored by the comsumption of hydroxyl ions in the discharge reaction: The lower pH, which is expected to result in the KOH film, causes the solubility of cadmium species to decrease. Once formed, many of the larger $Cd(OH)_2$ crystals do not appear to be reduced on continuous cycling (compare Figure 82) and, hence, do not contribute to the capacity. During periods of extensive reduction, the large $Cd(OH)_2$ crystals seem to dissolve (Figure 95), and dissolved cadmium species may then be electrodeposited on the test electrode. Due to the increased solubility of cadmium species at high pH, this process is favored by the formation of hydroxyl ions during charging and leads to a preliminary increase in the capacity up to factors of 3 (Figure 105).

The fact that the shape of the charge and discharge curves does not change during the initial 10 cycles (Figure 68) indicates that the mechanism does not change. The brown color which the electrode exhibits as a consequence of extensive cycling is probably related to the passivating film (cadmium oxide?) suggested earlier as the reason for the different shape of the curves after 4000 cycles. Unfortunately, no conclusive evidence for such a film could be found in the SEMs.

Effect of Electrolyte Film Thickness on Capacity and Morphology

The effect of electrolyte film thickness on capacity and morphology on cycling was studied on cadmium oxide electrodes with layer thicknesses of 3-6μ. The electrolyte film thickness was varied from 12.5 to 500μ. Figures 105-108 show the capacity as a function of the number of cycles for four different cadmium oxide electrodes, using electrolyte film thicknesses of 12.5, 25, 100 and 500μ. The initial capacities, referred to 1 cm^2 area and 1μ
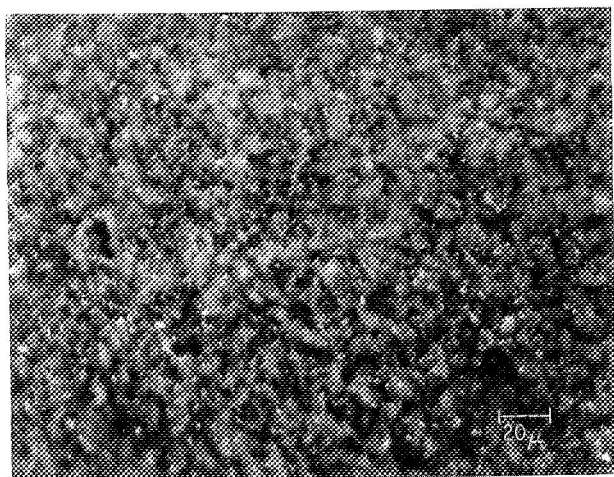
Fig. 99. Optical micrograph of 3.5μ CdO film in dry condition after more than 8000 cycles, using 12.5μ film of 6N KOH. (220X, dark field).
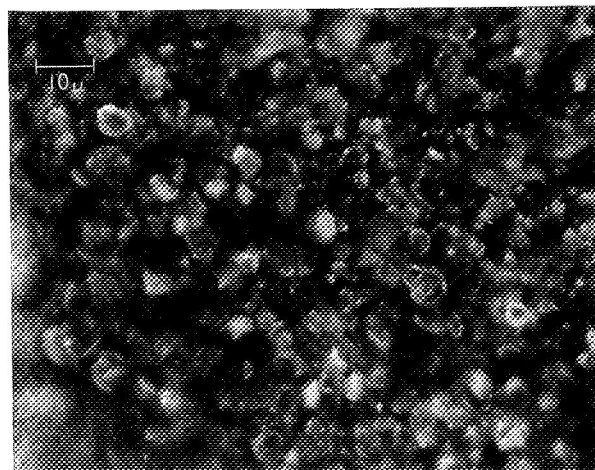
Fig. 102. Optical micrograph of same electrode, but at 500X (dark field).
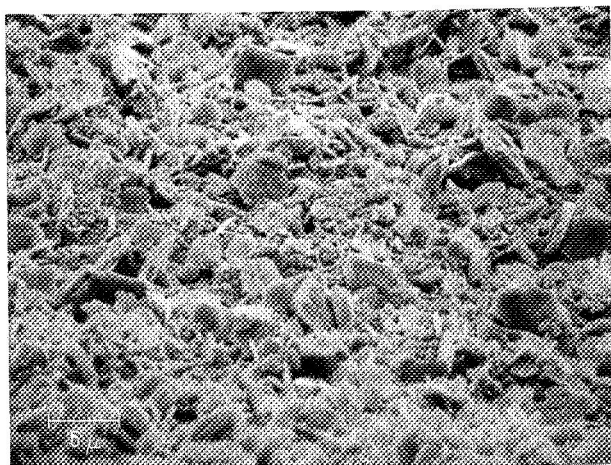
Fig. 100. SEM of same electrode at 2000X.
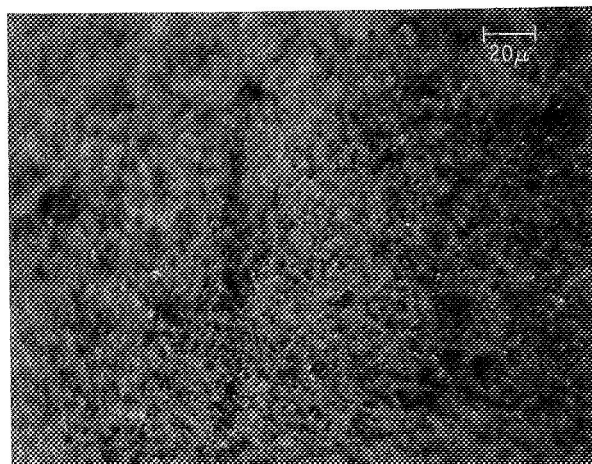
Fig. 103. Optical micrograph of CdO film as deposited by electrophoresis (220X, dark field, dry).
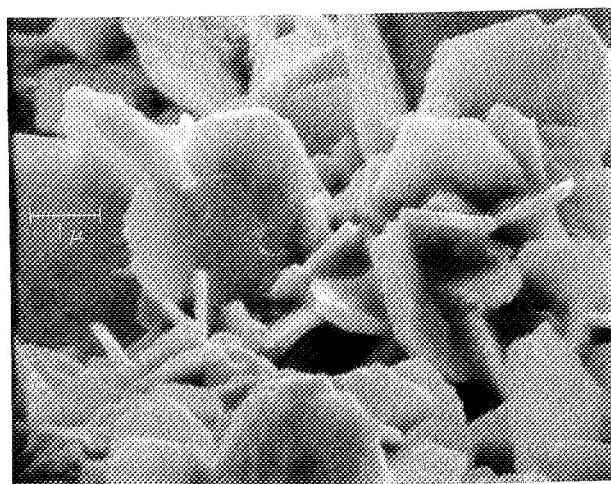
Fig. 101. SEM of same electrode at 10,000X.
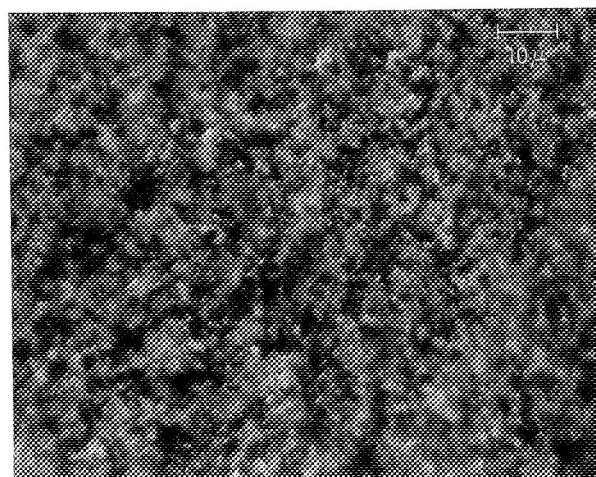
Fig. 104. Optical micrograph of same electrode, but at 500X (dark field).

63
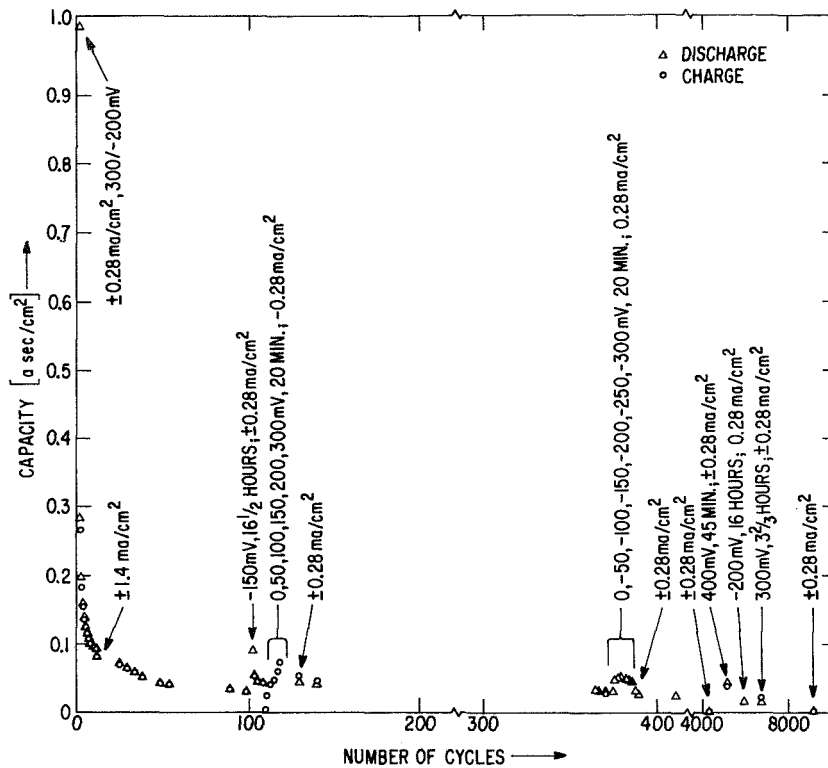
Fig. 105 Capacity of 3.5μ CdO film electrode vs. number of cycles, using 12.5μ film of 6 N KOH.
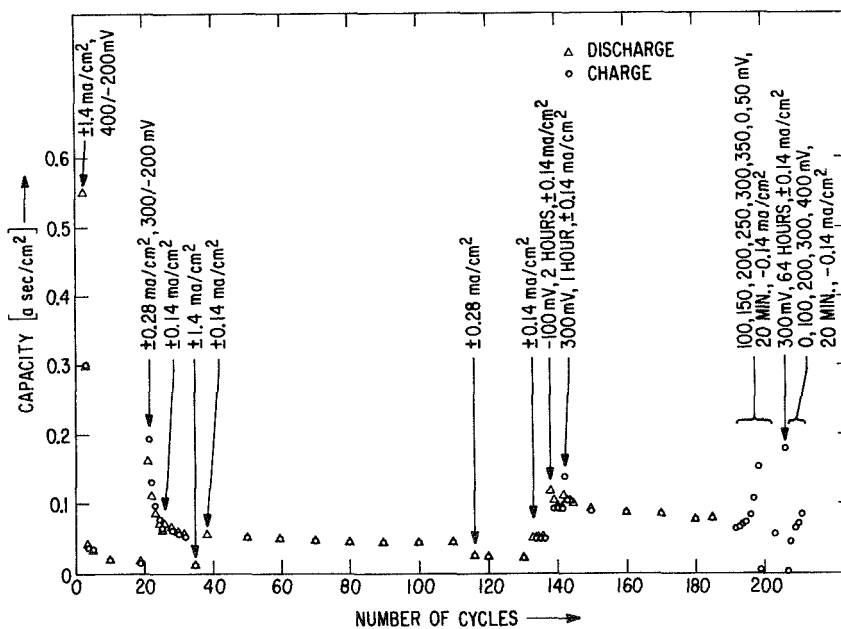
Fig. 106 Capacity of 6μ CdO film electrode vs. number of cycles, using 25μ film of 6 N KOH.

64
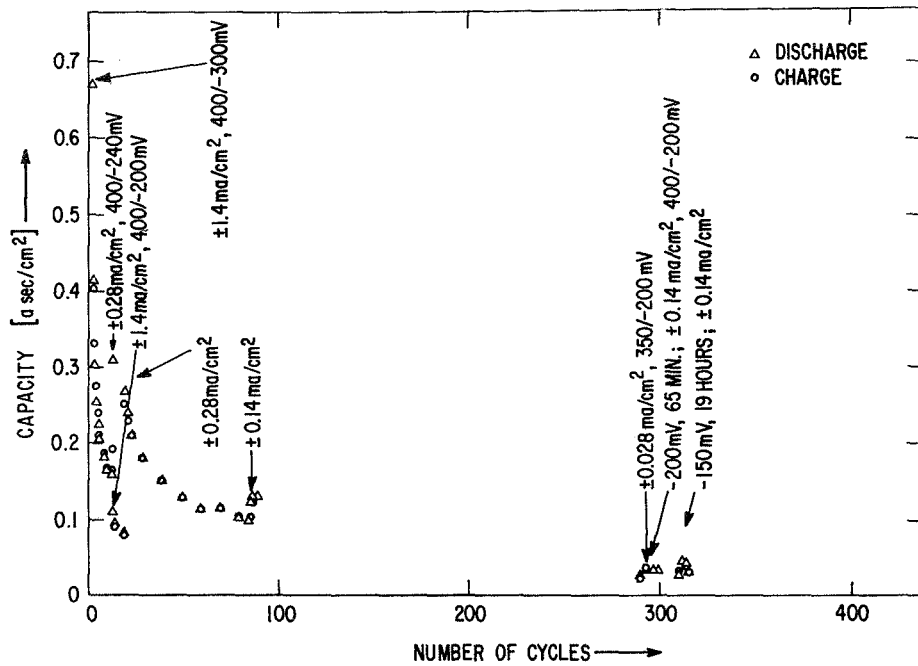
Fig. 107 Capacity of 4μ CdO film electrode vs. number of cycles, using 100μ film of 6 N KOH.
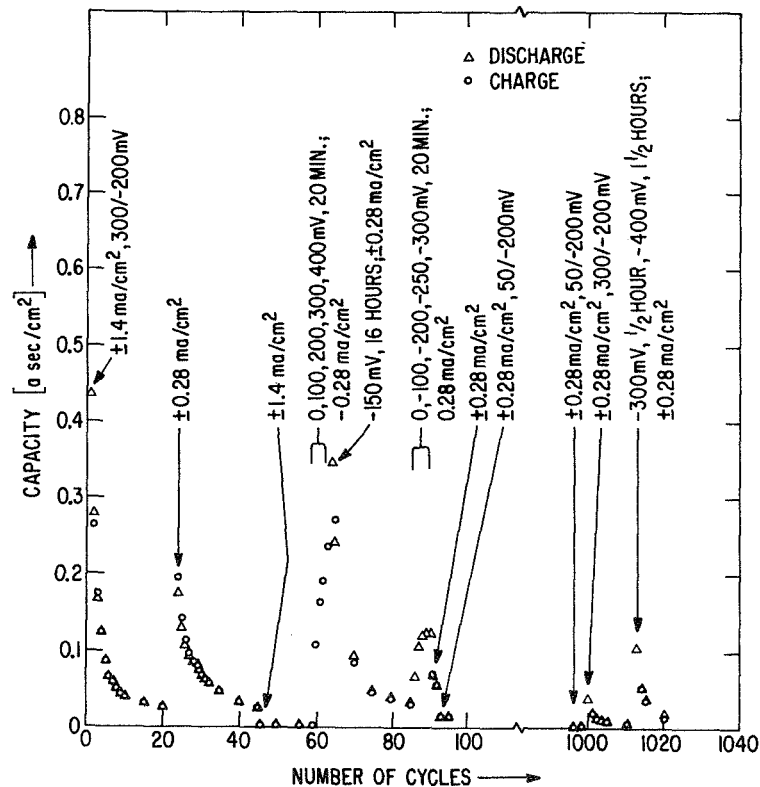
Fig. 108 Capacity of 4μ CdO film electrode vs. number of cycles, using 500μ film of 6 N KOH.

thickness of these four electrodes are 0.28, 0.09, 0.17 and
0.12 asec/cm^{2}μ. With the exception of the 25μ KOH film, the
capacities become somewhat smaller as the KOH film thickness
increases.

The capacity on cycling decreases very steeply in all cases.
Values between 3 and 13% of the initial values are obtained during
the first 100 cycles. No systematic effect of the KOH film thick-
ness on the loss of capacity during cycling could be detected.

The effects of changing the current density and voltage limits,
and the effects of extensive oxidation and reduction, are approxi-
mately the same in all cases: Lower current densities and larger
anodic voltage limits during cycling lead to the recovery of
larger capacities, extensive oxidation produces larger charge
capacities and extensive reduction has little effect on the dis-
charge capacities.

In all cases only small and gradual changes in the morphology
occur on cycling so that they become clearly visible only after
100 or more cycles. More noticeable changes relate to the color
of the electrodes. As a result of continued cycling and in
particular after periods of extensive oxidation, the surfaces
exhibit a definite brown color. In no case was this brown color
observed during the initial ten cycles. No effect of KOH film
thickness on the color changes was observed.

Effect of Electrode Preparation

While all of the previous results with electrolyte films
were obtained on cadmium oxide layers deposited electrophoretically,
some experiments were also performed on cadmium oxide layers of
considerably larger thickness, produced by brushing cadmium oxide-
binder mixtures on copper strips. This method is very similar to
preparing pasted battery plates as used in certain types of com-
mercial nickel-cadmium batteries.

Figures 109 and 110 show the cycling behavior of an electrode with a 63μ cadmium oxide film, using 6N KOH film thicknesses of 400 and 100μ, respectively. The initial capacities in Figure 109 amount to about 55% of the theoretical value. The loss of capacity on cycling was found to be much less pronounced than in any other case. After 10 cycles the capacity decreases to 88% of the initial value. The changes in morphology are characterized by the formation of a few large and transparent crystals while the surface in general does not show drastic changes as viewed in the microscope at a magnification of 220X.

When reducing the KOH film thickness from 400 to 100μ on the same electrode, a more pronounced loss of capacity is observed on cycling. This is evident from Figure 110. After 850 cycles the capacity amounts to 44% of the initial capacity.

On cycling with the 100μ KOH film, a layer of white particles formed near the solution edge, most likely by precipitation. This layer became very pronounced after about 400 cycles and had a noticeable effect on the charge and discharge curves. Charge and discharge occurred at noticeably increased cathodic and anodic potentials. Figure 111 shows the effect of current density during charge and discharge on the voltage at the state of half charge and discharge. The straight-line behavior of the curves in Figure 111 show that the layer of precipitated particles near the solution edge constitutes an additional ohmic resistance. After removing the precipitated layer by washing in distilled water, the ohmic polarization was eliminated and the capacity values were increased by 30% (compare Figure 110).

The much reduced loss of capacity on cycling observed with the painted cadmium oxide layers as compared to electrophoretic cadmium oxide layers suggests that the organic binder and the method of applying it, plays a significant role in maintaining intimate particle contact and in reducing the rate of particle growth during cycling. The painted layers displayed a much better mechanical integrity, evidenced for example by better resistance to wiping.
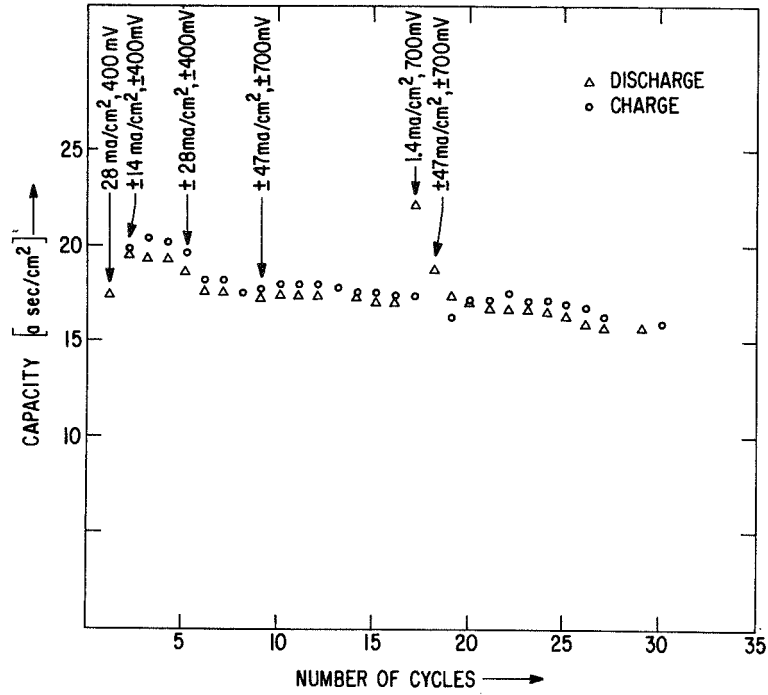
Fig. 109 Capacity of 63μ painted CdO film electrode vs. number of cycles, using 400μ film of 6 N KOH.
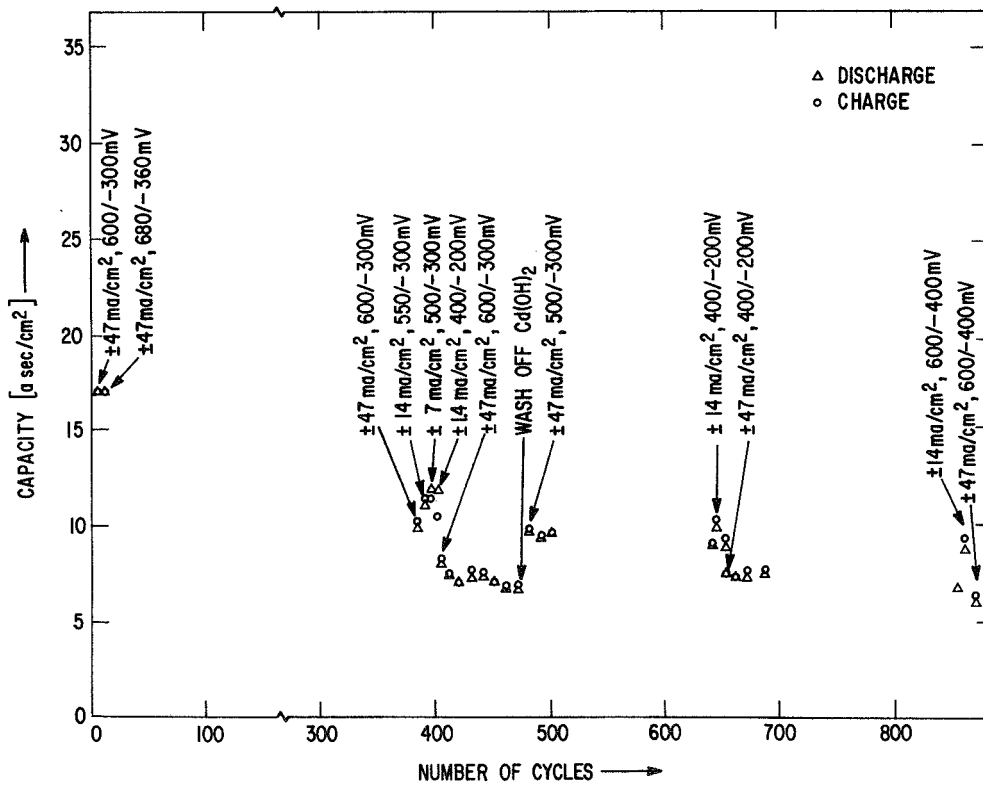
Fig. 110 Same electrode, but using 100μ film of 6 N KOH.
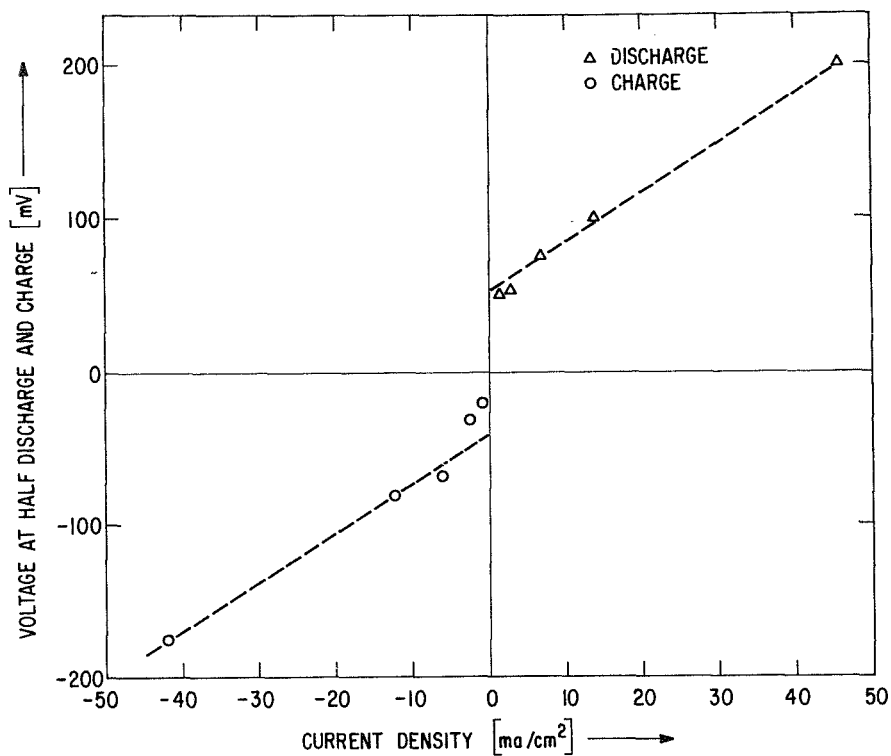
Fig. 111 Polarization curve at state of half charge and discharge of electrode in
Fig. 110 after formation of white precipitate.
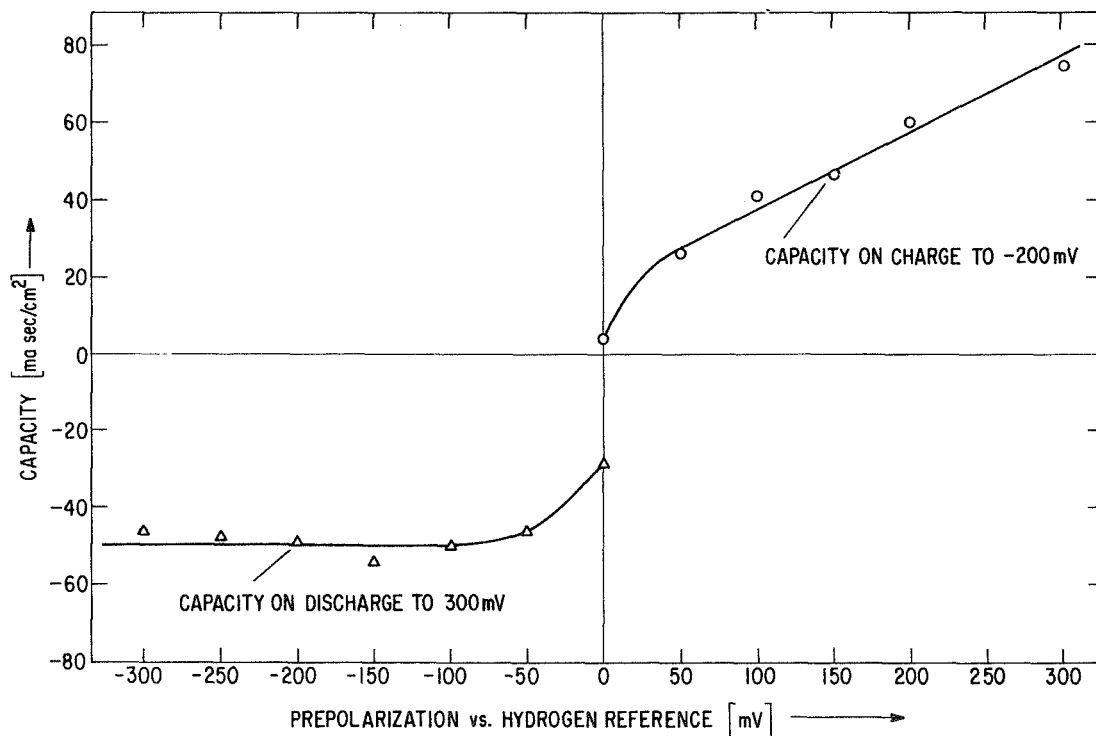
Fig. 112 Charge and discharge capacity of 3. 5μ CdO film electrode vs. prepolari-
zation, using a 12. 5μ film of 6 N KOH and ±0. 28 ma/cm².

69

Effect of Voltage on Capacity

The effect of the magnitude of the (anodic) discharge voltage on the charge capacity and the effect of the magnitude of the (cathodic) charge voltage on the discharge capacity was studied on electrodes with electrophoretic cadmium oxide films of 4-6μ and KOH films of 12.5, 25 and 500μ thickness.

The procedure adopted for the 12.5 and 500μ KOH thicknesses was as follows: In determining the effect of anodic voltages on the charge capacity, a cathodic voltage of -150 mV was always applied for 20 minutes between each new measurement. A given anodic voltage was then applied for 20 minutes and the capacity determined by applying a cathodic current density of -0.28 ma/cm^2 until a cutoff voltage of -200 mV was obtained. Conversely, the effect of cathodic voltages on the discharge capacity was determined by applying an anodic voltage of 300 mV for 20 minutes, then applying the cathodic voltage of interest followed by applying an anodic current density of 0.28 ma/cm^2 until a cutoff voltage of 300 mV was obtained. The procedure adopted for the 25μ KOH film was different in that the electrode was oxidized at a particular voltage for 20 minutes then reduced with a constant current density of -0.14 ma/cm^2 to a cutoff voltage of -200 mV followed by immediate oxidation at the next selected anodic voltage.

The results of these measurements are shown in Figures 112-114. Above anodic voltages of 100 mV, the charge capacity increases linearly with the oxidizing voltage. In contrast, the discharge capacity for voltages more cathodic than -100 mV is independent of the magnitude of the reducing voltage. Figure 113 shows the curve obtained for the 25μ KOH film. The deviations from a straight line behavior are due to incomplete reduction of oxidized species during the short duration of the charging curve.

The linear dependence of the charge capacity on the magnitude of the discharge voltage was observed previously when performing identical experiments in 0.1N KOH bulk electrolyte (Figure 44). This behavior had been explained in terms of the formation of
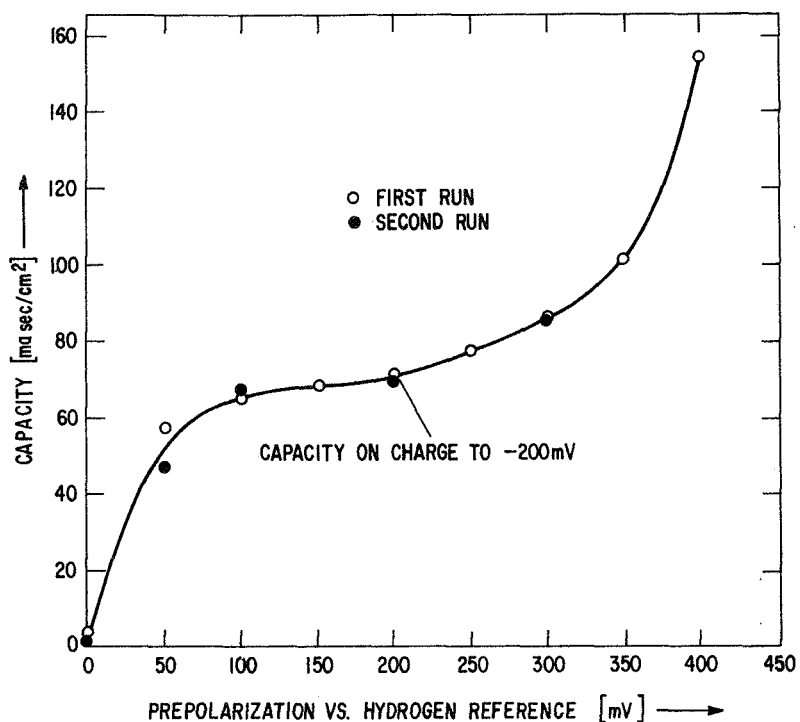
Fig. 113 Capacity on charge of 6μ CdO film electrode vs. anodic prepolarization, using a 25μ film of 6 N KOH and ±0.28 ma/cm².
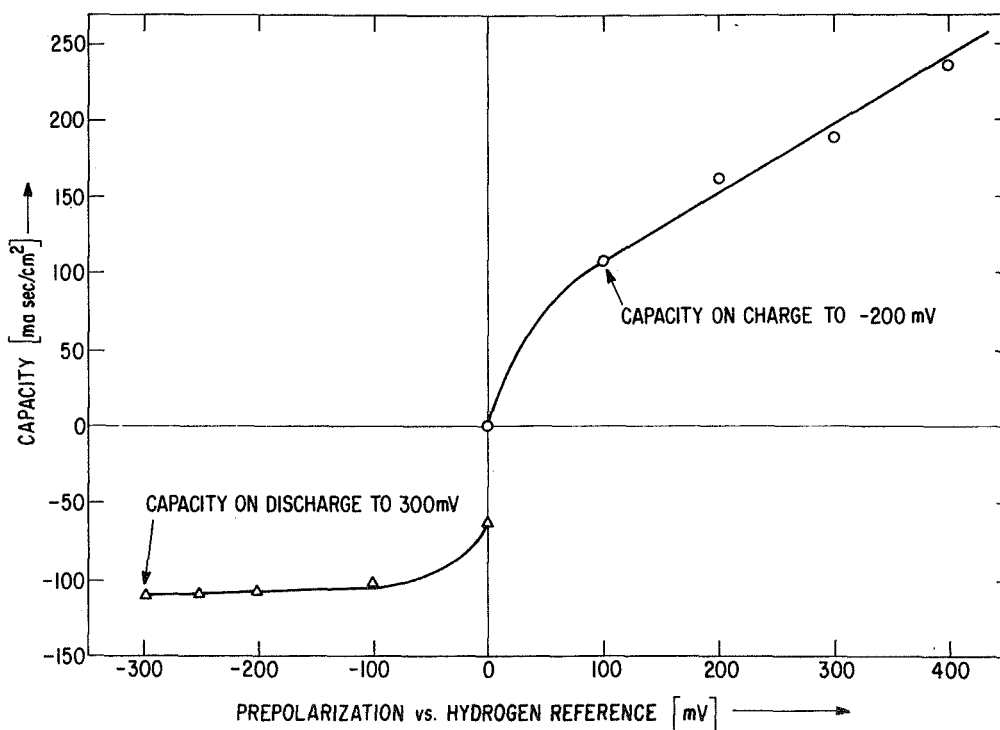
Fig. 114 Charge and discharge capacity of 4μ CdO film electrode vs. prepolarization, using a 500μ film of 6 N KOH and ±0.28 ma/cm².

passivating films during oxidation and the subsequent transport
of ions through these films. In the present case the original
layer consists of individual cadmium oxide particles rather than
a continuous cadmium film. Hence, after the first reduction to
cadmium, it is appropriate to think in terms of the formation of
passivating films around each individual particle. The question
regarding the nature of these passivating films must be left
open; they may consist of either $Cd(OH)_2$ or CdO. Since their
thickness is found to be proportional to the amount of charge
applied to the electrode, Figures 44 and 112-114 signify that the
thickness of the film increases linearly with the voltage across
the film. The deviation from the straight-line behavior at
voltages between 0 and 100 mV is very likely caused by the in-
creasing penetration of the electrolyte film by the electric
field. The same phenomenon applies to the discharge capacity as
a function of the reducing voltage. The independence of the
discharge capacity on the reducing voltage between -100 and
-300 mV implies that within the reduction time of 20 minutes,
all reducible particles were in fact reduced with voltages as
low as -100 mV while the large $Cd(OH)_2$ particles remain unre-
duced during short-term reductions. "Reducible" are considered
the small particles (compare Figure 82) in good contact with the
substrate surface.

Effect of Temperature on Capacity and Morphology

Changes in capacity and morphology of 5-6μ cadmium oxide films
on cycling were examined at 75°C with 6N KOH films of 12.5 and
100μ thickness. Figures 115 and 116 show the capacity as a function
of cycling. The initial capacities on discharge are comparable
to those obtained at room temperature. However, the loss of capa-
city on cycling is more pronounced. Thus, within ten cycles, the
capacity decreases to 7.7 and 5.8% of the initial capacity with
a KOH film of 12.5 and 100μ, respectively. This compares with
typical values between 17 and 35% at room temperature. Extensive
reduction leads to proportionally larger capacities on subsequent
discharge than at room temperature. This behavior is similar to
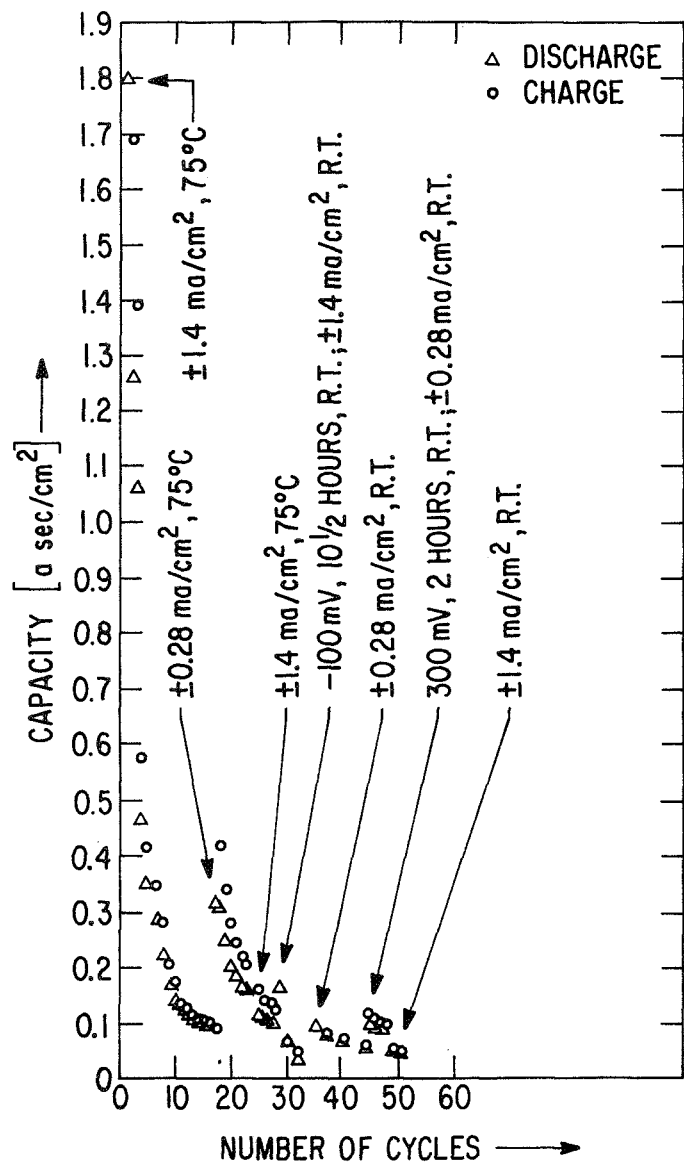
Fig. 115 Capacity of 5μ CdO film electrode vs. number of cycles at 75°C, using 12.5μ film of 6 N KOH and limits 300/-200mV.
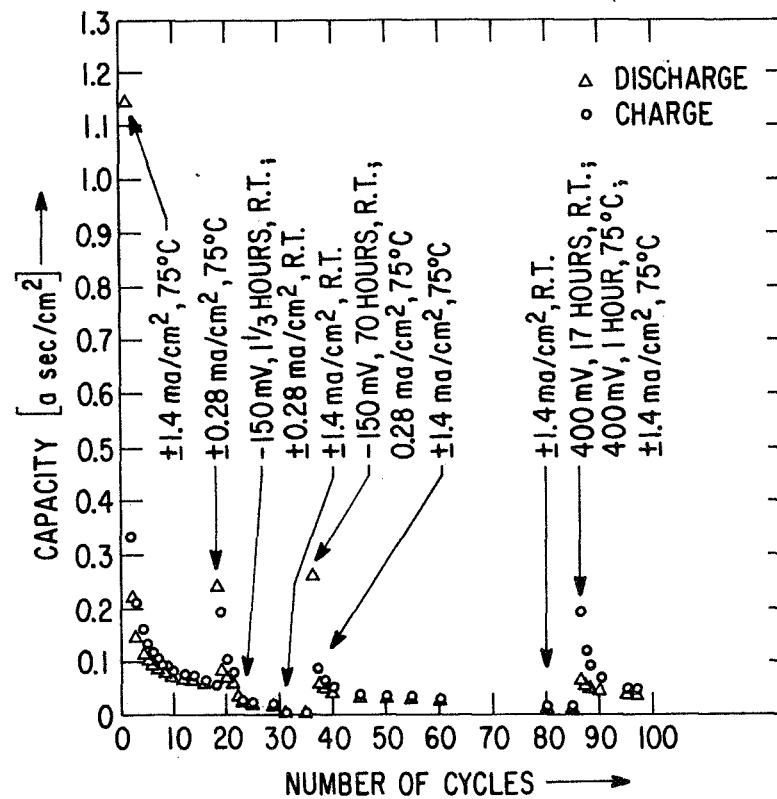
Fig. 116 Capacity of 6μ CdO film electrode vs. number of cycles at 75°C, using 100μ film of 6 N KOH and limits 300/-200 mV.

73

that observed in 6N KOH bulk electrolyte (Figure 12) and is indicative of the increasing significance of a mechanism involving the electrodeposition of dissolved cadmium species during extensive reduction (compare Figure 12).

The morphology of the electrode changes at a considerably faster rate than at room temperature. During the very first discharge, especially in the case of the 100µ KOH film, the formation of large crystals near the solution edge can be clearly observed at a magnification of 220X (Figure 117). At the far edge of the electrode, essentially no large crystals are found even after 21 cycles at 75°C. At the same time, the crystals close to the solution edge have grown in size (Figure 118).

Also in contrast to the observations at room temperature, the electrodes develop a brown appearance during the first seven cycles. Simultaneously, cadmium species become entirely depleted from some parts of the electrode. During reduction at -150 mV for 70 hours at room temperature, after cycling at 75°C, tree-like structures are formed at the solution edge in lengths up to 140µ. Subsequent cycling at 75°C and at room temperature has essentially no effect on these tree-like deposits.

The appearance of the electrode after 97 cycles is shown in Figures 119-122. All of these micrographs were obtained at a magnification of 500X after rinsing and drying the electrode. Figures 119 and 121 were obtained in dark field and show an abundance of large, mostly transparent crystals of sizes up to 15µ. These crystals tend to escape observation in the bright field (Figures 120 and 112). However, the existence of a number of well-developed hexagonal particles and of a surface film containing holes is clearly evident. It cannot be said with certainty whether this surface film causes the brown appearance of the electrode.

The formation of large hexagonal $Cd(OH)_2$ crystals during the first discharge (Figure 117) is due to a dissolution-precipitation mechanism. The formation of tree-like structures on extended reduction, together with the recovery of much increased capacities

74
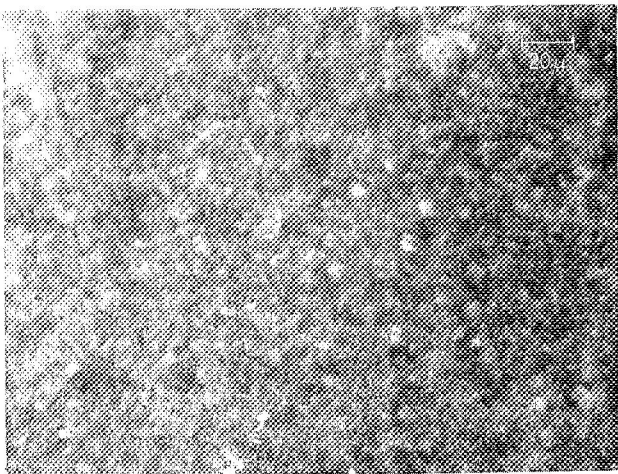
Fig. 117. Optical micrograph of 6µ CdO film near solution edge after 1st discharge at 75°C using 100µ film of 6N KOH (220X,dark field,wet).
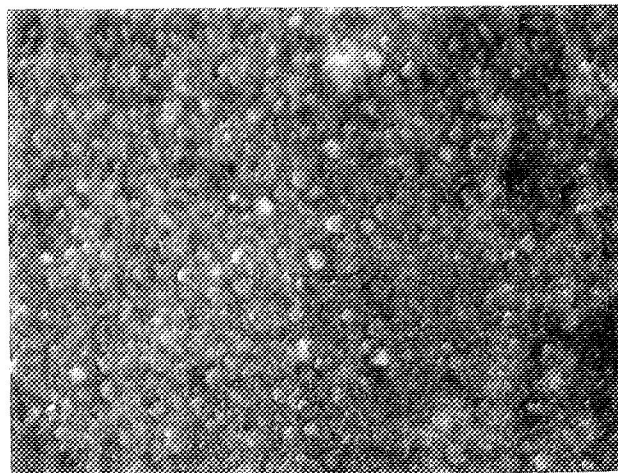
Fig. 118. Optical micrograph of same electrode same area after 21 cycles at 75°C (220X, dark field, wet).
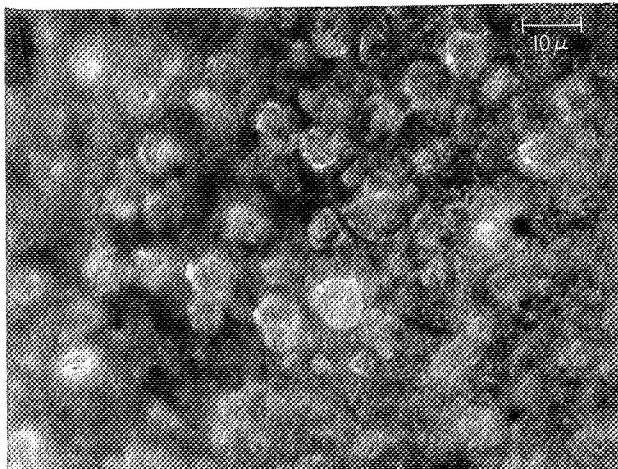
Fig. 119. Optical micrograph of same electrode in dry state after 97 cycles at 75°C (500X, dark field).
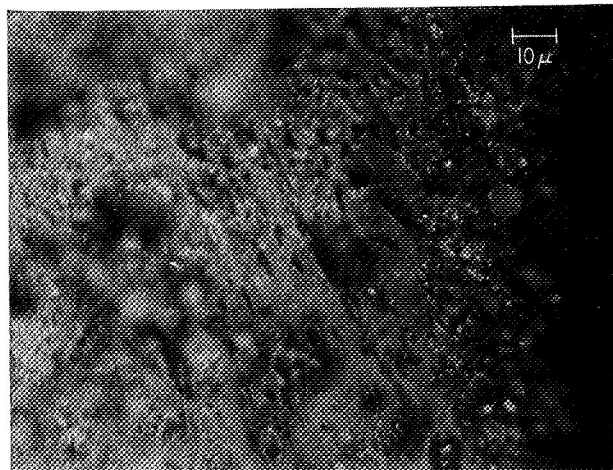
Fig. 120. Optical micrograph near solution edge after 97 cycles. (500X, bright field, dry).
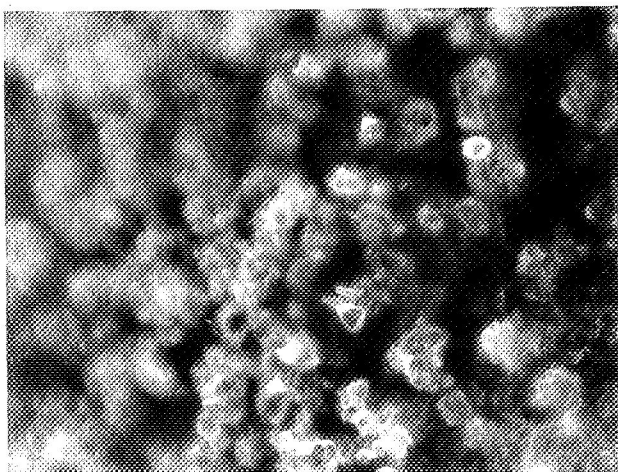
Fig. 121. Optical micrograph of different area near solution edge after 97 cycles (500X, dark field, dry).
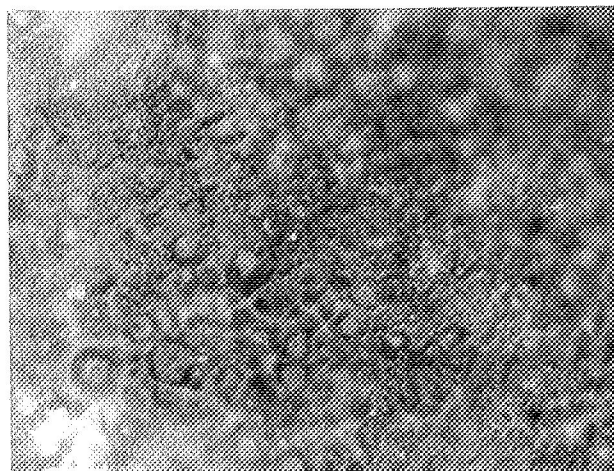
Fig. 122. Optical micrograph near far edge after 97 cycles (500X, bright field, dry).

75

on subsequent discharge, suggests that electrodeposition of dissolved cadmium species occurs on charge. This latter mechanism was found to be dominant in 6N KOH bulk electrolyte. The appearance of a brown film after seven cycles suggests the formation of cadmium oxide. The significance of this film in the loss of capacity is not clearly understood. The increased rate of capacity loss on cycling at 75°C as compared to room temperature is most likely due to the increased rate of particle growth caused by the increased rate of dissolution and the much higher solubility of cadmium species at 75°C as compared to room temperature.[6]

Concentration Changes in Film Electrolyte

The combination of equations [1] and [2] shows that hydroxyl ions are consumed on discharge and formed on charge. In thin films of electrolyte, pH-changes on charge and on discharge may, therefore, be expected and have, in fact, been demonstrated to exist in films with thicknesses of 0.5 to 2 mm.[26] A study of pH-changes in the present case of a miniature electrode was initiated but not completed.

In the previous study of pH-changes on a macroelectrode, narrow strips of $Cd/Cd(OH)_2$ at a minimum distance of 5 mm from each other were used as probes.[26] These probes served to apply small alternating current signals and thus to determine the electrolyte resistance from the measured alternating current impedance. After calibration with KOH electrolyte of known concentrations, the pH-profile was determined from the measured values of the local electrolyte resistance.

In preparation for an identical approach, cover plates containing miniature probes of silver were prepared for the electrolytic cell. The cover plates consisted of quartz plates 1 x 1 inch by 10/1000 of an inch thick. Due to the small dimensions and the small spacing of the silver probes, a masking technique recently developed for semiconductor processing[32] was applied. The silver probes are 1 mm long, 0.1 mm wide and 15-20μ thick and

are spaced at a distance of 0.3 mm on centers. Silver strips of double the width, that is 0.2 mm, are conducted to the edge of the quartz plate over a distance of about 1 cm. Since the dimension of the test electrode is 1 x 1 mm, four silver probes can be accomodated in the section of the quartz plate covering the test electrode.

The method of preparing the cover plate consists of using a photographic mask containing the desired pattern. A molybdenum film of 5,000Å thickness is evaporated on the quartz plate and then covered with a photoresist layer of 1μ thickness. The photoresist is exposed through the mask and the exposed part of the resist removed with developer in the usual way. Channels of the desired depth are introduced by etching in buffered hydrofluoric acid (1 part of 48% HF:10 parts of 40% NH_4F) for four hours. The photoresist and molybdenum adjoining the etched channels are then removed with hot 97% H_2SO_4. Fast-drying conducting silver paint (Micro-Circuits Co., New Buffalo, Michigan, Type SC12) is subsequently used to fill the etched channels. Before drying the paint, silver wires of 12.5μ diameter are inserted in the channels with their free ends emerging from the quartz plate and fastened to a microcircuit board. The excess silver paint between the channels is finally wiped off with ketone. The resulting silver probes are flush with the surface of the quartz plate.

While in the present study these cover plates were actually not applied to measure the pH-gradient in the electrolyte film covering the test electrode, the existence of pH-changes had been qualitatively established in a gross way in previous experiments. Two probes were located at the solution edge and the far edge and the impedance was measured immediately after fully charging and discharging the test electrode. Pronounced changes in the impedance were found, suggesting major changes in the electrolyte concentration during charge and discharge.

In addition to changes in the KOH concentration, changes in the concentration of cadmiate ions in the film during charge and discharge are expected to occur (compare equation [1] and [2]). The formation of soluble cadmium species, that is either $Cd(OH)_3^-$ or $Cd(OH)_4^{--}$, is evidenced by the formation of precipitated particles during discharge. The particular conditions of charge and discharge will affect the cadmiate concentration which in turn has a decisive effect on the morphology.

Mechanism for Changes in Capacity and Morphology

The results in this study are consistent with the following mechanism: On discharge, a solid state- and a dissolution-precipitation mechanism occur simultaneously, both contributing to the measured capacity and the latter leading to the formation of large crystals. The net reactions may be written as:

$$Cd + 2\ OH^- \rightleftarrows Cd(OH)_2 + 2e^- \qquad \text{(solid state)} \qquad [3]$$

$$Cd + 3\ OH^- \rightleftarrows Cd(OH)_3^- + 2e^- \qquad \text{(dissolution)} \qquad [4a]$$

$$Cd(OH)_3^- \rightleftarrows Cd(OH)_2 + OH^- \qquad \text{(precipitation)} \qquad [4b]$$
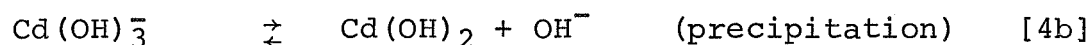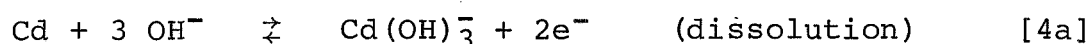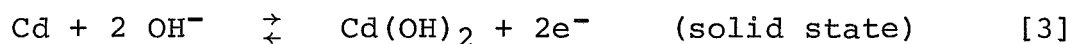
Many of the precipitated particles have poor contact with the substrate. The particles oxidized via solid state reaction[3] become surrounded by a layer of cadmium hydroxide which hinders subsequent charge transfer and requires increasing overvoltages. This is evident from those parts of the discharge curves, where the voltages rises steeply with further discharge (compare curve after 4000 cycles in Figure 68).

On charging, the rate and duration of charging is significant in determining the reaction mechanisms. On short and high-rate charges, the solid state reaction [3] (in reverse direction) dominates and explains the observed persistence of the large pre-cipitated $Cd(OH)_2$ crystals. On prolonged and low-rate charges, the reaction [4b] leads to the observed dissolution of $Cd(OH)_2$ crystals. In this case, sufficient time is available for this slow process[18] to occur. The dissolution process is furthermore

78

favored by the increase in pH during charging which raises the solubility of cadmiate ions. The dissolution is followed by the reverse of reaction [4a] which leads to the electrodeposition of cadmium. In parallel to the dissolution-electrodeposition process, the solid state reduction of many particles takes place, in particular the smaller ones which are in good contact with the substrate surface. As this process proceeds, the particles become surrounded with a conducting layer of cadmium which facilitates further reduction. This is very likely the reason why charging occurs with smaller overvoltages than discharging.

Cadmiate ions are expected to diffuse and, during discharge, to migrate toward the counter electrode. Once they have left the small volume of the film electrolyte, very long charging times are required to electrodeposit them on the test electrode. The areas of the test electrode near the electrolyte well are preferred sites for deposition. The observed growth of tree-like structures during prolonged reduction is evidence for this mechanism.

CONCLUSIONS

In bulk solutions of KOH under conditions of stirring and uniform current distribution we arrive at the following conclusions with regard to the changes in capacity and morphology of cadmium film electrodes during cycling:

1. In concentrated bulk solutions of KOH, prolonged discharge and especially continuous cycling lead to a drastic loss in capacity and complete change in morphology due to extensive dissolution of cadmium species. The soluble species leaves the electrode before supersaturation and precipitation can occur.

2. The discharge occurs via a dissolution mechanism to the extent of 70 to 80% and via a solid state transport mechanism to the extent of 20 to 30%. The latter part of the discharged species remains at the surface and passivates readily. The proportions of cadmium dissolving and undergoing solid state oxidation depend upon the initial morphology of the electrode.

3. Prolonged charging leads to electrodeposition of previously dissolved cadmium species and hence, to the recovery of capacities near the theoretical values.

4. As the KOH concentration decreases, the dissolution mechanism becomes less and the solid state transport mechanism more important.

5. In 0.1N KOH there is very little change in morphology and capacity on cycling, but the capacity corresponds to the oxidation and reduction of only a few atom layers. The limited extent of reactions is due to the formation of and subsequent ionic transport through passivating layers.

6. The passivating layers are likely to consist of cadmium oxide as implied by the appearance of a brown film and cubic particles.

In thin films of concentrated KOH under conditions of highly non-uniform current distribution, simulating conditions in a single pore of a cadmium battery plate, we arrived at the following conclusions:

1. The first discharge leads to the recovery of typically 60% of the theoretical capacity, but the capacity decreases steeply during cycling, typically to 12% of the theoretical value in ten cycles. Discharge leads to the formation of large well-behaved crystals of β-Cd(OH)$_2$ and some γ-Cd(OH)$_2$ due to dissolution and subsequent precipitation of soluble cadmium species which is favored by the decreasing pH during discharge.

2. The large crystals do not contribute to the capacity on subsequent cycling and, hence, are responsible for the pronounced loss of capacity observed during the initial cycles.

3. The remaining capacity is due to the charge and discharge of particles of the original size via a solid state transport mechanism.

4. The formation of passivating films, probably cadmium oxide, is suggested by the appearance of a brown film accompanied by a further decrease of the capacity on continued cycling.

5. Prolonged reduction leads to the dissolution of the Cd(OH)$_2$ crystals due to the increase in pH on charging. Electrodeposition of cadmium leads to increased capacity on subsequent discharge.

6. The thickness of the electrolyte film has very little effect on the observed phenomena.

7. The method of preparing the electrode may have significant effects on the morphology and capacity. Pasted cadmium oxide electrodes display better coherence between particles than electrophoretic cadmium oxide electrodes and show considerably smaller loss of capacity on cycling.

8. Increased temperature enhances the rate of particle growth and results in increased loss of capacity on cycling.

REFERENCES

1. A. J. Salkind and G. W. Bodamer, Proc. 4th Internat. Symp. on Batteries Brighton, England, D. H. Collins, ed., Pergamon Press (1964), p. 55.

2. J. P. Harivel, B. Morignat, and J. Migeon, ibid., p. 107.

3. E. Lifshin and J. L. Weininger, Electrochem. Tech. 5, 5 (1967).

4. O. C. Wagner, J. Electrochem. Soc. 116, 693 (1969).

5. R. Scholder and E. Staufenbiel, Z. Anorg. Chem., 247, 257 (1941).

6. P. E. Lake and J. M. Goodings, Can. J. Chem., 36, 1089 (1958).

7. R. E. Visco and R. H. Sonner, Electrochem. Soc., Extended Abstracts, Detroit Meeting, Oct. 1969, p. 18.

8. K. Huber, J. Electrochem. Soc. 100, 376 (1953).

9. K. Huber and S. Stucki, Helv. Chim. Acta, 51, 1343 (1968).

10. P. E. Lake and E. J. Casey, J. Electrochem. Soc. 105, 52 (1958).

11. P. E. Lake and E. J. Casey, ibid., 106, 913 (1959).

12. I. Sanghi, S. Visvanathan, and S. Ananthanarayanan, Electrochim. Acta 3, 65 (1960).

13. S. Yoshizawa and Z. Takehara, ibid., 5, 240 (1961).

14. M. A. V. Devanathan and S. Lakshmanan, ibid., 13, 667 (1968).

15. G. T. Croft, J. Electrochem. Soc. 106, 278 (1959).

16. G. T. Croft and D. Tuomi, ibid., 108, 915 (1961).

17. J. P. G. Farr and N. A. Hampson, Electrochem. Technol., 6, 10 (1969).

18. Y. Okinaka, J. Electrochem. Soc. 117, 289 (1970).

19. P. C. Milner and U. B. Thomas "Advances in Electrochem. and Electrochem. Eng.," C. W. Tobias, Editor, Vol. 5, Interscience Publishers, New York (1967).

20. M. W. Breiter and J. L. Weininger, J. Electrochem. Soc. 113, 651 (1966).

21. M. W. Breiter and W. Vedder, Trans. Faraday Soc., 63, 1042 (1967).

22. S. U. Falk, J. Electrochem. Soc. 107, 661 (1960).

23. R. D. Armstrong, E. H. Buolt, D. F. Porter and H. R. Thirsk, Electrochim. Acta 12, 1245 (1967).

24. F. G. Will, Electrochem. Soc. Extended Abstracts, Detroit Meeting, Oct. 1969, p. 62.

25. Y. Okinaka and C. M. Whitehurst, J. Electrochem. Soc. 117, 583 (1970).

26. F. G. Will, Proc. 6th Intern. Symp. on Batteries, Brighton, England, 1968, p. 149, D. H. Collins, ed., Pergamon Press.

27. M. D. Zhoulder and V. V. Stender, Zhur. Priklad. Khim., 31, 711 (1958).

28. R. W. Powers, Electrochem. Technol. 2, 274 (1964).

29. R. Haul and D. Just, J. Applied Physics 33, 487 (1962).

30. F. G. Will, to be published

31. F. G. Will, J. Electrochem. Soc. 110, 145 (1963).

32. D. M. Brown, W. E. Engeler, M. Garfinkel, and F. K. Heumann, J. Electrochem. Soc. 114, 730 (1967).

DISTRIBUTION LIST

National Aeronautics & Space Administration
Lewis Research Center
21000 Brookpark Road
Cleveland, Ohio   44135
Attn: Dr. L. Rosenblum (MS 302-1)
        H. J. Schwartz (MS 309-1)
        Dr. J. S. Fordyce (MS 309-1)
        J. E. Dilley (MS 500-309)
        Technology Utilization Office (MS 3-19)
        D. G. Soltis (MS 309-1)
        V. Hlavin (MS 3-14)
        Library (MS 60-3)
        Report Control (MS 5-5)
        G. M. Ault (MS 3-13)

National Aeronautics & Space Administration
Washington, D. C. 20546
Attn: RNW/E. M. Cohn
        MTG/Richard Livingston
        FC/A. M. Greg Andrus
        RN/William H. Woodward
        UT/Dr. S. J. Glassman
        U/Dr. E. N. Case

National Aeronautics & Space Administration
Goddard Space Flight Center
Greenbelt, Maryland   20771
Attn: Thomas Hennigan, Code 716.2
        Gerald Halpert, Code 735
        Joseph Sherfey, Code 735
        Louis Wilson, Code 450

National Aeronautics & Space Administration
Langley Research Center
Instrument Research Division
Hampton, Virginia   23365
Attn: M. B. Seyffert, MS 112
        Jack E. Zanks MS 488

National Aeronautics & Space Administration
Geo. C. Marshall Space Flight Center
Huntsville, Alabama   35812
Attn: Philip Youngblood
        C. B. Graff (S&E-ASTR-EP)

National Aeronautics & Space Administration
Manned Spacecraft Center
Houston, Texas   77058
Attn: William R. Dusenbury (EP-5)
        W. E. Rice (EP-5)
        Robert Cohen
            Gemini Project Office
        Forrest E. Eastman (EE-4)

National Aeronautics & Space Administration
Langley Research Center
Langley Station
Hampton, Virginia   23365
Attn: Harry Ricker

National Aeronautics & Space Administration
Scientific & Technical Information
   Center: Input
P. O. Box 33
College Park, Maryland   20740
   (2 copies plus 1 reproducible)

National Aeronautics & Space Administration
Ames Research Center
Pioneer Project
Moffett Field, California   94035
Attn: Arthur Wilber/A. S. Hertzog

National Aeronautics & Space Administration
Ames Research Center
Moffett Field, California   94035
Attn: Jon Rubenzer
        Code PBS, MS 244-2

Jet Propulsion Laboratory
4800 Grove Drive
Pasadena, California   91103
Attn: Mr. Paul Goldsmith (MS 198-223)/
        A. Uchiyami

Department of the Army

U. S. Army Mobility Equipment R & D Center
MERDC
Fort Belvoir, Virginia   22060
Electro Technology Lab -
Energy Conversion Research Division

Commanding General
U. S. Army Weapons Command
Attn: AMSWE-RDR, Mr. G. Reinsmith
Rock Island Arsenal
Rock Island, Illinois   61201

U. S. Army Research Office
Box CM, Duke Station
Durham, North Carolina   27706
Attn: Dr. Wilhelm Jorgensen

U. S. Army Research Office
Chief, R & D
Department of the Army
3D442, The Pentagon
Washington, D. C.   20546

Commanding Officer
U. S. Army Electronics R & D Labs
Fort Monmouth, New Jersey   07703
Attn: Power Sources Division (SELRA/PS)

Army Materiel Command
Research Division
AMCRD-RSCM-T-7
Washington, D. C.   20315
Attn: John W. Crellin

Army Materiel Command
Development Division
AMCRD-DE-MO-P
Washington, D. C.   20315
Attn: Marshall D. Aiken

U. S. Army TRECOM
Fort Eustis, Virginia   23604
Attn: Leonard M. Bartone (SMOFE-ASE)
       Dr. R. L. Eshols (SMOFE-PSG)

U. S. Army Mobility Command
Research Division
Warren, Michigan   48090
Attn: O. Renius (AMSMO-RR)

Harry Diamond Laboratories
Room 300, Building 92
Conn. Ave. & Van Ness St., N. W.
Washington, D. C.   20438
Attn: Nathan Kaplan

Department of the Navy

Office of Naval Research
Washington, D. C.   20360
Attn: Director, Power Program
       Code 473

Office of Naval Research
Department of the Navy
Arlington, Virginia   22217
Attn: H. W. Fox (Code 472)

Naval Research Laboratory
4555 Overlook Avenue
Washington, D. C.   20360
Attn: Dr. J. C. White, Code 6160

Naval Ship R & D Center
Annapolis, Maryland   21402
Attn: J. H. Harrison, Code A731

Commanding Officer
U. S. Naval Ammunition Depot
Crane, Indiana   47522
Attn: D. Miley, Code QEWE

Naval Ordnance Laboratory
Silver Spring, Maryland   20910
Attn: Philip D. Cole (Code 232)

Naval Ship Engineering Center
Center Bldg., Prince George's Center
Hyattsville, Maryland   20782
Attn: C. F. Viglotti (Code 6157D)

Bureau of Naval Weapons
Department of the Navy
Washington, D. C.   20360
Attn: Whitewall T. Beatson
      (Code RAAE-52)

Naval Ship Systems Command
Washington, D. C.   20360
Attn: Bernard B. Rosenbaum
      Code 03422

Mr. Robert Trumbule, STIC
4301 Suitland Road
Suitland, Maryland   20390

Department of the Air Force

Aero Propulsion Laboratory
Wright-Patterson AFB, Ohio   45433
Attn: James E. Cooper, APIP-1

AF Cambridge Research Lab
Attn: CRFE
L. G. Hanscom Field
Bedford, Massachusetts   01731
Attn: Dr. R. Payne

AF Cambridge Research Lab
L. G. Hanscom Field
Bedford, Massachusetts   01731
Attn: Francis X. Doherty, CRE
      Edward Raskind (Wing F)

Headquarters, U. S. Air Force (AFRDR-AS)
Washington, D. C.   20325
Attn: Major G. Starkey

Headquarters, U. S. Air Force (AFRDR-AS)
Washington, D. C.   20325
Attn: Lt. Col. William G. Alexander

Rome Air Development Center, ESD
Attn: Frank J. Mollura   (EMEAM)
Griffis AFB, New York   13440

Space Systems Division
Los Angeles Air Force Station
Los Angeles, California   90045
Attn: HQ SAMSO (SMTAE/Lt. R. Ballard)

Other Government Agencies

National Bureau of Standards
Washington, D. C.   20234
Attn: Dr. W. J. Hamer

National Bureau of Standards
Washington, D. C.   20234
Attn: Dr. A. Brenner

Office, Sea Warfare System
The Pentagon
Washington, D. C.   20310
Attn: G. B. Wareham

Bureau of Mines
4800 Forbes Avenue
Pittsburgh, Pa.   15213
Attn: Dr. Irving Wender

Clearing House for Scientific &
  Technical Information
5285 Port Royal Road
Springfield, Virginia   22151

Private Organizations

Aerojet-General Corporation
Von Karman Center
Bldg. 312, Dept. 3111
Azusa, California   91703
Attn: Mr. Russ Fogle

Aerospace Corporation
P. O. Box 95085
Los Angeles, California   90045
Attn: Library Acquisition Group

A.M.F.
Attn: R. J. Mosny/M. S. Mintz
689 Hope Street
Stamford, Connecticut   06907

Arthur D. Little, Inc.
Acorn Park
Cambridge, Massachusetts   02140
Attn: Dr. James D. Birkett

Battelle Memorial Institute
505 King Avenue
Columbus, Ohio 43201
Attn: Dr. John MaCallum

Dr. Carl Berger
13401 Kootenay Drive
Santa Ana, California 92705

Bell Laboratories
Murray Hill, New Jersey 07974
Attn: Dr. P.C. Milner

The Boeing Company
P.O. Box 3999
Seattle, Washington 98124
Attn: Sid Gross, MS 85-86, 2-7814

Burgess Battery Company
Foot of Exchange Street
Freeport, Illinois 61032
Attn: Mr. M.E. Wilke

C & D Batteries
Division of Electric Autolite Co.
Conshohocken, Pennsylvania 19428
Attn: Dr. Eugene Willihnganz

Calvin College, Science Bldg.
3175 Burton Street, S.E.
Grand Rapids, Michigan 49506
Attn: Prof. T.P. Dirkse

Communications Satellite Corporation
1835 K Street, N.W.
Washington, D.C. 20036
Attn: Mr. Robt. Strauss

ChemCell Inc.
150 Dey Road
Wayne, New Jersey 07470
Attn: Peter D. Richman

Cubic Corporation
9233 Balboa Avenue
San Diego, California 92123
Attn: Librarian

Delco Remy Division
General Motors Corporation
2401 Columbus Avenue
Anderson, Indiana 46011
Attn: J.A. Keralla

Bellcomm, Inc.
955 Lenfant Plaza North, S.W.
Washington, D.C. 20024
Attn: B.W. Moss

Eagle-Picher Company
Post Office Box 47
Joplin, Missouri 64801
Attn: E.P. Broglio

ESB Inc.
Post Office Box 11097
Raleigh, North Carolina 27604
Attn: Director of Engineering

Electromite Corporation
2117 South Anne Street
Santa Ana, California 92704
Attn: R.H. Sparks

Energy Research Corp.
15 Durant Avenue
Bethel, Connecticut 06801
Attn: M. Klein

ESB Inc.
Research Center
P.O. Box 336
Yardley, Pennsylvania 19067
Attn: Dr. G. Frysinger

Electrochimica Corporation
1140 O'Brien Drive
Menlo Park, California 94025
Attn: Dr. Morris Eisenberg

Energetics Science, Inc.
4461 Bronx Blvd.
New York, New York 10470
Attn: Dr. H.G. Oswin

Elgin National Watch Company
107 National Street
Elgin, Illinois   60120
Attn: T. Boswell

Engelhard Industries, Inc.
497 Delancy Street
Newark, New Jersey   07105
Attn: Dr. J. G. Cohn

Dr. Arthur Fleischer
466 South Center Street
Orange, New Jersey   07050

General Electric Company
Missile & Space Division
Spacecraft Department
P. O. Box 8555
Philadelphia, Pennsylvania   19101
Attn: K.L. Hanson, Room M-2614

General Electric Company
Battery Business Section
P. O. Box 114
Gainesville, Florida   32601
Attn: Director of Engineering

General Electric Company
Research & Development Center
Post Office Box 8
Schenectady, New York   12301
Attn: Whitney Library

Dr. P. L. Howard
Centreville, Maryland   21617

General Telephone & Electronics Labs
Bayside, New York   11352
Attn: Library

Globe-Union, Inc.
P. O. Box 591
Milwaukee, Wisconsin   53201
Attn: Dr. E. Weissmann

Mr. David Schmidt
General Electric Company
777 - 14th Street, N. W.
Washington, D. C.   20005

Gould-National Batteries, Inc.
Engineering & Research Center
2630 University Avenue, S. E.
Minneapolis, Minnesota   55418
Attn: D. L. Douglas

Gulton Industries
Alkaline Battery Division
1 Gulton Street
Metuchen, New Jersey   08840
Attn: D. J. Mager

Hughes Aircraft Corporation
Centinda Avenue & Teale Street
Culver City, California   90230
Attn: T. V. Carvey

Hughes Aircraft Corporation
Bldg. 366, M.S. 524
El Segundo, California   90245
Attn: M. E. Ellion

ITT Federal Laboratories
500 Washington Avenue
Nutley, New Jersey   07110
Attn: Dr. P. E. Lighty

ITT Research Institute
10 West 35th Street
Chicago, Illinois   60616
Attn: Dr. H. T. Francis

Institute for Defense Analyses
R & E Support Division
400 Army-Navy Drive
Arlington, Virginia   22202
Attn: Mr. R. Hamilton/Dr. R. Briceland

Heliotek
12500 Gladstone Avenue
Sylmar, California 91342
Attn: Dr. H. N. Seiger

Idaho State University
Department of Chemistry
Pocatello, Idaho   83201
Attn: Dr. G. Myron Arcand

International Nickel Company
1000-16th Street, N. W.
Washington, D. C.   20036
Attn: Mr. N. A. Matthews

Leesona Moos Laboratories
Lake Success Park, Community Drive
Great Neck, New York   11021
Attn: Dr. A. Moos

Honeywell Inc.
Livingston Electronic Laboratory
Route 309
Montgomeryville, Pennsylvania   18936
Attn: Library

Life Systems, Inc.
23715 Mercantile Road
Cleveland, Ohio   44122
Attn: Dr. Richard Wynveen

Lockheed Missiles & Space Company
Technical Information Center
3251 Hanover Street
Palo Alto, California   93404

P. R. Mallory & Co., Inc.
Northwest Industrial Park
Burlington, Massachusetts   01803
Attn: Dr. Per Bro

P. R. Mallory & Co., Inc.
3029 E. Washington Street
Indianapolis, Indiana   46206
Attn: Technical Librarian

Martin Company
Electronics Research Department
P. O. Box #179
Denver, Colorado   80201
Attn: William B. Collins, MS 1620
        M. S. Imanura, MS 8840
        J. Leuthard, MS 8840

Mauchly Systems, Inc.
Montgomeryville Industrial Park
Pennsylvania   18936
Attn: John H. Waite

Melpar
Technical Information Center
7700 Arlington Boulevard
Falls Church, Virginia   22046

McDonnell Douglas Corp.
5301 Bolsa Avenue
Huntington Beach, California   92647
Attn: A. D. Tonelli, MS-17, Bldg. 22
        Dr. G. Moe, MS 12, Bldg. 11-3-12

North American Rockwell
Autonetics Division
P. O. Box 4181
Anaheim, California   92803
Attn: R. F. Fogle GFIG

Midwest Research Institute
425 Volker Boulevard
Kansas City, Missouri   64110
Attn: Physical Science Laboratory

North American Aviation Co.
S & ID Division
Downey, California   90241
Attn: Dr. James Nash

Oklahoma State University
Stillwater, Oklahoma   74075
Attn: Prof. William L. Hughes
        School of Electrical Engineering

Dr. John Owen
P. O. Box 87
Bloomfield, New Jersey   07003

Power Information Center
University City Science Institute
3401 Market St., Room 2107
Philadelphia, Pennsylvania   19104

Prime Battery Corporation
15600 Cornet Street
Santa Fe Springs, Calif.,   90670
Attn: David Roller

Portable Power Sources Corp.
122 East 42nd Street
New York, New York   10017
Attn: L. Schulman

RAI Research Corporation
225 Marcus Blvd.
Hanppange L.I., New York   11787

Radio Corporation of America
Astro Corporation
P. O. Box 800
Hightstown, New Jersey   08540
Attn: Seymour Winkler

Philco-Ford Corporation
Space Power & Prop. Dept, MS W-49
3825 Fabian Way
Palo Alto, California   94303
Attn: Mr. D. C. Briggs

Southwest Research Institute
P. O. Drawer 28510
San Antonio, Texas   78228
Attn: Library

Sonotone Corporation
Saw Mill River Road
Elmsford, New York   10523
Attn: A. Mundel

Thomas A. Edison Research Laboratory
McGraw Edison Company
Watchung Avenue
West Orange, New Jersey   07052
Attn: Dr. P. F. Greiger

TRW Systems Inc.
One Space Park
Redondo Beach, California   90278
Attn: Dr. A. Krausz
       Bldg. 60, Rm. 1047

TRW Systems, Inc.
One Space Park
Redondo Beach, California   90278
Attn: Dr. Herbert P. Silverman (R-1/2094)
       Dr. W. R. Scott (M-2/2154)

TRW, Inc.
2355 Euclid Avenue
Cleveland, Ohio   44117
Attn: Librarian TIM 3417

Tyco Laboratories, Inc.
Bear Hill
Hickory Drive
Waltham, Massachusetts   02154
Attn: Dr. Jose Giner

Union Carbide Corporation
Development Laboratory Library
P. O. Box 6056
Cleveland, Ohio   44101

Union Carbide Corporation
Parma Laboratory
Post Office Box 6116
Parma, Ohio   44130
Attn: Dr. Robert Powers

University of California
Space Science Laboratory
Berkeley, California   94720
Attn: Dr. C. W. Tobias

University of Pennsylvania
Electrochemistry Laboratory
Philadelphia, Pennsylvania   19104
Attn: Prof. John O'M. Bockris

Westinghouse Electric Corporation
Research and Development Center
Churchill Borough
Pittsburgh, Pennsylvania   15235
Attn: Dr. C. C. Hein/Dr. A. Langer

Whitakker Corporation
3850 Olive Street
Denver, Colorado   80237
Attn: Mr. L. K. White

Western Electric Company
Suite 802, RCA Building
Washington, D. C.   20006
Attn: R. T. Fiske

Yaroney Electric Corp.
82 Mechanic Street
Pawcatuck, Connecticut   02891
Attn: Director of Engineering